Hochschule für Angewandte Wissenschaften Hamburg
Hamburg University of Applied Sciences

Masterarbeit

Fabian Brandes

Mehrskalen-Modellierung eines Vanadium Redox-Flow-Batterie Stacks

Fakultät Technik und Informatik
Department Maschinenbau und Produktion

Faculty of Engineering and Computer Science
Department of Mechanical Engineering and Production

Fabian Brandes

Mehrskalen-Modellierung eines Vanadium Redox-Flow-Batterie Stacks

Masterarbeit eingereicht im Rahmen der Masterprüfung

im Studiengang Master of Science Maschinenbau / Berechnung und Simulation
am Department Maschinenbau und Produktion
der Fakultät Technik und Informatik
der Hochschule für Angewandte Wissenschaften Hamburg

Erstprüfer: Prof. Dr. Thorsten Struckmann
Zweitprüfer: Prof. Dr. Achim Schmidt

Eingereicht am: 28.05.2020

Fabian Brandes

Thema der Arbeit
Mehrskalen-Modellierung eines Vanadium Redox-Flow-Batterie Stacks

Stichworte
Redox-Flow-Batterie, RFB, VRFB, RFB Stack, Mehrskalen-Modellierung, Modellierung

Kurzzusammenfassung
In dieser Arbeit wird die Entwicklung eines Mehrskalen-Modells eines Vanadium Redox-Flow-Batterie Stacks beschrieben. Das Modell besteht aus einem Mikro- und einem Makro-Modell und ermöglicht die Bewertung von verschiedenen Stack-Designs. Das Mikro-Modell wird in COMSOL implementiert und simuliert eine einzelne Zelle auf mikroskopischer Ebene. Das Makro-Modell wird in Matlab Simulink implementiert und kann benutzt werden um eine beliebige Anzahl Zellen in beliebiger elektrischer Verschaltung auf makroskopischer Ebene zu simulieren. Eine abschließende Bewertung des Modells ergibt, dass es zur Auslegung von Stacks geeignet ist.

Fabian Brandes

Title of the paper
Multiscale Modeling of a Vanadium Redox Flow Battery Stack

Keywords
redox flow battery, RFB, VRFB, RFB Stack, multiscale modeling, modeling

Abstract
In this thesis the development of a multiscale model of a vanadium redox flow battery stack is described. The model consists of a Micro- and a Macro-Model and allows the evaluation of different stack designs. The Micro Model is implemented in COMSOL and simulates a single cell on a microscopic level. The Macro Model is implemented in Matlab Simulink and can be used to simulate any number of cells in any electrical connection on a macroscopic level. An evaluation of the model shows, that it is suitable for the dimensioning of stacks.

Contents

List of Abbreviations

ASR	Area specific cell resistance
CC	Current Collector
LUT	Lookup Table
NaN	Not a Number
OCV	Open Circuit Voltage
RFB	Redox Flow Battery
SHE	Standard Hydrogen Electrode
SOC	State of Charge
VRFB	All-Vanadium Redox Flow Battery

Physical Constants

elementary charge	$e = 1.60217662 \cdot 10^{-19}\ \mathrm{C}$
Avogadro constant	$N_A = 6.02214086 \cdot 10^{23}\,\mathrm{mol}^{-1}$
Faraday constant	$F = 96483.33289\,\mathrm{C\,mol}^{-1}$
universal gas constant	$R = 8.314472\,\mathrm{J\,K}^{-1}\,\mathrm{mol}^{-1}$

List of Symbols

a	activity	$\mathrm{mol\,m^{-3}}$
A	area	$\mathrm{m^2}$
ASR	area specific cell resistance	$\Omega\,\mathrm{cm^2}$
c	(bulk) concentration	$\mathrm{mol\,m^{-3}}$
c^s	surface concentration	$\mathrm{mol\,m^{-3}}$
d	diameter	m
D	diffusion coefficient	$\mathrm{m^2\,s^{-1}}$
E^{00}_{cell}	standard cell potential	V
$E^{00}_{neg/pos}$	standard electrode potential	V
$E^{00'}_{cell}$	formal standard cell potential	V
$E^{00'}_{neg/pos}$	formal standard electrode potential	V
$E^{0}_{neg/pos}$	Nernst-Potential of the negative or positive electrode	V
E_{cell}	cell potential	V
i	current density per membrane area	$\mathrm{mA\,m^{-2}}$
i_0	exchange current density per membrane area	$\mathrm{mA\,m^{-2}}$
i_{lim}	limiting current density per membrane area	$\mathrm{mA\,m^{-2}}$
I	electric current	A
j	current density per electrode surface	$\mathrm{mA\,m^{-2}}$
j_0	exchange current density per electrode surface	$\mathrm{mA\,m^{-2}}$
k	chemical reaction rate	$\mathrm{s^{-1}}$
l	length	m
n	amount of substance	mol
N	flux of species	$\mathrm{mol\,m^{-2}\,s^{-1}}$
OCV	Open Circuit Voltage	V
R	electric resistance	Ω
p	pressure	Pa
Q	electric charge	C
SOC	State of charge	%
T	temperature	T
u	mobility	$\mathrm{m^2\,s^{-1}\,V^{-1}}$
U	voltage	V
v	velocity	$\mathrm{m\,s^{-1}}$
$\dot{V}$	volume flow rate	$\mathrm{m^3\,s^{-1}}$
W	Work	J
z	number of transferred electrons per reaction	-

α	charge transfer coefficient	-
δ_0	thickness of the Nernst Diffusion layer	m
ΔG	Gibb's free enthalpy	J
ΔH	reaction enthalpy	J
ΔS	reaction entropy	$\mathrm{J\,K^{-1}}$
ε	porosity	-
ζ	pore-wall flux density	$\mathrm{mol\,m^{-2}\,s^{-1}}$
η	overpotential	V
η_{act}	activation overpotential	V
η_{con}	concentration overpotential	V
η_{ohm}	ohmic overpotential	V
ϑ	stoichiometric factor	mol
λ	pipe coefficient	-
μ	dynamic viscosity	Pa s
ρ	density	$\mathrm{kg\,m^{-3}}$
σ	conductivity	$\mathrm{S\,m^{-1}}$
ϕ	electric potential	V

1 Introduction

Electricity generation from renewable energy sources has risen considerably in the last two decades. The worldwide generation of eletricity by wind grew from roughly 31000 GWh in 2000 to 1127000 GWh in 2017, while solar photovoltaic generation grew from 994 to 444000 GWh in the same time period [1]. International agreements like the Paris Agreement emphasize the focus on renewable energy sources in order to reduce CO2 emissions. Thus, it can be expected that these numbers will continue to grow. However, power generation from wind or solar sources is dependent on weather conditions and therefore volatile.

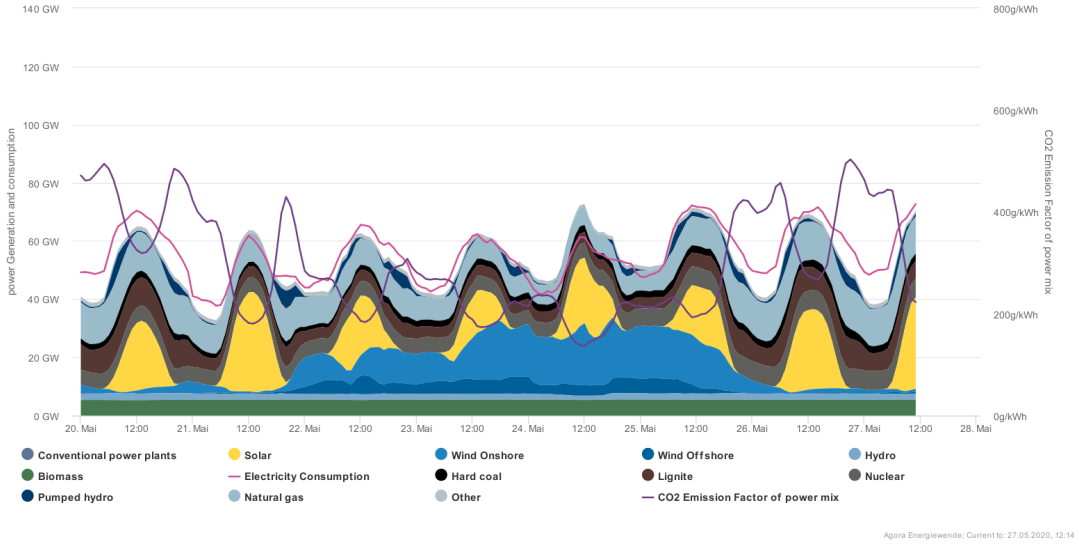

Figure 1.1: Power generation and consumption in Germany over the course of one week [2]

Figure 1.1 shows the power generation and consumption in Germany over the course of one week [2]. The volatile nature of solar (in yellow) and wind (blue) power generation is clearly visible. A customized energy storage is crucial to use these renewable energy sources to their full extent. Among them are pumped hydro, compressed air energy storage or batteries. While the former two are dependent on geographical features, batteries can be set up nearly everywhere. Many variations of the battery can be considered to be technologically mature. However, concerns regarding reliability, cycle life, energy density, cost or safety remain and hinder a wider application of batteries in stationary storage applications. *Redox Flow Batteries* (RFB) have the potential to overcome these

challenges.

1.1 State of the Art

1.1.1 Redox Flow Batteries

The Redox Flow Battery is a type of battery that combines high cycle life expectancy, safety, environmental compatibility, scalability and performance and is therefore a potential candidate to solve the aforementioned issues. A RFB is an electrochemical energy converter. Its basic setup is shown in figure 1.2. As can be seen in the figure (taken from the work of Arenas [3]), it consists mainly of two electrolyte cycles and a conversion unit. The conversion unit consists of two half cells, negative and positive, which are connected to each other via electric wiring and separated from each other by an ion permeable separator, often in the form of a membrane. Each half cell features an electrode. The two electrolyte cycles both consist of a tank and a pump, which are connected to each other and to the respective half cell via piping. Redox couples are dissolved in the electrolyte. The electrolytes can be charged by applying electricity to drive the non-spontaneous redox reactions of the dissolved species, which take place at the electrode-electrolyte surface. Discharge is also possible: in this case the reactions take place spontaneously in the reverse direction, which releases electricity.

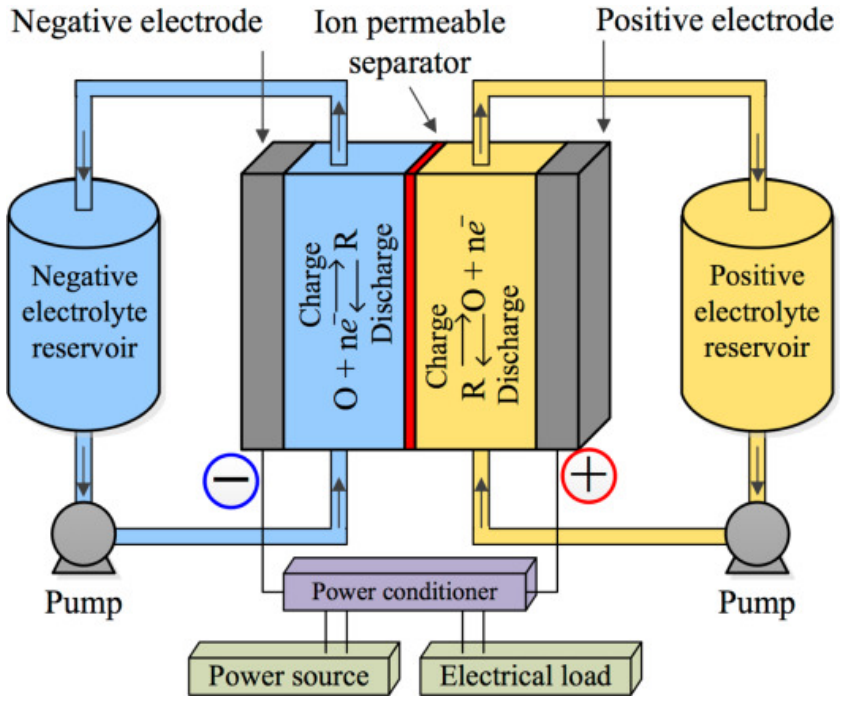

Figure 1.2: A classical RFB system, showing a divided cell, electrolyte recirculation to holding tanks and electrical controls as found in the work of Arenas [3]

The big advantage of the RFB is, that the power of the system is not equal to its energy capacity, as the latter is stored in the electrolyte and depends on the electrolyte volume and the concentration of the active species. This makes scaling possible. In combination with their decreasing cost with larger scale, their relatively low energy density, the fact that they produce no pollution emissions and their capability to operate at ambient temperature and pressure, RFBs are well-suited for medium- and large-scale energy storage [3].

Single RFB cells are usually connected electrically to form modules, which are in turn connected to stacks. The stacks use a common electrolyte reservoir and are electrically connected to the power grid.

1.1.2 All Vanadium Redox Flow Batteries

There are many different redox couples, which were tested in RFBs: Fe-Ti, Fe-Cr or Zn-Br are just exemplary pairings. However, none of the pairings appears as promising as the *All-Vanadium Redox Flow Battery* (VRFB), proposed by Maria Skyllas-Kazacos in 1984. True to its name, it utilizes four different oxidation states of vanadium, which circumvents the negative effects of cross-mixing of the electrolytes. [4].

Figure 1.3 shows a schematic illustration of the VRFB. It follows the classic setup of RFBs: two electrolyte cycles with a conversion unit, separated by an ion exchange membrane. The negative electrolyte consists of V^{2+}/V^{3+} vanadium ions, while the positive consists of VO^{2+}/VO_2^+ vanadium ions, which are also often referred to by V^{4+}/V^{5+}. Both of them are dissolved in aqueous solutions with added sulfuric acid in order to increase ionic conductivity. A porous graphite electrode in conjunction with a current collector (CC) is used in each half cell. The electrolyte flows through the electrode. Choosing a porous structure increases the electrode surface, which in turn increases the reaction surface for charging or discharging, as the reactions take place at the electrolyte-electrode interface. Electrons are transported from one half cell to the other by connecting the electrodes to a current collector and connecting the current collectors to each other.

As the cell is charged, V^{3+} is reduced to V^{2+} at the negative electrode for a standard potential of $E_{neg}^{00} = -0.26V$ (against the standard hydrogen electrode SHE), while VO^{2+} oxidizes to VO_2^+ at the positive electrode for a standard potential of $E_{pos}^{00} = 1.00V$ vs SHE. To maintain the conservation of charge, H^+-ions are transferred through the ion exchange membrane. When discharging, the reactions are proceeding in reversed direction.

$$\mathrm{V^{3+} + e^- \underset{\text{discharge}}{\overset{\text{charge}}{\rightleftharpoons}} V^{2+}} \tag{1.1}$$

$$\mathrm{VO^{2+} + H_2O \underset{\text{discharge}}{\overset{\text{charge}}{\rightleftharpoons}} VO_2^+ + e^- + 2\,H^+} \tag{1.2}$$

Both partial reactions contribute to a total potential of the cell of $E_{cell}^{00} = 1.26V$.

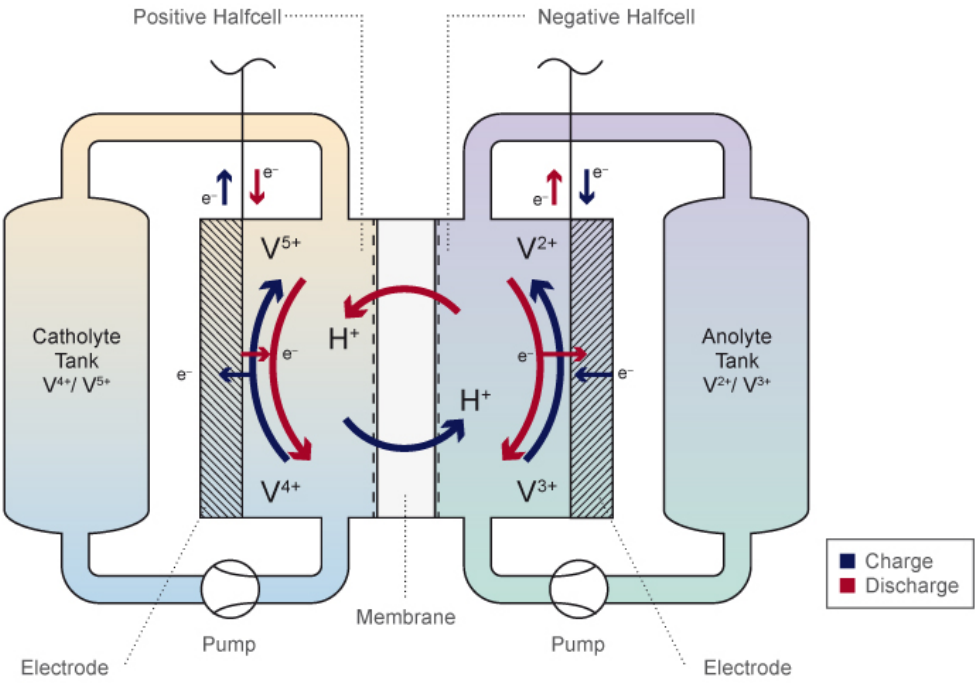

Figure 1.3: A schematic illustration of the All Vanadium Redox Flow Battery, taken from the work of Ressel [5]

1.1.3 StaTuR

The dominating cell geometry for VRFBs is the planar cell, shown in figure 1.4 A. Two electrodes are separated by a membrane. Flow frames transport the electrolyte to the electrodes. All the components are fabricated in a sheet-like geometry. Planar cells can be stacked in a bipolar manner, which allows the easy fabrication of modules. However, only serial connection is possible with the bipolar approach. Additionally, manufacturing costs remain high for this geometry.

The goal of the project *StaTuR* is to develop a stack of tubular VRFBs [6]. Figure 1.4 B shows the geometry. The components from the inside to the outside are: inner current collector, inner electrode, membrane, outer electrode and outer current collector. The tubular geometry might allow to produce the components via extrusion, possibly reducing manufacturing costs. As the cell only has to be sealed at the ends, the sealing length is also reduced significantly. Additionally, abandoning the bipolar approach allows for the electrical parallel connection in addition to the serial connection. By using the parallel connections, parasitic shunt currents, which are a major loss source for big serial stacks [7] could be prevented. Extensive studies on the tubular design were carried out by Simon Ressel [5].

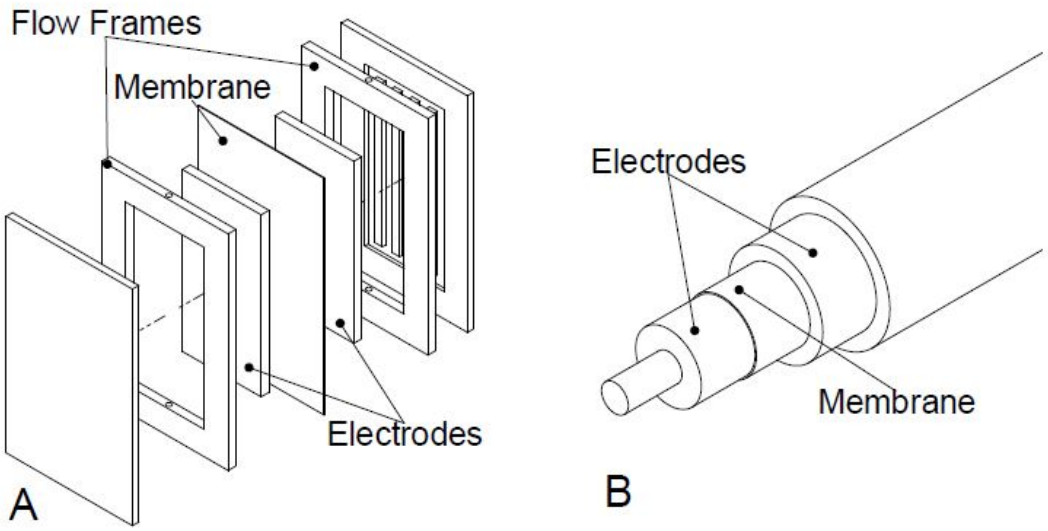

Figure 1.4: Comparison of the planar geometry (A) to the tubular geometry (B) [8]

1.2 Aim of the Thesis

The aim of this study is to develop a design tool for an All Vanadium Redox Flow Battery Stack, which allows to compare different module designs quantitatively. Therefore, two models are developed: a Micro Model in COMSOL Multiphysics and a Macro Model in

Matlab Simulink.

The Micro Model will be capable of simulating a Redox Flow Battery Cell on a microscopic scale, based on existing literature models (see the works of Knehr [9], Gandomi [10] or Nix [11]). To simplify the model, the geometry of the cell will be two-dimensional planar, derived from the tubular geometry of the cells described beforehand.

The Macro Model will be capable of simulating a variable amount of All Vanadium Redox Flow Battery cells. While several stack models already exist (see the works of Moro [12], Koenig [13], Wandschneider [14], Xing [15] or others), none of them combines the following characteristics. All major overvoltages (activation, concentration and ohmic) in the cells will be considered. The cells can be connected electrically in serial, in parallel or in a combination of both to form modules. Hydraulically, the cells will be connected in parallel by pipes containing the electrolyte. To emphasize the design aspect of the model, the performance of a cell will be defined by either design parameters, actual measurements or by results of the Micro Model (thus requiring an interface between the two models). Furthermore it will be possible to assign different performances to each cell, representing variation in manufacturing quality. The model will provide outputs, which are suitable for the comparison of different module designs.

1.3 Thesis Outline

The second chapter of the thesis will clarify the fundamentals needed to understand a VRFB and develop a model of it. In a first section, the electrochemical principles are stated, followed by hydraulic principles. The third section contains information on the modeling of VRFB modules or stacks. It features brief overviews of selected models from literature.

In the third chapter, a brief overview of the two developed models is provided. The division into the two models is clarified and crucial design aspects of the models are mentioned.

The fourth chapter will discuss the developed Micro Model in detail. After clarifying the assumptions, each one of the three domains of the model is described through the applied equations. The remaining boundary conditions needed to fully describe the model are explained in the last section of the chapter alongside the in- and outputs.

Chapter five contains the modeling of the Macro Model. The first section provides an overview of the Macro Model and the data flows that take place in it. After that, each part of the model is discussed in detail, regarding the questions of why the part is needed and how it was implemented in the model. The resulting outputs complete the chapter.

Results of both models are shown in chapter six. In order to prove its validity, selected parts of the Macro Model are compared to analytic calculations or, if possible, to results from literature models or measurements, that were conducted within the working group. The results are discussed.

The last chapter of this work provides a conclusion and suggests possible extensions to the model.

2 Fundamentals

In order to develop a model of a *All-Vanadium Redox Flow Battery*, it is necessary to state the fundamental processes. The processes leading to the energy conversion in a RFB are described by the principles of electrochemistry. Electrolyte has to be transported to the cell, therefore hydraulic principles have to be discussed as well. The last section of the chapter will provide an overview over the methods and principles to combine multiple cells into stacks.

2.1 Electrochemistry

2.1.1 Chemical Reactions

A chemical reaction which involves the shifting of electrons is either called an *Oxidation* or a *Reduction*. In the case of an Oxidation, electrons are released while in the case of a Reduction electrons are received, see formula 2.1. z describes the number of involved electrons.

$$\mathrm{Ox} + z \cdot \mathrm{e}^- \underset{\text{oxidation}}{\overset{\text{reduction}}{\rightleftharpoons}} \mathrm{Red} \tag{2.1}$$

In order to move one or more electrons from one reaction partner to another, Oxidation and Reduction are coupled in a so called *Redox* system. Electrochemical cells use Redox systems to convert chemical energy into electrical energy or vice versa. A cell consists of two half cells. Each half cell contains an electrode immersed in electrolyte. Electrons can move from one electrode to the other through electrical wiring. Ions are transported through the electrolytes. The electrolytes are often separated by a semi-permeable membrane, which allows only certain species to cross through it. The chemical reactions take place at the electrolyte-electrode boundaries. The electrode which is releasing electrons is called the anode while the electrode which is receiving electrons is called cathode.

In the case of an all vanadium redox flow battery, V^{2+}/V^{3+} and VO^{2+}/VO_2^+ redox couples are used as electrolyte in the negative and positive half cell, respectively. The active substances are dissolved in aqueous solutions. In order to further enhance the ionic conductivity sulfuric acid is used as a supporting electrolyte. This results in the following two reactions, for the negative half cell and for the positive half cell.

$$\mathrm{V}^{3+} + \mathrm{e}^- \underset{\text{discharge}}{\overset{\text{charge}}{\rightleftharpoons}} \mathrm{V}^{2+} \tag{2.2}$$

$$\mathrm{VO}^{2+} + \mathrm{H_2O} \underset{\text{discharge}}{\overset{\text{charge}}{\rightleftharpoons}} \mathrm{VO_2^+} + \mathrm{e}^- + 2\,\mathrm{H}^+ \tag{2.3}$$

The ratio in which the different species are consumed or produced is described by stoichiometric factors ϑ_i. The stoichiometric factors of each vanadium species in the reactions taking place in the VRFB for example are 1, see 2.2 and 2.3.

$$\vartheta_{\mathrm{A}}\,\mathrm{A} + \vartheta_{\mathrm{B}}\,\mathrm{B} \longrightarrow \vartheta_{\mathrm{C}}\,\mathrm{C} + \vartheta_{\mathrm{D}}\,\mathrm{D} \tag{2.4}$$

2.1.2 Faraday's Law

The amount of electric charge Q needed to separate the molar amount n of a z-valant ion is described by Faraday's law, see equation 2.6. It uses the Faraday constant F, which is a proportional constant. The Faraday constant is defined as the amount of charge according to 1 mol of electrons (see equation 2.5). Therefore it is the product of the elementary charge e_0 and the Avogadro constant N_A.

$$\frac{Q}{1mol} = e_0 \cdot N_A = F = 96485\frac{As}{mol} \tag{2.5}$$

$$Q = n \cdot z \cdot F \tag{2.6}$$

2.1.3 Thermodynamics

Using the first and second law of thermodynamics, one can derive that the maximum non volume work of a thermodynamic system at constant pressure and temperature is equal to the electrical work of an electrochemical cell.

$$W_{el} = \Delta G \tag{2.7}$$

The *Gibb's Free Enthalpy* ΔG can be calculated from the reaction enthalpy ΔH and entropy ΔS, which in turn can be calculated from the stoichiometric factors of the respective chemical reaction (see equation 2.4).

$$\Delta G = \Delta H - T\Delta S \tag{2.8}$$

$$W_{el} = -z \cdot F \cdot E^{00} \tag{2.9}$$

$$E^{00} = -\frac{\Delta G^0}{zF} \tag{2.10}$$

By utilizing Faraday's law (equation 2.9), the standard potential E^{00} of a redox, metal/ metal ion or gas electrode is defined in equation 2.10. ΔG^0 is the Gibb's Free Enthalpy at a set of defined standard conditions: $T_0 = 298.15K$, $p_0 = 101300Pa$ and $c_0 = 1000\frac{mol}{m^3}$. As potentials can not be measured directly, the potentials are listed against a defined electrode, usually the *Standard Hydrogen Electrode* or SHE. It's potential is defined as $0V$.

2.1.4 Cell Potential

The Cell Potential E_{cell} of an electrochemical cell is obtained by the potential difference of its electrodes. Therefore, the standard cell potential E^{00}_{cell} can be obtained by:

$$E^{00}_{cell} = E^{00}_{pos} - E^{00}_{neg} \tag{2.11}$$

However, this potential is only valid for the aforementioned standard conditions. If the temperature, pressure or concentration parameters defer from the standard conditions, a correction is necessary. This correction term is called the *Nernst Potential* and is utilized in the *Nernst Equation*.

$$E^{0}_{neg,pos} = E^{00}_{neg,pos} + \frac{RT}{zF} ln \frac{a^{\vartheta_{Ox}}_{Ox}}{a^{\vartheta_{Red}}_{Red}} \tag{2.12}$$

As can be seen in equation 2.12, the potential of a electrode at non-standard conditions $E^{0}_{neg,pos}$ is equal to the standard electrode potential E^{00} modified by a correction term, with a_i being the activity of the species i, participating in the respective chemical reaction.

The activities are not measurable. For a diluted solution though, it is possible to set the activity coefficient f_i of species i to be 1 [16].

$$a_i = f_i \cdot c_i \tag{2.13}$$

The approach used in this work however, is to assume constant activity coefficients. If their impact on the electrode potential is incorporated into the standard electrode potential, one can derive the formal standard electrode potential $E^{00'}_{neg,pos}$ [17]. The Nernst Potential in the Nernst Equation is now only dependent on the concentrations.

$$E^{0}_{neg,pos} = E^{00'}_{neg,pos} + \frac{RT}{zF} ln \frac{c^{\vartheta_{Ox}}_{Ox}}{c^{\vartheta_{Red}}_{Red}} \tag{2.14}$$

For the VRFB the Nernst Equation of the whole cell, which is often denoted as the *Open Circuit Voltage* or OCV, becomes this (see the reactions stated in equations 2.2 and 2.3).

$$OCV = E^{00'}_{cell} + \frac{RT}{zF} ln \left(\frac{c_{VO^+_2} \cdot c_{V^{2+}} \cdot \left(c^+_{H^+}\right)^2}{c_{VO^{2+}} \cdot c_{V^{3+}}} \right) \tag{2.15}$$

An additional potential arises from the difference of the proton concentrations on each side of the membrane which separates the two half cells. By incorporating this potential, the *Donnan Potential*, into the Nernst Equation, we derive the complete Nernst Equation for the Vanadium Redox Flow Battery [18].

$$OCV = E^{00'}_{cell} + \frac{RT}{zF} ln \left(\frac{c_{VO^+_2} \cdot c_{V^{2+}} \cdot \left(c^+_{H^+}\right)^2 \cdot c^+_{H^+}}{c_{VO^{2+}} \cdot c_{V^{3+}} \cdot c^-_{H^+}} \right) \tag{2.16}$$

2.1.5 State of Charge and Concentrations

The state of charge (SOC) of an All-Vanadium Redox Flow Battery is a value that indicates the remaining amount of energy in the electrolytes. If the electrolyte is fully charged, its SOC will be at 100 percent, while it will be at 0 percent, if fully discharged. The state of charge can be calculated by simply relating the charged vanadium species (V^{2+} and VO_2^+) to all vanadium species in the respective electrolyte.

$$SOC_{neg} = \frac{c_{V^{2+}}}{c_{V^{2+}} + c_{V^{3+}}} \tag{2.17}$$

$$SOC_{pos} = \frac{c_{VO_2^+}}{c_{VO^{2+}} + c_{VO_2^+}} \tag{2.18}$$

The second interesting concentration is the H^+-concentration. It depends heavily on the method of the electrolyte formation and the concentration in both half cells will differ. The following equations are derived from the formation process of $V3.5$. c_{acid} describes the total concentration of sulfuric acid and $c_{V_{tot,neg/pos}}$ the total concentration of vanadium in the negative or positive electrolyte. β is a factor that is based on the formation process [19].

$$c^-_{H^+}(SOC_{neg}) = \left(c_{acid} - \frac{1}{4}c_{V_{tot,neg}}\right) \cdot (1+\beta) + SOC_{neg} \cdot c_{V_{tot,neg}} \cdot \frac{1}{2} \cdot (1+\beta) \tag{2.19}$$

$$c^+_{H^+}(SOC_{pos}) = \left(c_{acid} + \frac{1}{4}c_{V_{tot,pos}}\right) \cdot (1+\beta) + SOC_{pos} \cdot c_{V_{tot,pos}} \cdot \frac{1}{2} \cdot (1+\beta) \tag{2.20}$$

2.1.6 Transport Processes

The movement of a charged ion and therefore the mass transport in a electrochemical cell is influenced by three main factors. While a chemical reaction takes place, a concentration gradient will form within the cell, leading to Diffusion. With the development of electrical fields, the second effect resulting in a mass transport occurs: Migration. Finally, the electrolyte, which is pumped through the cell will lead to Convection. Combining these three factors results in the Nernst-Planck equation, describing the molar flux $\vec{N_i}$ of the ionic species i in a dilute solution:

$$\vec{N_i} = -D_i^{eff}\nabla c_i - z_i u_i c_i F \nabla \phi_l + \vec{v_j} c_i \tag{2.21}$$

D_i^{eff} is the effective diffusion coefficient in porous media of species i, c_i denotes the concentration of species i, z_i is the charge number of species i, u_i is the ion mobility of the species i, ϕ_l denotes the electric potential in the electrolyte and $\vec{v}$ is the velocity of the electrolyte j.

2.1.7 Reaction Kinetics

Reactions in a RFB cell take place at the electrolyte-electrode interface, at which a electrolyte double-layer will form. Under the assumption that the transport from the bulk electrolyte to the double-layer and vice versa happens fast, the speed of the reactions only depends on the reaction kinetics. The reaction rate r is defined as the product of the chemical reaction rate k (unit: $\frac{1}{s}$) and the concentration of the educt c_E:

$$r = k \cdot c_E^{\vartheta} \tag{2.22}$$

By applying Faraday's law (see equation 2.6), the current density per electrode area $j_{ox/red}$ for an oxidation or a reduction becomes obvious:

$$j_{ox} = z \cdot F \cdot k_{ox} \cdot c_{red}^{\vartheta} \tag{2.23}$$

$$j_{red} = -z \cdot F \cdot k_{red} \cdot c_{ox}^{\vartheta} \tag{2.24}$$

Both of these reactions happen at the same time. By adding them both up, we obtain the total exchange current density j. Note that, in case of a VRFB, the stoichiometric factors are all 1 (monovalent reactions).

$$j = j_{ox} + j_{red} = z \cdot F \cdot k_{ox} \cdot c_{red} - z \cdot F \cdot k_{red} \cdot c_{ox} \tag{2.25}$$

As we have already established, no net current flow exists at standard potential. Therefore, the total current density j_0 at standard potential is:

$$j_0 = j_{ox} + j_{red} = 0 \tag{2.26}$$

Current densities vary with electrode potential. Consequently, the reaction rate constants k have to depend on the potential. Under this assumption, we can modify equations 2.23 and 2.24. The charge transfer coefficient α is introduced. It describes the change of the activation energy with the free enthalpy of reaction and has to have a value between 0 and 1 for monovalent reactions. The symmetry factor of the reduction can thus be defined to be $1 - \alpha$.

$$j_{ox} = z \cdot F \cdot k_{ox}^0 \cdot c_{red} \cdot e^{\frac{\alpha \cdot z \cdot F}{R \cdot T} E} \tag{2.27}$$

$$j_{red} = -z \cdot F \cdot k_{red}^0 \cdot c_{ox} \cdot e^{\frac{(1-\alpha) \cdot z \cdot F}{R \cdot T} E} \tag{2.28}$$

By defining the activation overpotential $\eta_{act}(j) = E(j) - E^{00}$, the current density can be modified to:

$$j_{ox} = z \cdot F \cdot k_{ox}^0 \cdot c_{red} \cdot \left(e^{\frac{\alpha \cdot z \cdot F}{R \cdot T} E^{00}} + e^{\frac{\alpha \cdot z \cdot F}{R \cdot T} \eta_{act}(j)} \right) \tag{2.29}$$

$$j_{red} = -z \cdot F \cdot k_{red}^0 \cdot c_{ox} \cdot \left(e^{-\frac{(1-\alpha) \cdot z \cdot F}{R \cdot T} E^{00}} - e^{-\frac{(1-\alpha) \cdot z \cdot F}{R \cdot T} \eta_{act}(j)} \right) \tag{2.30}$$

By utilizing equation 2.26, the exchange current density is obtained:

$$j_0 = z \cdot F \cdot k_{ox}^0 \cdot c_{red} \cdot e^{\frac{\alpha \cdot z \cdot F}{R \cdot T} E^{00}} = -z \cdot F \cdot k_{red}^0 \cdot c_{ox} \cdot e^{-\frac{(1-\alpha) \cdot z \cdot F}{R \cdot T} E^{00}} \tag{2.31}$$

This results in the *Butler-Volmer Equation*:

$$j = j_0 \cdot \left[e^{\left(\frac{\alpha z F}{RT} \cdot \eta_{act}(j) \right)} - e^{\left(-\frac{(1-\alpha) z F}{RT} \cdot \eta_{act}(j) \right)} \right] \tag{2.32}$$

2.1.8 Concentration Overpotential

The former formulation of the Butler-Volmer equation is valid if the mass transfer of the reactant from the bulk-electrolyte to the double-layer is reasonably fast. However, from the definition of mass transfer (see equation 2.21), we can see that the transfer is dependent on the effects of Migration, Diffusion and Convection, and is therefore limited. A layer with a concentration gradient forms in front of the double layer and a concentration overpotential η_{conc} has to be added to the activation overpotential:

$$\eta = \eta_{act} + \eta_{conc} \tag{2.33}$$

Now the concentration dependent Butler-Volmer equation can be obtained, with $c^s_{red/ox}$ describing the concentration of the reactant or product at the electrode surface while $c_{red/ox}$ is the concentration in the bulk electrolyte, respectively [16].

$$j = j_0 \cdot \left[\frac{c^s_{red}}{c_{red}} \cdot e^{\left(\frac{\alpha z F}{RT} \cdot \eta\right)} - \frac{c^s_{ox}}{c_{ox}} \cdot e^{\left(-\frac{(1-\alpha) z F}{RT} \cdot \eta\right)} \right] \tag{2.34}$$

2.2 Hydraulics

Hydraulics-wise, the interesting relation for this work is the relation of pressure drop Δp and volume flow rate $\dot{V}$. In every flow carrying network the total pressure will differ between two points. The difference in pressure is called pressure drop. It is caused by the friction forces of the walls of the flow channel acting on the moving fluid. Pressure losses are dependent on the flow velocity, the viscosity of the fluid and on the geometry and roughness of the flow channel.

Darcy's law describes that the amount of fluid $\dot{V}$ flowing through the cross sectional area A is proportional to the hydraulic gradient i. It is valid for laminar flow through porous media.

$$\frac{\dot{V}}{A} = -k_f \cdot i \tag{2.35}$$

The Darcy-Weisbach equation describes the pressure loss $\Delta p = p_1 - p_2$, where λ is a pipe coefficient, l and d are the length and diameter of a pipe, ρ is the density of the fluid, $\dot{V}$ is the volume flow rate of the fluid and A is the area cross-section of the pipe.

$$p_1 - p_2 = \lambda \cdot \frac{l}{d} \cdot \frac{\rho}{2} \cdot \left(\frac{\dot{V}}{A} \right)^2 \tag{2.36}$$

The value of lambda depends on the Reynolds number and therefore on whether the fluid flow is laminar or turbulent. For laminar flow lambda can be assumed to be $\lambda = \frac{64}{Re}$ with the Reynolds number being $Re = \frac{\rho u d}{\mu}$ (flow speed v and the dynamic viscosity of the fluid μ).

Another notation for this relation is the Hagen-Poiseuille equation. It describes the pressure drop for laminar flow of an incompressible Newtonian fluid flowing through a

pipe with a circular cross section.

$$\Delta p = \frac{8 \cdot \mu \cdot l}{\pi \cdot r^4} \cdot \dot{V} = \frac{8 \cdot \mu \cdot l}{\pi \cdot \frac{d^4}{16}} \cdot \dot{V} = \frac{128 \cdot \mu \cdot l}{\pi \cdot d^4} \cdot \dot{V} \tag{2.37}$$

μ is the dynamic viscosity of the fluid, d and l describe the geometry of the flow channel and $\dot{V}$ is the volume flow rate of the fluid.

2.3 Stack Models

As the output of a single electrochemical cell is limited by the potential generated by its governing chemical reaction, it is necessary to electrically connect multiple cells in order to achieve outputs that are of use in industrial applications. Electrolyte is provided via piping from tanks. The piping establishes a hydraulic connection between the cells.

Already in the 1980s it was discovered, that the hydraulic connection via electrolyte leads to a parasitic side effect in a stack of flow batteries [20]. The electrolyte features a electric conductivity, providing a different path for the electric current. This effect is called *shunt currents*. The design of the piping impacts the amount of emerging shunt currents. A model which investigates the tradeoff between shunt currents, pumping power and cell performance was developed by Hagedorn [7].

The approach to quantify shunt currents in a model consisting of multiple cells connected electrically in serial stayed the same even in recent models (for example Xing [15] or Ye [21]): An equivalent circuit diagram is set up, which treats the ionic paths as resistances (see figure 2.1).

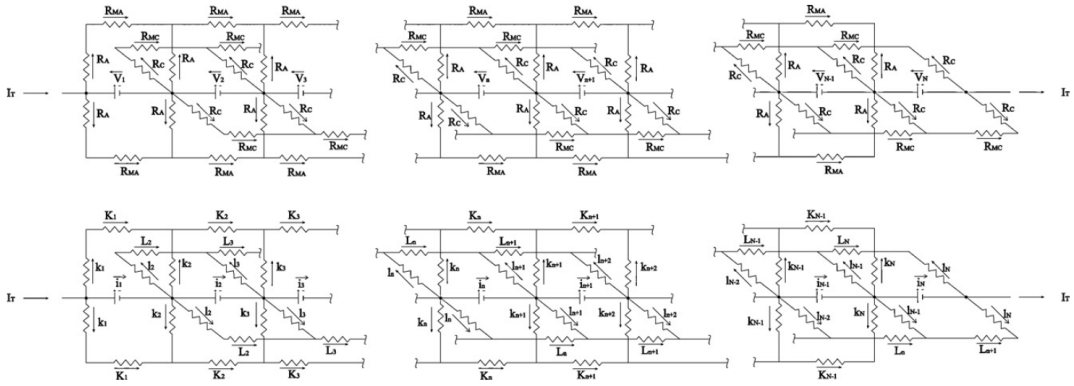

Figure 2.1: The equivalent circuit diagram used to calculate shunt currents in the work of Xing [15]

The ionic resistance R of a pipe is obtained by using the following equation, utilizing the conductivity if the electrolyte σ, and the length l and cross-sectional area A of the pipe, as described in for example Xing [15], Tang [22] or Koenig [13].

$$R = \frac{1}{\sigma} \frac{l}{A} \tag{2.38}$$

The Models of Tang and Koenig describe the conductivity of the electrolyte depending on its State of Charge, based on values from measurements found in own publications (in the case of Koenig) or in literature (see the work of Skyllas-Kazacos [23]).

Models that connect cells in parallel are rare, as the common geometry, the planar cell, doesn't allow for that connection. The work of Moro [12] features a parallel connection, but it consists only of two cells.

3 Modeling Approach

This short chapter will describe the modeling approach taken to provide a rough overview of the developed model.

3.1 Division into Micro and Macro model

It was decided to develop two models: a macroscopic one (*Macro Model*), which functions as a design tool for the simulation of multiple cells organized into modules, and a microscopic one (*Micro Model*), which allows a more accurate simulation of the electrochemical processes in a single cell. The focus of the work is set on the Macro Model. The Micro Model is mainly developed to prove that an interface can be used to use the results from the Micro Model within the Macro Model.

Both models share the design tool aspect. This means, that the cases which can be simulated with them, can be quickly changed by altering design parameters, like performance characteristics and setups. The aim is to provide a tool, which allows the quantitative comparison of different VRFB modules.

3.2 Modularity of the Macro Model

3.2.1 Interchangeability of the Calculations

The calculations used in the Macro Model need to function as black boxes. This means that inputs generate outputs dependent on boundaries or parameters. As long as the inputs and outputs remain the same, the block could be swapped out with a different block (with a possible alteration of the needed boundaries or parameters). This decision was made to be able to increase or reduce the accuracy of specific calculations.

As the author can't know which challenges might occur in the further development of the tubular VRFB stack, the model has to be also kept in a way, that allows quick extension. Choosing Simulink as the program makes adding additional components easy.

3.2.2 Data Basis

The performance of a cell is impacted by many factors like geometry, used materials, the way of manufacturing or aging. Many of these factors can be quantified by parameters. In order to be able to simulate a variety of different cells in the same setup, it was decided to store the characteristic of the cells in a Lookup Table (LUT). LUTs are basically multidimensional tables, that specify an output based on a combination of inputs. The generation of the LUTs is not part of the Simulink model, but is instead

conducted beforehand in Matlab, resulting in a reduced complexity of the Simulink model. Furthermore, as a LUT is a table with predefined values, measurements or results from the micro model can be used instead of the design parameters to generate it.

3.2.3 Electric and hydraulic Arrangement of the Cells or Modules

With the tubular design of the cells, electric connection of the cells can be realized in serial, parallel or a combination of both. Varying the position of good performing or bad performing cells in this setup only adds to the complexity. This results in a practically infinite number of ways to electrically connect the cells in a module.

The hydraulic setup was decided to be fixed. From a tank, the electrolyte flows through a manifold, which splits up into multiple parallel channels, one for each cell. This setup is mirrored for the other half of the electrolyte cycle and repeated for the other electrolyte type. However, the pressure drop characteristics of the half cells are stored in another LUT.

In order to simulate all the possible setups, addresses are used to access the correct values in vector-signals or in the LUTs.

3.3 Inputs, Outputs and Boundaries

The data is organized into four different types: inputs, outputs, boundaries or parameters and addresses. Inputs and outputs change with every time step of the simulation, while boundaries or parameters are set for the whole simulation. Addresses indicate which entries from vector quantities or LUTs should be taken. The two inputs are the electric current and the volume flow rate of the electrolyte applied to the top level: in case of a single cell, the top level is simply the cell, while in a module the top level would be module.

The main outputs of the model are the voltage and the pressure drop of the single cells and the module. Other values can be tracked to the nature of Simulink as well. In an optional step, additional outputs can be calculated after the Simulink Simulation in Matlab.

A multitude of parameters is needed to generate the outputs from the inputs. These will be collected in a single place, the parameter bus, for the sake of accessibility.

4 Micro Model

The Micro Model simulates the electrochemical behavior of one RFB cell on a microscopic level with the software COMSOL Multiphysics [24]. The model can be used as a stand-alone simulation or to generate inputs for the Macro Model. Because the Macro Model is the focus of this work, the Micro Model is kept simple. Instead of modeling a 3-dimensional tubular geometry, a planar 2-dimensional geometry is used, similar to the models presented by Knehr [9], Gandomi [10] or Nix [11].

Big parts of the developed model are based on the work of Knehr [9]. The Knehr-model features a 2-dimensional planar geometry which is capable of simulating the Vanadium crossover and water transport through the membrane. The model of Gandomi [10] however, features the calculation of surface and bulk electrolyte concentrations. Because the Micro Model is not the sole focus of this work, the Knehr-model is used without the crossover simulation and is modified by adding the surface and bulk electrolyte concentration calculation from the Gandomi-model and by adding the Donnan-Potential, elaborated by Knehr in [18]. The fluid dynamics are also simplified in order to reduce the modeling work. While in reality the cell would be in flow-by configuration, a flow-through cell is modeled. The volumetric flow rate within the porous electrode is approximated with a factor, based on studies of Ke [25]. A tutorial model published by COMSOL and based on the aforementioned Gandomi model was used as a baseline [26].

The intended use as a design tool led to the decision, that the model has to accept the two cell performance parameters ASR (area specific cell resistance) and i_0 (exchange current density per membrane area) as inputs. To further improve the design tool aspect, it has to be possible to simulate multiple operating points in one simulation run to achieve a polarization curve. This polarization curve is the connection to the Macro Model.

This chapter will present the implementations of the various electrochemical principals.

4.1 Overview

A 2-dimensional flow-through electrode model with planar geometry is developed. It is based on the following assumptions:

1. The cell is isothermal
2. The membrane can only be crossed by H^+-ions
3. Side reactions (e.g. gas evolution) are neglected
4. The dilute solution approximation can be used for the porous electrode

The model is divided into five domains, as shown in figure 4.1. From left to right they are: Negative current collector, negative electrode, membrane, positive electrode and positive current collector.

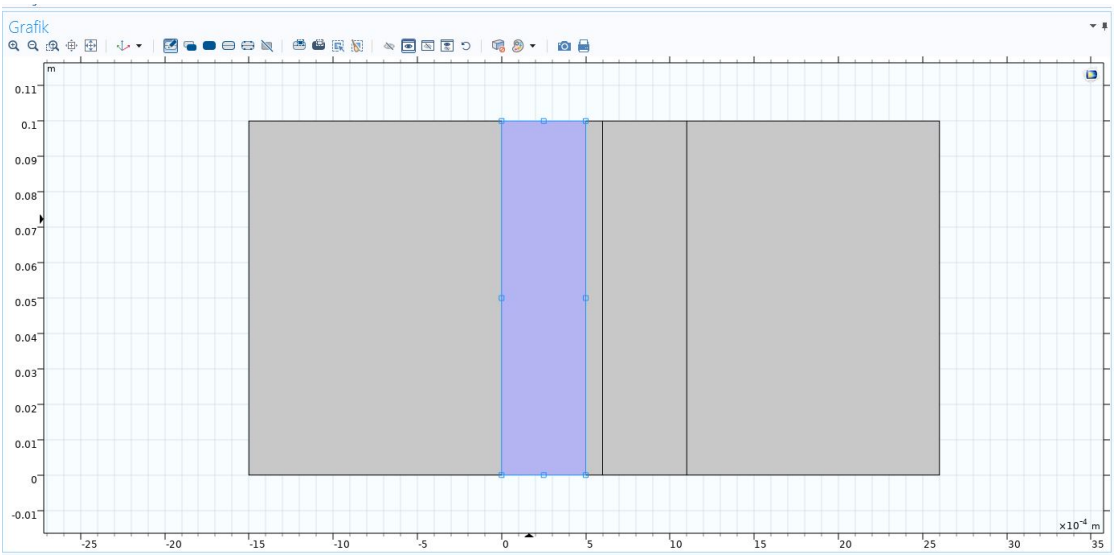

Figure 4.1: The five domains of the model. The negative electrode is highlighted

The software COMSOL Multiphysics utilizes the finite element method. Finite elements are organized in a mesh. By proper definition of a mesh, simulation time can be kept short and results can be specified more accurately. In this case, strongly varying results are anticipated near the electrode membrane boundary. As a result, the amount of elements is increased in the vicinity of the boundary. There is no need for more than one element for the current collectors however, because a linear behavior will be defined. The used mesh is shown in figure 4.2.

The model is solved for the solid state potential ϕ_s, the liquid state potential ϕ_l and the concentrations of the different species c_i.

4.2 Porous Electrode

The porous electrode domain consists of two different mediums: electrode and electrolyte. Electrolyte consisting of water, sulfuric acid and charged vanadium species flows through the porous electrodes. For each charged species, the conservation of mass has to be true:

$$\frac{\partial}{\partial t}\left(\varepsilon c_i\right) + \nabla \cdot \vec{N}_i = a\zeta_i \tag{4.1}$$

ε describes the porosity of the electrode, c_i denotes the bulk concentration of species i in the electrolyte, $\vec{N}_i$ is the flux of the charged species i, a the specific interfacial area and ζ_i the pore-wall flux density of species i. The flux of species is defined by the Nernst-Planck equation (see equation 2.21). In order to obtain the effective diffusion coefficient

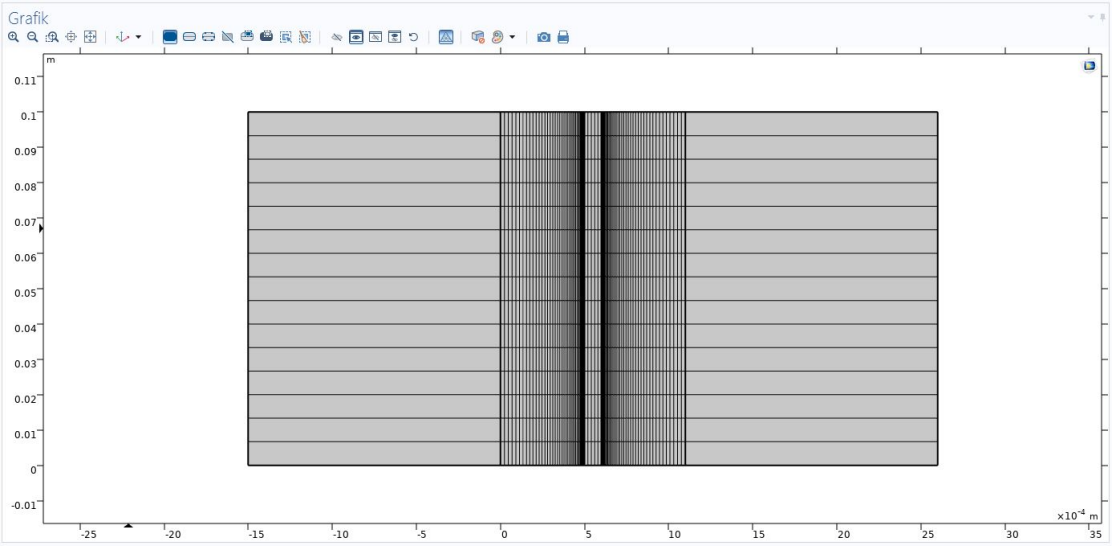

Figure 4.2: The mesh of finite elements used for the model

in a porous media, the Bruggemann-relation is utilized, with ϵ being the porosity of the electrode and D_i the diffusion coefficient of the species i, which can be obtained from literature [27].

$$D_i^{eff} = \varepsilon^{3/2} D_i \tag{4.2}$$

Assuming the dilute solution approximation, the ionic mobility can be represented by the Nernst-Einstein equation.

$$u_i = \frac{D_i^{eff}}{RT} \tag{4.3}$$

This leads to a modified version of the Nernst-Planck equation:

$$\vec{N_i} = -D_i^{eff} \nabla c_i - \frac{c_i z_i D_i^{eff} F}{RT} \nabla \phi_l + \vec{v}_j c_i \tag{4.4}$$

Through the conservation of charge it is possible to couple the species transport, the electrochemical reactions and the current in the electrode:

$$\nabla \cdot \vec{i_l} + \nabla \cdot \vec{i_s} = 0 \tag{4.5}$$

where $\vec{i_l}$ is the liquid and $\vec{i_s}$ is the solid current density. The liquid current density is defined by Faraday's law (see equation 4.6) while the solid current density is defined by Ohm's law (see equation 4.7; with σ_s^e being the bulk conductivity of the electrode).

$$\vec{i_l} = F \sum_i z_i \vec{N_i} \tag{4.6}$$

$$\vec{i_s} = \sigma_s^e \nabla \phi_s \tag{4.7}$$

By forming the divergence of the liquid current density, the following is obtained:

$$\nabla \cdot \vec{i_l} = F \sum_i z_i \nabla \cdot \vec{N_i} \tag{4.8}$$

The conservation of mass yields:

$$\nabla \cdot \vec{i_l} = F \sum_i z_i \left(a\zeta_i - \frac{\partial}{\partial t} (\varepsilon c_i) \right) = aF \sum_i z_i \zeta_i - \varepsilon F \frac{\partial}{\partial t} \sum_i z_i c_i \tag{4.9}$$

The solution is electroneutral, which can be described by equation 4.10.

$$\sum_i z_i c_i = 0 \tag{4.10}$$

Following this condition, the last term in 4.9 vanishes. j_n is defined as the transfer current per unit volume of the electrode.

$$j_n = \nabla \cdot \vec{i_l} = aF \sum_i z_i \zeta_i = a i_n \tag{4.11}$$

The Butler-Volmer equation expresses local current densities. In addition to the form of the equation presented in equation 2.32, surface concentrations c_i^s and bulk concentrations c_i are discerned. This leads to the two following expressions:

$$\begin{aligned} j_{n,neg} = aFk_{neg}(c_{V^{2+}})^{1-\alpha_{neg}}(c_{V^{3+}})^{\alpha_{neg}} \Bigg[& \left(\frac{c^s_{V^{2+}}}{c_{V^{2+}}} \right) e^{\left(\frac{-\alpha_{neg} F \eta_{neg}}{RT} \right)} \\ & - \left(\frac{c^s_{V^{3+}}}{c_{V^{3+}}} \right) e^{\left(\frac{(1-\alpha_{neg}) F \eta_{neg}}{RT} \right)} \Bigg] \end{aligned} \tag{4.12}$$

$$\begin{aligned} j_{n,pos} = aFk_{pos}(c_{VO^{2+}})^{1-\alpha_{pos}}(c_{VO_2^+})^{\alpha_{pos}} \Bigg[& \left(\frac{c^s_{VO_2^+}}{c_{VO_2^+}} \right) e^{\left(\frac{-\alpha_{pos} F \eta_{pos}}{RT} \right)} \\ & - \left(\frac{c^s_{VO^{2+}}}{c_{VO^{2+}}} \right) e^{\left(\frac{(1-\alpha_{pos}) F \eta_{pos}}{RT} \right)} \Bigg] \end{aligned} \tag{4.13}$$

α denotes the charge transfer coefficients, k is a reaction rate coefficient and η represents the overpotential of the respective electrode. While k_{pos} is obtained from literature, k_{neg} is calculated from the input $i_{0,neg}$:

$$k_{neg} = \frac{\frac{i_{0,neg}}{l_{el} A}}{\left(\frac{c_{V^{2+},0}}{c_{ref}} \right)^{(1-\alpha_{neg})} \cdot \left(\frac{c_{V^{3+},0}}{c_{ref}} \right)^{\alpha_{neg}} \cdot c_{ref} \cdot F} \tag{4.14}$$

The overpotential of an electrode is defined by:

$$\eta_{neg/pos} = \phi_l - \phi_s - E^0_{neg/pos} \tag{4.15}$$

$E^0_{pos/neg}$ is the formal potential of an electrode, defined by equation 2.14. Because the Donnan Potential will be incorporated into the membrane, the two potentials are defined as follows:

$$E^0_{neg} = E^{00'}_{neg} + \frac{RT}{F} ln \left(\frac{c_{V^{3+}}}{c_{V^{2+}}} \right) \tag{4.16}$$

$$E^0_{pos} = E^{00'}_{pos} + \frac{RT}{F} ln \left(\frac{c_{VO_2^+} \cdot (c_{H^+})^2}{c_{VO^{2+}}} \right) \tag{4.17}$$

As already mentioned the model discerns the bulk concentration and the surface concentration. The difference between these concentrations develops as a consequence of a minor convection contribution to the mass transport in close proximity of the electrode [28]. A common simplified approximation is to assume a layer of the thickness δ_0, the so called Nernst diffusion layer. In this layer, the only effective transport mechanism is the diffusion. Beyond this layer, convection contributes to the mass transport.

While the electrochemical reaction runs, the surface concentration c^s_i of species i will be lower than the bulk concentration c_i. By assuming a linear concentration gradient, the following is obtained:

$$N^s_i = \frac{D_{0,i}}{\delta_0}(c_i - c^s_i) \tag{4.18}$$

The diffusion coefficient within the Nernst diffusion layer $D_{0,i}$ as well as the thickness of the Nernst diffusion layer δ_0 are often unknown. Therefore, the local mass transfer coefficient k_m is introduced:

$$N^s_i = k_m(c_i - c^s_i) \tag{4.19}$$

This equation needs to be written for both electrodes and for all species undergoing faradaic reaction. The mass transfer flux is balanced by the flux of species production or consumption, expressed by the Butler-Volmer equation [29]. In the following the term $f = \frac{F}{RT}$ is used to increase the readability.

$$\begin{aligned} N^s_{V^{2+}} = k_m(c_{V^{2+}} - c^s_{V^{2+}}) = k_{neg} \cdot (c_{V^{3+}})^{\alpha_{neg}} \cdot (c_{V^{2+}})^{(1-\alpha_{neg})} \\ \cdot \left[\left(\frac{c^s_{V^{2+}}}{c_{V^{2+}}} \right) e^{((1-\alpha_{neg}) f \eta_{neg})} - \left(\frac{c^s_{V^{3+}}}{c_{V^{3+}}} \right) e^{(-\alpha_{neg} f \eta_{neg})} \right] \end{aligned} \tag{4.20}$$

$$\begin{aligned} N^s_{V^{3+}} = k_m(c_{V^{3+}} - c^s_{V^{3+}}) = k_{neg} \cdot (c_{V^{3+}})^{\alpha_{neg}} \cdot (c_{V^{2+}})^{(1-\alpha_{neg})} \\ \cdot \left[\left(\frac{c^s_{V^{3+}}}{c_{V^{3+}}} \right) e^{(-\alpha_{neg} f \eta_{neg})} - \left(\frac{c^s_{V^{2+}}}{c_{V^{2+}}} \right) e^{((1-\alpha_{neg}) f \eta_{neg})} \right] \end{aligned} \tag{4.21}$$

$$\begin{aligned} N^s_{VO^{2+}} = k_m(c_{VO^{2+}} - c^s_{VO^{2+}}) = k_{pos} \cdot (c_{VO_2^+})^{\alpha_{pos}} \cdot (c_{VO^{2+}})^{(1-\alpha_{pos})} \\ \cdot \left[\left(\frac{c^s_{VO^{2+}}}{c_{VO^{2+}}} \right) e^{((1-\alpha_{pos}) f \eta_{pos})} - \left(\frac{c^s_{VO_2^+}}{c_{VO_2^+}} \right) e^{(-\alpha_{pos} f \eta_{pos})} \right] \end{aligned} \tag{4.22}$$

$$N^s_{VO_2^+} = k_m(c_{VO_2^+} - c^s_{VO_2^+}) = k_{pos} \cdot (c_{VO_2^+})^{\alpha_{pos}} \cdot (c_{VO^{2+}})^{(1-\alpha_{pos})} \cdot \left[\left(\frac{c^s_{VO_2^+}}{c_{VO_2^+}} \right) e^{(-\alpha_{pos} f \eta_{pos})} - \left(\frac{c^s_{VO^{2+}}}{c_{VO^{2+}}} \right) e^{((1-\alpha_{pos}) f \eta_{pos})} \right] \tag{4.23}$$

These equations can be solved for the surface concentrations:

$$c^s_{V^{2+}} = \frac{\Psi_2 c_{V^{3+}} + (1+\Psi_2) c_{V^{2+}}}{1+\Psi_1+\Psi_2} \tag{4.24}$$

$$c^s_{V^{3+}} = \frac{\Psi_1 c_{V^{2+}} + (1+\Psi_1) c_{V^{3+}}}{1+\Psi_1+\Psi_2} \tag{4.25}$$

$$c^s_{VO^{2+}} = \frac{\Psi_4 c_{VO_2^+} + (1+\Psi_4) c_{VO^{2+}}}{1+\Psi_3+\Psi_4} \tag{4.26}$$

$$c^s_{VO_2^+} = \frac{\Psi_3 c_{VO^{2+}} + (1+\Psi_3) c_{VO_2^+}}{1+\Psi_3+\Psi_4} \tag{4.27}$$

The coefficients Ψ_i are calculated by the following equations.

$$\Psi_1 = \left(\frac{k_{neg}}{k_m} \right) \cdot \left(\frac{(c_{V^{2+}})^{(1-\alpha_{neg})}}{(c_{V^{3+}})^{\alpha_{neg}}} \right) \cdot e^{((1-\alpha_{neg}) f \eta_{neg})} \tag{4.28}$$

$$\Psi_2 = \left(\frac{k_{neg}}{k_m} \right) \cdot \left(\frac{(c_{V^{3+}})^{\alpha_{neg}}}{(c_{V^{2+}})^{(1-\alpha_{neg})}} \right) \cdot e^{(-\alpha_{neg} f \eta_{neg})} \tag{4.29}$$

$$\Psi_3 = \left(\frac{k_{pos}}{k_m} \right) \cdot \left(\frac{(c_{VO_2^+})^{\alpha_{pos}}}{(c_{VO^{2+}})^{(1-\alpha_{pos})}} \right) \cdot e^{((1-\alpha_{pos}) f \eta_{pos})} \tag{4.30}$$

$$\Psi_4 = \left(\frac{k_{pos}}{k_m} \right) \cdot \left(\frac{(c_{VO^{2+}})^{(1-\alpha_{pos})}}{(c_{VO_2^+})^{\alpha_{pos}}} \right) \cdot e^{(-\alpha_{pos} f \eta_{pos})} \tag{4.31}$$

The key parameter for these equations is k_m, which is a function of electrolyte velocity [30].

$$k_m = 1.6 \cdot 10^{-4} \cdot |v|^{0.4} \tag{4.32}$$

The last remaining undefined term is the reaction source term ζ_i. It represents the change in concentrations of species i due to the electrochemical reactions in the half cells. An overview is given in table 4.1.

4.3 Membrane

A reduced model of a membrane is used in this work, not allowing crossover of species other than H^+. Therefore, the liquid current density 4.6 reduces under the condition of electroneutrality 4.10 to:

$$\vec{i_l} = -\sigma_l \nabla \phi_l \tag{4.33}$$

Term	Negative Electrode	Positive Electrode
$\zeta_{V^{2+}}$	$\frac{j_n}{aF}$	-
$\zeta_{V^{3+}}$	$-\frac{j_n}{aF}$	-
$\zeta_{VO^{2+}}$	-	$-\frac{j_n}{aF}$
$\zeta_{VO_2^+}$	-	$\frac{j_n}{aF}$
ζ_{H^+}	-	$\frac{2j_n}{aF}$

Table 4.1: Reaction Source Terms

4.4 Current Collector

The current collectors are composed of impermeable solid graphite. Therefore, the current j_{CC} within the domain is governed by Ohm's law.

$$j_{CC} = -\sigma_{CC}\nabla\phi CC, s \tag{4.34}$$

σ_{CC} is the electric conductivity of the current collector. In order to incorporate the ASR (which includes contact resistances) into the model, the following formulation of the electric conductivity is defined in the model.

$$\sigma_{CC,neg/pos} = \frac{l_{CC,neg/pos}}{ASR_{neg/pos}} \tag{4.35}$$

4.5 Initial Values and Boundary Conditions

In order to solve the model for the species concentrations and the liquid state potential as well as the solid state potential, boundary conditions and initial values have to be determined. Figure 4.3 assigns a number to each boundary in the model. The respective conditions are listed in table 4.2. i_{avg} describes the desired average current density for the cell.

Finally the initial values for concentrations can be calculated by using a defined initial state of charge. Using equations 2.17 to 2.20 (which will be explained in the following chapter) it is possible to define a starting concentration for each species.

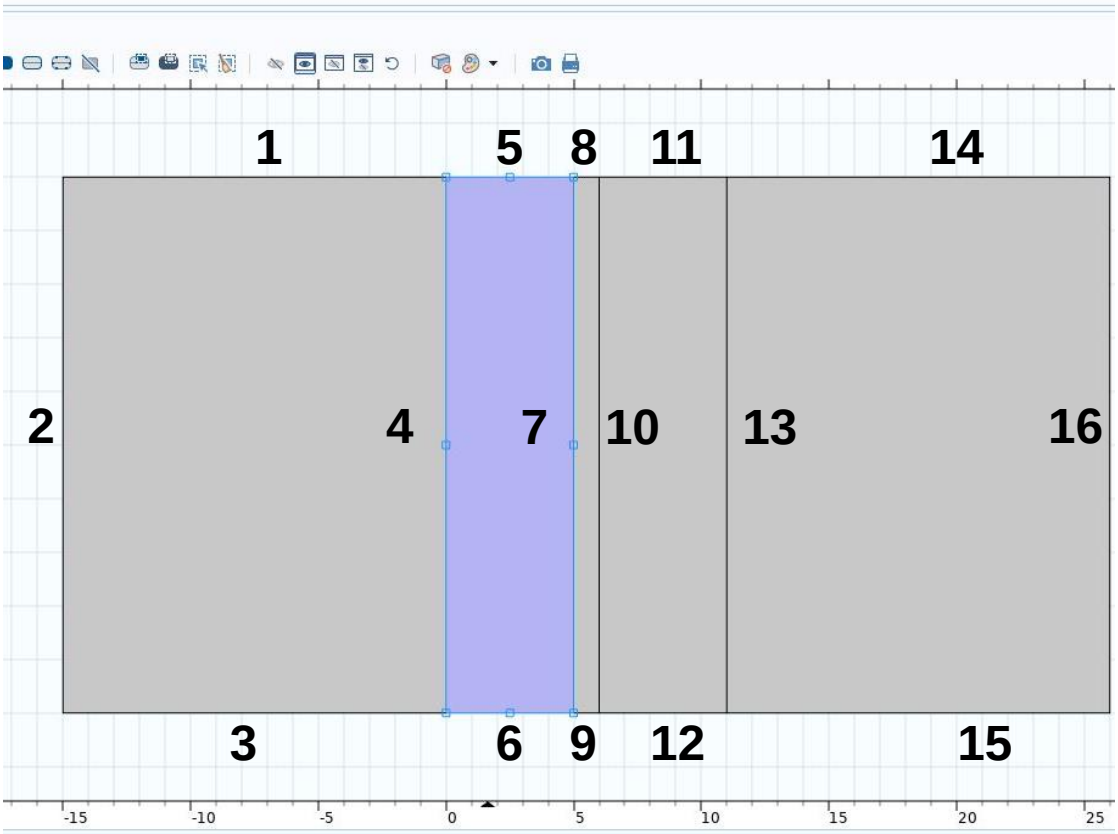

Figure 4.3: Boundaries in the Micro Model

Boundaries	Description	Expression
2	Electric ground	$\phi_{s,CC,neg} = 0$
16	Electric current	$-n \cdot i_{s,CC,pos} = i_{avg}$
4 13	Continuous Solid State Potential	$\phi_{s,el} = \phi_{s,CC}$
7	Continuous Liquid State Potential with Donnan Correction	$\phi_{l,el,neg} - \phi_{mem} = \frac{RT}{F} ln\left(\frac{c_{H,neg}}{c_{H,mem}}\right)$
10	Continuous Liquid State Potential with Donnan Correction	$\phi_{l,el,pos} - \phi_{mem} = \frac{RT}{F} ln\left(\frac{c_{H,pos}}{c_{H,mem}}\right)$
6 12	Inflow	$n \cdot (N_i + uc_i) = n \cdot (uc_{0,i})$
5 11	Outflow	$n \cdot D_i \nabla c_i = 0$
4 7-10 13	No Flux	$-n \cdot (N_i + uc_i) = 0$
1 3 5 6 8 9 11 12 14 15	Electric Insulation	$-n \cdot i_l = 0; -n \cdot i_s = 0$

Table 4.2: Boundary Conditions for the Micro Model

5 Macro Model

The Macro model serves as a design-tool for the simulation of multiple VRB cells combined into modules or stacks. It is implemented in Matlab Simulink R2019b [31]. Inputs are the volume flow rate of the electrolytes and the electrical current applied to the top level. Boundaries include the cell characteristics, the geometry of the electrolyte supply pipes and the setup of the hydraulic and electrical connections of the cells. Figure 5.1 shows the module level model with its components.

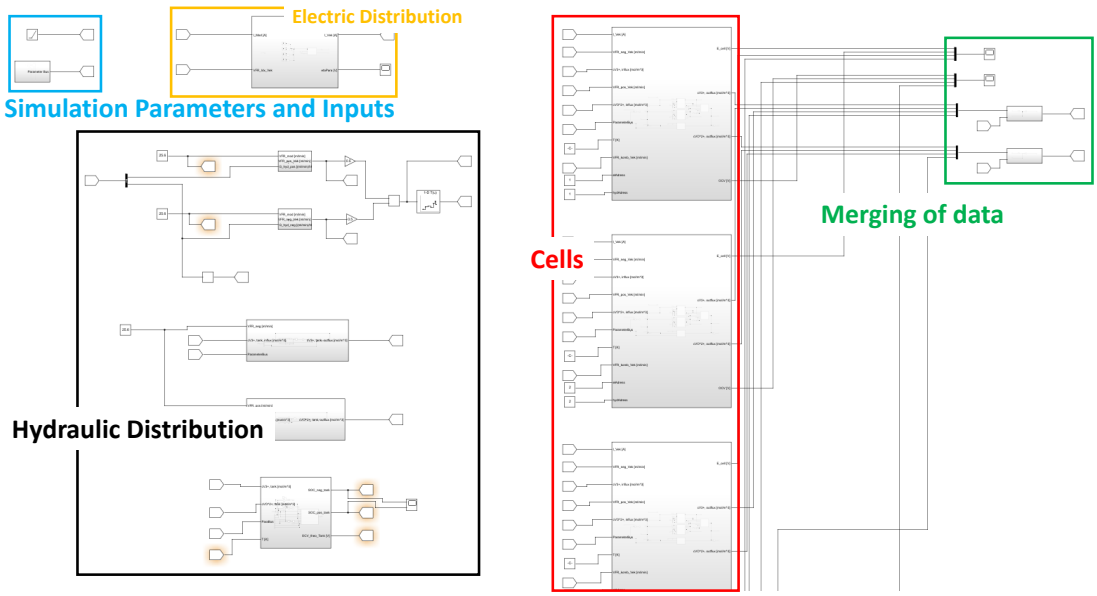

Figure 5.1: The Model on Module Level with its different components

5.1 Overview and Data Flow

Because the resulting model is rather complicated, a short overview is given in this section. Figure 5.2 shows the main elements that are used for the calculation of a single time step. The arrows in between the blocks represent the data flow happening between the elements. The arrows leaving to the right hand side represent the model outputs.

As already mentioned, the two inputs for the model are the current and the volume flow rate applied to the top level, in this case the module level. The model computes the main outputs of voltage and pressure drops. The concentration of the used electrolytes

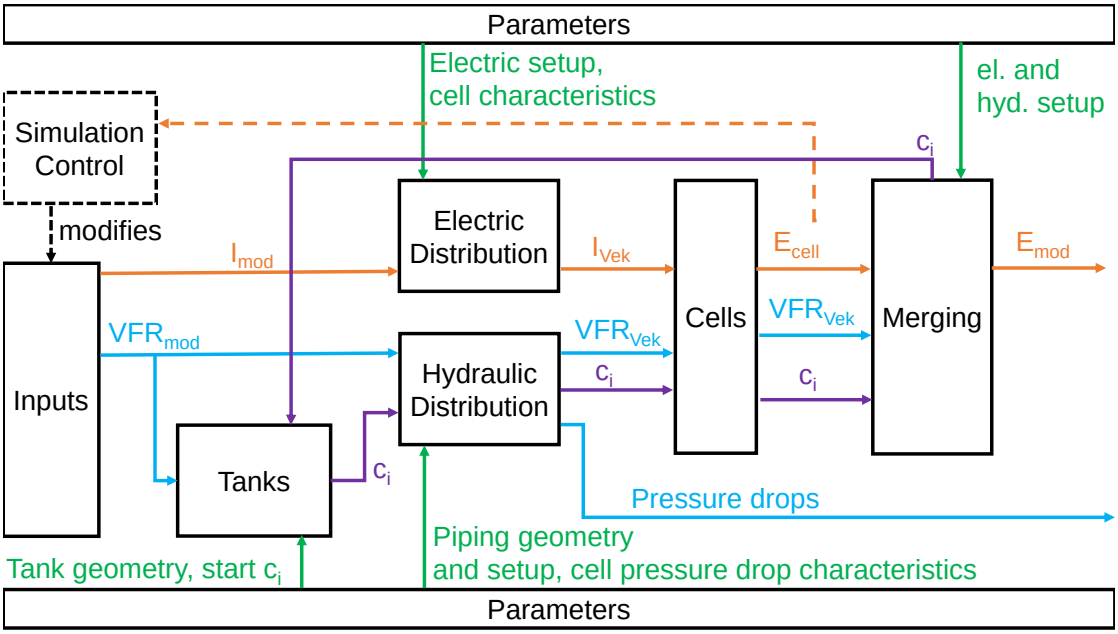

Figure 5.2: The main components of the macro model and the data that flows between them

is also very important: it impacts the resulting voltage and the applied current will alter it with time.

For a single time step, read figure 5.2 from left to right. In a first step, the concentrations in the electrolyte tanks are updated, using the volume flow rate of the electrolytes and the concentrations calculated in the previous time step. For a correct calculation, the tank geometry and the starting concentration (as an integral approach is used) have to be imported from the collected parameters.

The required variable setup of the cells makes a distribution of the inputs necessary. This step transforms the module level inputs into cell level inputs on a vector basis. The electric distribution changes the single value input of the module current into a vector containing the current for each cell, according to the electric setup and the electric characteristics of the cells. In a similar fashion. the hydraulic distribution changes the single value input of the module volume flow rate into a vector, according to the hydraulic setup and the hydraulic characteristic of the cells. In order to calculate the resulting pressure drops, the piping geometry is also provided to the block, and the first major output can be quantified.

The main calculation block of the model is the cell block. For each cell in the module, a cell block is used. Each cell block is provided with addresses, which indicate which values of the vectors generated in the distribution step have to be used for the cell. Another address is used to decide which cell characteristic is used for the cell. The cell block calculates the resulting voltage of each cell and updates the concentration of the electrolyte in the respective cell.

The last regular step of a time step in the simulation is to merge the produced data, according to the used electric and hydraulic setup. This step contains adding the voltages up in the way the electric setup dictates, in order to gain the second major output. The computing of a new concentration of the electrolyte, that is fed into the tank, is as well conducted in this step.

The last remaining block is the simulation control. Based on the outputs of the time step, the inputs for the next time step are modified if necessary. This block allows the simulation of complex measurements with relative ease.

5.2 Cell-Block

Input	I_{cell}, $\dot{V}_{cell,neg/pos,in}$, $c_{cell,i,in}$
Parameter	$c_{i,initial}$, β, $V_{cell,neg/pos}$, OCV-adjustments
Settings	Addresses
Output	E_{cell}, $c_{cell,i,out}$, OCV

Table 5.1: Cell Block Summary

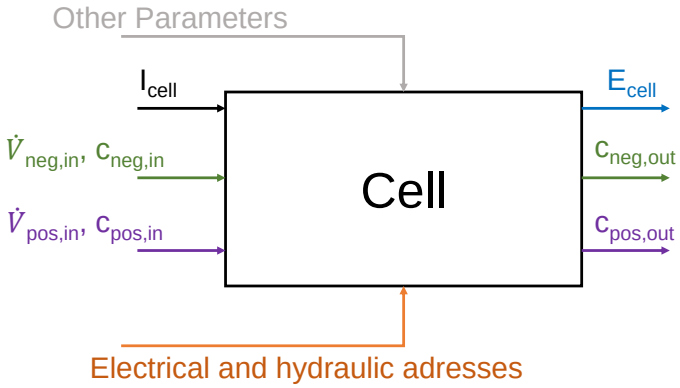

Figure 5.3: A Black Box Model of a Single Vanadium Redox Flow Cell as used in the model

The cell serves as the central calculation element of the model. A Black Box approach is shown in figure 5.3. As can be seen in the figure, the inputs consist of the electric current I_{cell} (which is in vector form if more than one cell is simulated) as well as the the volume flow rate $\dot{V}_{cell,neg/pos,in}$ and the concentrations $c_{neg/pos,in}$ of the respective electrolytes. The model calculates the changes in the electrolyte resulting in the output of the updated concentrations $c_{neg/pos,out}$ of the respective electrolytes. In addition the resulting cell voltage E_{cell} (which includes the OCV) is calculated.

Because the inputs alone are not sufficient to calculate the outputs, additional information in the form of addresses is needed. These addresses ensure two things: If multiple cells are simulated, the inputs I_{cell} and $\dot{V}_{neg/pos,in}$ will be handed over in vector form. The addresses indicate which value has to be taken from the vector for the specific cell. A third address indicates which characteristic has to be picked from the LUT, in which the current-voltage characteristics of the simulated cells are collected.

Some other constant parameters (see table 5.1) are needed as well, for example the volume of the half cells. However these are assumed to be the same for every cell used in the model, and therefore are concentrated in a parameter input.

Following these considerations, it is derived that 4 different calculations are needed in the cell block in Simulink: the concentration change in the electrolyte for both of the electrolytes, the calculation of the open circuit voltage and the calculation of the overpotentials. The overpotentials will be looked up from a table rather than be calculated to enable the import of electric cell characteristics from different sources. Figure 5.4 shows the implementation in Simulink.

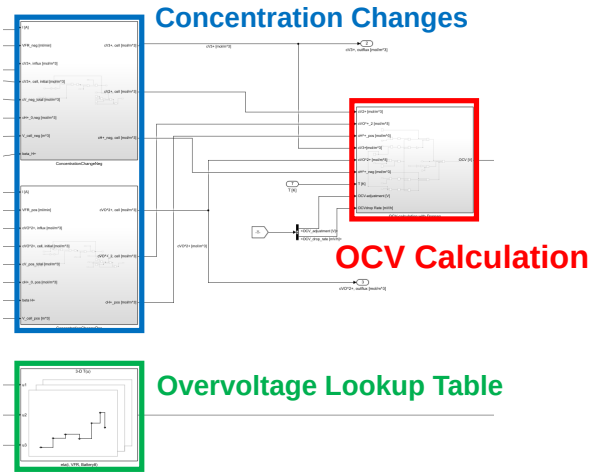

Figure 5.4: The Cell Block in Simulink

5.2.1 Concentration Change

In order to correctly calculate the potential of the cell, it is necessary that the concentrations of the different vanadium ions in the electrolytes are known. If no current is applied, the concentrations will stay the same if diffusion across the membrane and side reactions are neglected. However, if a current is applied, the concentrations of the vanadium ions will change.

Input	I_{cell}, $\dot{V}_{cell,neg/pos,in}$, $c_{cell,i,in}$
Parameter	$c_{i,initial}$, $V_{cell,neg/pos}$
Settings	none
Output	$c_{cell,i,out}$

Table 5.2: Concentration Change Summary

An integral approach to calculate the updated concentrations is presented by Li [32]. Because this method is also used in the extensive model developed by Koenig [13], it is implemented in this work as well. The new concentration of the V^{3+}-ions in the cell $c_{V^{3+},cell}(t_1)$ for the control volume V_{cell} is obtained by integrating all the gains and losses of concentration between time t_0 and time t_1 and adding it to the concentration at the time t_0. Note that the volume flow rate of the electrolyte $\dot{V}_{neg,cell}$ has to be the same for influx and outflux at each time step t, because the cell volume is assumed to be constant and the electrolyte to be incompressible.

$$c_{V^{3+},cell}(t_1) = c_{V^{3+},cell}(t_0) + \frac{1}{V_{cell}} \cdot \int_{t_0}^{t_1} \left(\left(c_{V^{3+},cell,in}(t) - c_{V^{3+},cell,out}(t) \right) \cdot \dot{V}_{neg,cell}(t) - \frac{I(t)}{F} \right) dt \quad (5.1)$$

If the electrolyte in the cell is perfectly mixed, the outflux concentration $c_{V^{3+},cell,out}(t)$ is equal to the cell concentration $c_{V^{3+},cell}(t)$, resulting in equation 5.2.

$$c_{V^{3+},cell}(t_1) = c_{V^{3+},cell}(t_0) + \frac{1}{V_{cell}} \cdot \int_{t_0}^{t_1} \left(\left(c_{V^{3+},cell,in}(t) - c_{V^{3+},cell}(t) \right) \cdot \dot{V}_{neg,cell}(t) - \frac{I(t)}{F} \right) dt \quad (5.2)$$

The implementation of this equation in Simulink is shown in figure 5.5. The same equation can be used for the VO^{2+}-ions. By comparing these two concentrations to their respective total vanadium concentration in the electrolyte defined in the parameter bus, the complementary concentrations $c_{V^{2+}}$ and $c_{VO_2^+}$ can be obtained.

It is also necessary to calculate the H^+-concentrations for both electrolytes. In order to use the equations 2.19 and 2.20, the State of Charge SOC for both electrolytes is required. It can be calculated by equations 2.17 and 2.18.

The SOC-independent first term is already calculated in the parameter bus. Cite the paper in preparation.

5.2.2 Open Circuit Voltage

The OCV of a RFB cell in an empiric model can be obtained by the complete Nernst equation 2.16 (which already incorporates the Donnan Potential, elaborated by Knehr

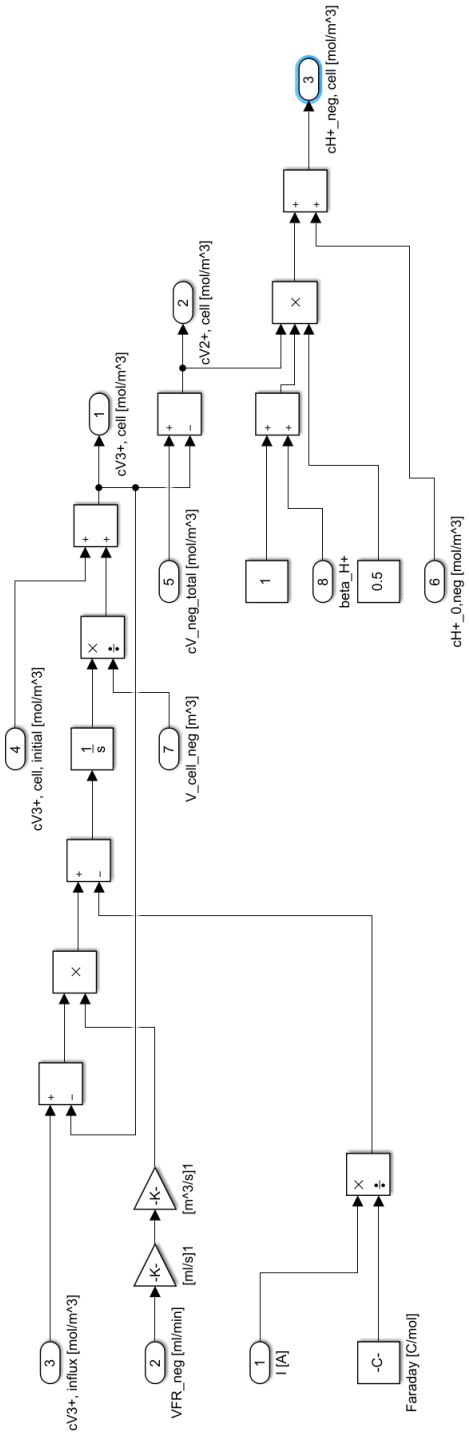

Figure 5.5: Implementation of the concentration change in Simulink

Input	$c_{cell,i,out}$
Parameter	OCV-adjustments
Settings	none
Output	OCV

Table 5.3: Open Circuit Voltage Summary

[18]). This complete formulation can be split up into the positive (see equation 5.3) and the negative electrode (see equation 5.4) according to equation 2.11. While the split is completely optional, it falls in line with the modular approach to modeling in this work.

$$E_{pos} = E^0_{pos} + \frac{RT}{zF} \ln\left(\frac{c_{VO_2^+}}{c_{VO^{2+}}}\right) + 3\frac{RT}{zF} \ln\left(\frac{c^+_{H^+}}{c_{ref}}\right) \tag{5.3}$$

$$E_{neg} = E^0_{neg} + \frac{RT}{zF} \ln\left(\frac{c_{V^{3+}}}{c_{V^{2+}}}\right) + \frac{RT}{zF} \ln\left(\frac{c^-_{H^+}}{c_{ref}}\right) \tag{5.4}$$

The implementation of this in Simulink can be seen in figure 5.6. Two optional adjustments are implemented as well. The first is the correction of the OCV by a specified amount. It was introduced to counter a constant offset between the measurements and the expectation by a few mV noticed in the working group. The second is a time dependent factor, which decreases the OCV, based on elapsed time, which is a simple way to implement the OCV-drop of around $0.46mVh^{-1}$, described by Ressel [5]. Both of these parameters are defined by the user in the parameter Bus block. If no adjustment is needed or wanted, the factors have to be set to 0.

5.2.3 Overpotentials

Input	I_{cell}, $\dot{V}_{cell,neg/pos,in}$
Parameter	none
Settings	Addresses, LUT, Breakpoints
Output	η_{cell}

Table 5.4: Overpotentials Summary

If a net current flux occurs, overpotentials arise and add to the open circuit voltage. In order to increase flexibility and to reduce calculation time, it was decided beforehand to model overpotentials by using Lookup tables for the current-overpotential characteristic. Known models from literature don't handle overpotentials in this way in a macroscopic stack model, but instead use equivalent resistances (Ontiveros [33]), calculate the overpotentials solely in a microscopic model (Yin [34] or Moro [12]) or forego overpotentials other than the ohmic overpotentials completely (Xing [15] or Ye [21]).

The Simulink Lookup Table block requires a n-dimensional matrix with n breakpoint vectors, which are defined in the block itself. In order to output a value, the block needs

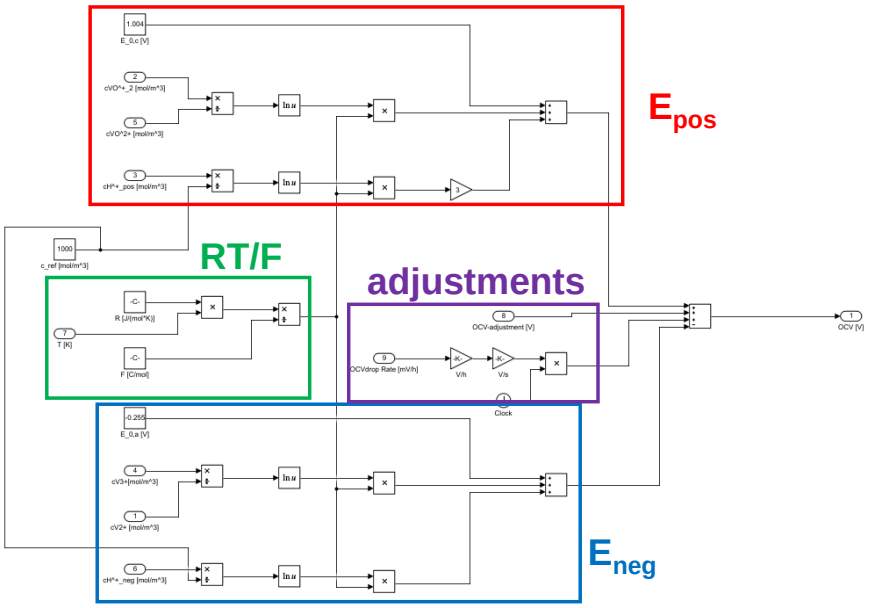

Figure 5.6: The OCV calculation block

an input for each breakpoint vector. In this model the output of the LUT η_{cell} (the overpotential of the cell) will depend on the inputs cell current I_{cell} and the volume flow rate of the electrolyte $\dot{V}_{cell}$. Note that the volume flow rate used here is the average of the volume flow rate of the negative and the positive electrolyte. The third input battery number $battNum$ is implemented to gather several different cells into one lookup table.

There are three ways to acquire the data needed to create the LUTs. The first is to use actual measurements of cells. Secondly, parameters can be used to create hypothetical cells. The third method uses the output of the micro model simulated in COMSOL. For each method, a table will be created, which describes polarization curves at different volume flow rates and for different cells.

In empiric 0-D models, the cell voltage E_{cell} can be described by the sum of the OCV and the various overvoltages η_i (activation, concentration and ohmic).

$$E_{cell}(i) = OCV + \eta_i(i) = OCV + \eta_{act}(i) + \eta_{ohm}(i) + \eta_{conc}(i) \tag{5.5}$$

From Measurements

The first method of generating the LUTs with the current-overpotential characteristic is to use measurements. A supplement program was created in Matlab based on previous works of the author, for example [35].

The algorithm starts by prompting the user to select a measured polarization curve. Followed by that, the user is asked to enter the volume flow rate $\dot{V}$ and a number used to distinguish the batteries, in the following called *battnum*. The program proceeds by checking the vector containing the electric current and the vector containing the

cell voltage for duplicate values, because these would cause problems in the following operations. If duplicate values are spotted, they will be removed. Afterwards, the electric current and the cell voltage will be transferred into a struct. By subtracting the open circuit voltage from the cell voltage, the accumulated overpotentials are obtained. The OCV is assumed to be the value that is measured at the current value that is closest to zero. The last step before the user is asked whether he wants to repeat the process is to gather the minimum and maximum value of the electric current.

The user can then opt to load another measurement. The program expects at least two different batteries at two volume flow rates each. The volume flow rates have to be the same for every battery. After loading every desired measurement, the user can opt to proceed in the program. In this case the program creates a new evenly spaced electric current vector ranging from the minimum to the maximum provided electric current. Linear Interpolation is performed for each measurement to match the polarization curve to the new current vector. If the original polarization curve has minimum and maximum electric currents larger or smaller than the global minimum or maximum, the rest of the values is filled up with NaNs. The interpolated overpotentials are then arranged into a 3-dimensional matrix $etaMat$ with the dimensions I, $\dot{V}$ and $battNum$.

In a last step the program creates the breakpoint vectors (I, $\dot{V}$ and $battNum$) necessary for the Simulink model. The resulting data can be saved.

From Micro Model

The second option to generate the LUT containing the current-overvoltage characteristic of the cell is to use the results from the micro model. This step connects the two models and while it is important for the goal of the work, its implementation is rather simple: The datapoints of the simulated polarization curve have to be exported from COMSOL into a csv-file.

Now the user can run a customized version of the program described beforehand. The procedure stays mostly the same with the obvious exception of importing the csv-files instead of the actual measurements.

From Parameters

The third method to generate the current-overpotential LUTs is to utilize parameters. Polarization curves can also be obtained by adding up functions that describe the single overpotentials.

Another variation of the program for the LUT-generation is implemented. In a first step the user is asked to provide a lower and an upper eta-value. These values serve as boundaries for the generation. The user is also asked for values of the temperature T and the number of transferred electrons z (1 in the case of a VRFB).

After that, the user has to provide several parameters that describe the different overpotentials. An ASR-value for the ohmic overpotentials, the exchange current density i_0 for the activation overpotentials and the limiting current density i_{lim} for the concentration overpotentials. Additionally the user is asked to provide the actice membrane area

A_{memb} of the cell. Changing the Tafel-Slope is possible but not recommended. This process is repeated as long as the user demands.

Based on these parameters the overpotentials are calculated in a loop until the aforementioned upper or lower eta value is hit. Other than that, the procedure stays mostly the same as described beforehand. Missing values for worse performing cells are replaced with NaN.

In order to calculate the ohmic overpotentials η_{ohm} Ohm's law is utilized.

$$\eta_{ohm}(i) = R_{cell} \cdot I_{cell} = R_{cell} \cdot i_{cell} \cdot A_{memb} = ASR \cdot i_{cell} \tag{5.6}$$

For the calculation of the activation overpotentials η_{act}, the Butler-Volmer equation (see equation 2.32) is used. However, solving the Butler-Volmer equation is rather complex. By assuming a transfer coefficient $\alpha = 0.5$, the hyperbolic sine can be utilized to simplify the equation.

$$sinh(x) = \frac{e^x - e^{-x}}{2} \tag{5.7}$$

$$2 \cdot sinh(x) = e^x - e^{-x} \tag{5.8}$$

$$i(\eta_{act}) = i_0 \cdot 2 \cdot sinh\left(\frac{\alpha z F \eta_{act}}{RT}\right) \tag{5.9}$$

Now, η_{act} can be obtained by using the arcus hyperbolic sine.

$$\eta_{act} = \frac{2RT}{zF} \cdot arcsinh\left(\frac{i}{2i_0}\right) \tag{5.10}$$

The last remaining overpotential is the concentration overpotential η_{conc}. Solving the concentration dependent Butler-Volmer equation (see equation 2.34) for η for the anodic reaction yields the following:

$$\eta = \frac{RT}{\alpha z F} \cdot \left(ln\left(\frac{j(\eta)}{j_0}\right) + ln\left(\frac{c_{red,el}}{c_{red,s}}\right)\right) \tag{5.11}$$

The first of the two ln-terms is obviously the activation overpotential part. The concentration overpotential becomes apparent:

$$\eta_{conc} = \frac{RT}{\alpha z F} \cdot ln\left(\frac{c_{red,el}}{c_{red,s}}\right) \tag{5.12}$$

And for the cathodic reaction:

$$\eta_{conc} = \frac{RT}{(1-\alpha) z F} \cdot ln\left(\frac{c_{ox,el}}{c_{ox,s}}\right) \tag{5.13}$$

If all ions are consumed at the electrode, maximum current occurs. This current is called the limiting current density i_{lim}. The concentration overpotential becomes the following:

$$\eta_{conc} = \frac{RT}{\alpha z F} \cdot ln\left(1 - \frac{i}{i_{lim}}\right) \tag{5.14}$$

For the calculation of the overpotentials in the program, it is assumed that every cell has the same electrode surface and active membrane area. Therefore, the current densities can be exchanged with the current I.

Adding all overpotentials yields the desired $\eta(I)$ characteristic.

5.3 Electrolyte Tanks

Input	$\dot{V}_{cell,neg/pos,in}$, $c_{tank,i,in}$
Parameter	$c_{i,initial}$, $V_{tank,neg/pos}$
Settings	none
Output	$c_{tank,i,out}$

Table 5.5: Electrolyte Tanks Summary

While tanks are an integral part of any VRFB, they are modeled fairly simple in this work. Following the same method that was used for the concentration change within the cell, equation 5.2 is used to update the concentrations for each simulated time step for both the negative as well as the positive electrolyte tank. Of course, there is no electric current applied to the tank, so the Faraday term is neglected.

This approach means, that in this work, electrolyte is assumed to be either in a tank or in one of the cells. While the connecting elements in the form of pipes are used in a following chapter to calculate pressure drops, the transition of electrolyte from the tank to one of the cells is instant. It is also assumed, that the electrolyte in the tank is perfectly mixed all the time.

5.4 Parameter Bus

Input	none
Parameter	defined in here
Settings	none
Output	every Parameter

Table 5.6: Parameter Bus Summary

In order to collect the boundaries for the simulation in a single place, a block called Parameter Bus is set up. This block includes simulation parameters which don't change over time. It has only one output called *Parameter Bus* and no inputs. The contained parameters describe the electrolyte and the geometries of cells, tanks and electrolyte pipes. Because the parameters don't change over time, the Simulink Constant element can be used for each one of them. The constant signals are collected in a Bus Creator element. A Bus Creator element collects and bundles signals into a single bus signal. Accessing one or more elements of the bus signal requires a Bus Selector element. It is crucial to precisely name the signals that go into the bus, to clarify which signals have to be read out at a Bus Selector element. Therefore, each signal in the Parameter Bus block is given a name with a description of the signal and its unit.

A few calculations also take place in this block. By subtracting the number of cells times the cell volume from the electrolyte volume, the volume of electrolyte in the tank

is determined (electrolyte in the model can only be in the tank or in a cell). This operation is performed for the negative and the positive electrolyte circuit (note that the cell volumes are different due to the tubular geometry). The other two calculations taking place in this block apply to the starting concentrations of the different species in the electrolyte, refer to the equations found in section 2.1.5.

With this block implemented, the simulation of a single cell is possible. The next sections in this chapter discuss the methods to simulate multiple cells organized into modules.

5.5 Electric Distribution

In order to reach voltages that are high enough for industrial use, the electric connection of cells is necessary. Cells can be connected in series, in parallel or in a combination of both. Cells connected in this way are called a module. Similar to the connection of cells, modules can be connected in different ways as well. Each connection bears its own advantages and disadvantages as well as its own challenges from a modeling perspective. In the following chapter these advantages, disadvantages and challenges will be described using the example of a module consisting of a variable amount of cells. They take place in the yellow block in figure 5.1.

5.5.1 Serial Connections without Shunt Currents

Input	I_{mod}
Parameter	none
Settings	Number of Cells in Serial
Output	I_{cell}

Table 5.7: Electric Distribution for Serial Connections without Shunt Currents Summary

Connecting multiple cells in series bears the benefit of an increased resulting voltage while current stays the same. In order to connect two redox flow batteries in series, the positive current collector of the first cell has to be connected electrically to the negative current collector of the second cell. Their voltages E_{cell} will add up to the resulting module voltage E_{mod}, while the current I_{mod} for each cell is the same.

$$I_{mod} = I_1 = I_2 = ... = I_n \tag{5.15}$$

$$E_{mod} = \sum_{k=1}^{n} E_{cell,k}(I_{mod}) \tag{5.16}$$

Because the module current is defined as an input in the model, calculating the module voltage is only a matter of adding the cell voltages, if shunt currents between the cells are ignored. This step is conducted at the end of each simulation time step. The only operation that has to be done in this step is vectorize the module current in order to cause no adjustments to the rest of the model.

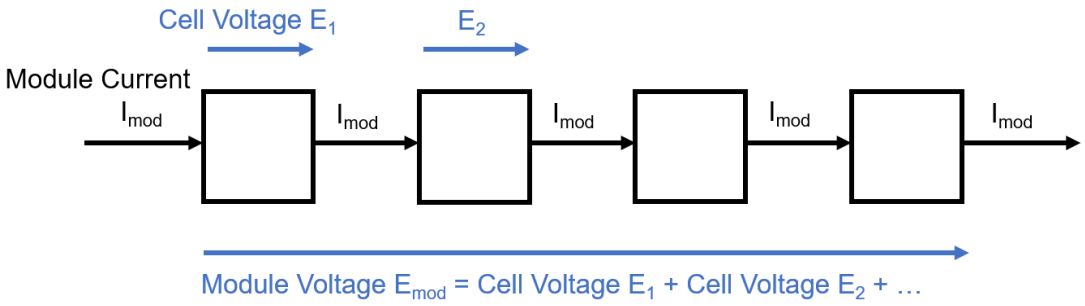

Figure 5.7: A Module consisting of 4 Cells connected in Series

5.5.2 Serial Connections with Shunt Currents

Input	I_{mod}, $OCV(t-1)$, $c_{tank,i,out}$
Parameter	piping-geometry, conductivities of the electrolyte
Settings	Number of Iterations per simulation time step
Output	I_{cell}, shunt currents in manifolds or channels

Table 5.8: Electric Distribution for Serial Connections with Shunt Currents Summary

In reality, if multiple redox flow batteries are connected in series, shunt currents will occur. Instead of the current passing through the electrodes, it may instead pass through the electrolyte that connects the individual cells if the ionic resistance is low enough[20]. The amount of emerging shunt currents depends on many factors, therefore a model has to be developed.

Ionic resistance of a channel

Input	$c_{tank,i,out}$
Parameter	piping-geometry, conductivities of the electrolyte
Settings	none
Output	$R_{channel,neg/pos}$

Table 5.9: Ionic Resistance of a channel Summary

The ionic resistance of a channel is dependent on its geometry and the conductivity of the medium that flows through it. The models of Xing [15], Tang [22], Wandschneider [14] or Koenig [13] all use the following equation, which is implemented in this model as well:

$$R_{channel,neg,pos}(SOC_{neg/pos}) = \frac{1}{\sigma_{A,C}(SOC_{neg/pos})} \frac{l_{channel}}{A_{channel}} \tag{5.17}$$

Conductivities of the different electrolytes at $SOC = 0$ and $SOC = 1$ and at different temperatures are published in various sources. The values used in this work are pre-

sented by Wandschneider and listed in table 5.10. Assuming a linear behavior, the SOC dependent conductivity of the anolyte σ_A and the catholyte σ_C at a set temperature can be calculated by the following equation. This approach is common in literature models and is used for example in the models of Tang, Koenig or Wandschneider.

$$\sigma_A(SOC_{neg}) = SOC_{neg} \cdot \sigma_{V^{2+}} + (1 - SOC_{neg}) \cdot \sigma_{V^{3+}} \tag{5.18}$$

$$\sigma_C(SOC_{pos}) = SOC_{pos} \cdot \sigma_{VO_2^+} + (1 - SOC_{pos}) \cdot \sigma_{VO^{2+}} \tag{5.19}$$

Piping is separated into channels and manifolds: Manifolds are bigger pipes connected to the tanks, that split into smaller channels, that are connected to the cells.

Vanadium Species	Conductivity $\sigma[\frac{mS}{cm}] \pm 10[\frac{mS}{cm}]$
V^{2+}	303
V^{3+}	196
VO^{2+}	308
VO_2^+	454

Table 5.10: Conductivities according to the work of Wandschneider [14] at a temperature of $T = 298[K] \pm 0.5[K]$

Equivalent circuit

Kirchhoff's circuit laws provide a powerful method to calculate currents in complex electrical circuits. They are used in many models in literature that focus on the calculation of shunt currents, dating back to the 1980s with the model of Hagedorn [7]. Recent models follow the same approach with examples in the models of Xing [15], Wandschneider [14], Moro [12] and many more. The calculation method is adapted in the model of this work to make it work with the LUTs. Kirchhoff states:

- The total current entering any junction is equal to the total current leaving that junction
- The sum of all voltages around a loop is equal to zero.

By defining the channels that provide the electrolyte to the cells as resistors, an equivalent electric circuit can be set up, as shown in figure 5.8. The cells are colored yellow and their respective voltages are named U. The currents that flow through the cells are called I. The red elements belong to the anolythe circuit, where R is the resistance of the manifold (capital A) and channel (a). The respective currents are called A and a. The elements belonging to the catholyte circuit are colored blue and named accordingly: R for the resistance of the manifold (capital C) and channel (c), as well as the respective currents C and c. I_{mod} is the current of the module. Note that only half of both circuits are shown. However, due to the symmetrical setup, it is possible to incorporate the symmetry into the equation system. With exceptions of the first and the last cell, a set

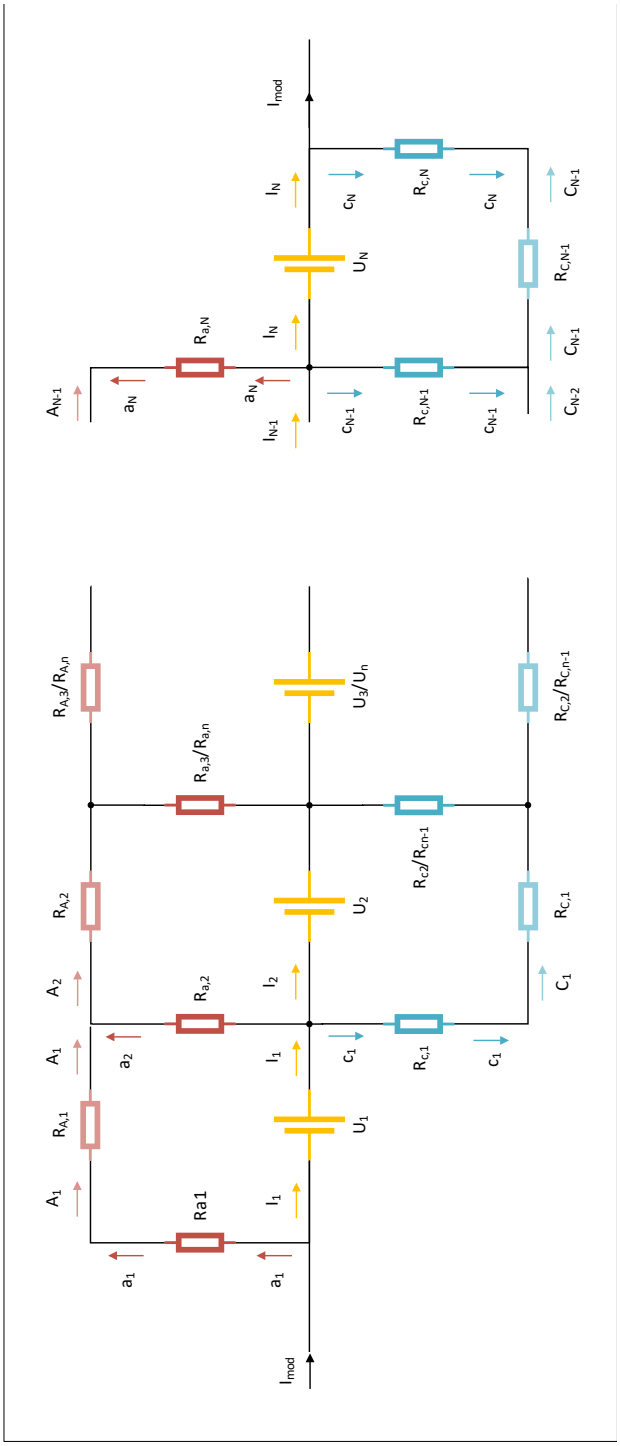

Figure 5.8: Equivalent circuit diagram of shunt currents in a serial connection

of periodically repeating linear equations can be derived from the circuit diagram.

$$-I_{n-1} + I_n + 2a_n + 2c_n = 0 \tag{5.20}$$

$$-a_n - A_{n-1} + A_n = 0 \tag{5.21}$$

$$-c_{n-1} - C_{n-2} + C_{n-1} = 0 \tag{5.22}$$

$$R_a \cdot (-a_{n-1} + a_n) + R_A \cdot A_n = E_{cell,n}(I_n) \tag{5.23}$$

$$R_c \cdot (c_{n-1} - c_n) + R_C \cdot C_{n-1} = E_{cell,n}(I_n) \tag{5.24}$$

The equations for the first cell are the following:

$$I_1 + 2a_1 = I_{mod} \tag{5.25}$$

$$a_1 - A_1 = 0 \tag{5.26}$$

$$R_a \cdot (a_1 - a_2) + R_A \cdot A_1 = E_{cell,1}(I_1) \tag{5.27}$$

For the last cell the special equations are as follows.

$$-I_{N-1} + I_N + 2a_N + 2c_N = 0 \tag{5.28}$$

$$A_{N-1} + a_N = 0 \tag{5.29}$$

$$C_1 - c_1 = 0 \tag{5.30}$$

$$R_c \cdot (c_{N-1} - c_N) + R_C \cdot C_{N-1} = E_{cell,N}(I_N) \tag{5.31}$$

$$I_N - 2 \cdot c_N = I_{mod} \tag{5.32}$$

This results in $5N - 2$ equations for $5N - 2$ unknowns, which can be solved with standard Matlab operations. Note that the cell voltage E_{cell} is obtained by adding the overpotentials $\eta(I)$ to the OCV, which is calculated from the concentrations.

Iteration

In contrary to the models from literature that also use this approach, in this work the activation and concentration overpotentials are considered on top of the ohmic overpotentials. This leads to a non-linear behavior of the cell voltage E_{cell}, or more specifically the overpotentials η. In order to use the aforementioned approach to calculating the shunt currents, an iteration is necessary. The first step of the iteration assumes, that no shunt currents occur, so the voltage for every cell is calculated by using I_{mod}. After the first iteration, different I will have been computed for every cell. New voltages can be calculated from these values and be used as the voltage for another iteration.

To implement this approach in Simulink, the Matlab function block is utilized.

Input	I_{mod}, $c_{tank,i,out}$, ionic resistances of the piping
Parameter	none
Settings	number of iterations, addresses, LUT, breakpoints
Output	I_{vec}, shunt currents

Table 5.11: Shunt Current Function Summary

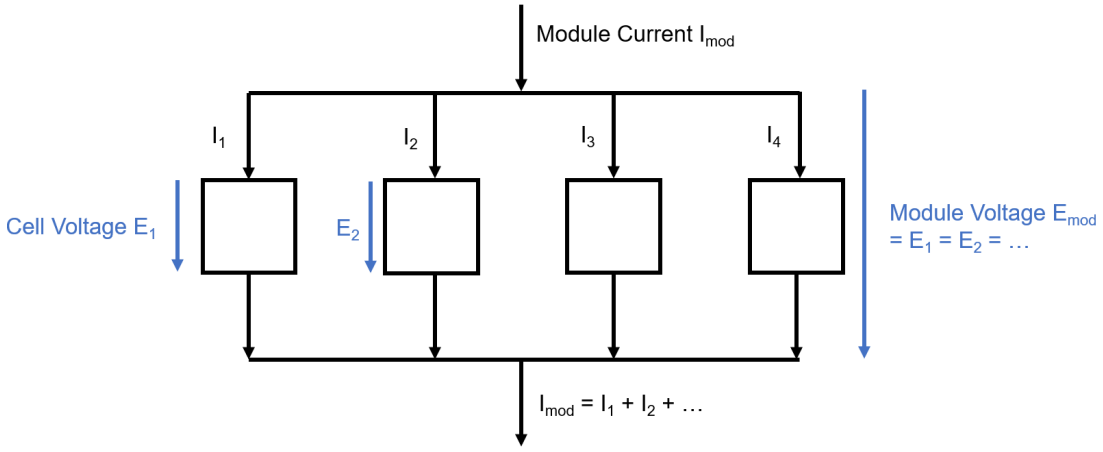

Figure 5.9: A Module consisting of 4 Cells connected in Parallel

5.5.3 Parallel Connections

The cells can also be electrically connected in parallel, see figure 5.9. In a parallel setup, each cell connected in parallel will have the same cell voltage E_{cell}. The module current I_{mod} will be distributed accordingly.

This connection type is not covered by literature models, as they focus on serial connections due to the different construction of the cell. The notable exception is the model of Moro [12]. However, this model doesn't incorporate overpotentials in a way that is compatible with the LUT-approach used in this work, nor does the electric characteristic of the cells vary. Therefore, an own model had to be developed for the electric distribution in parallel connections.

The fact, that the electric current is defined as an input in the model, presents a challenge. If the current-voltage characteristic of the cells were linear, the distribution would be rather easy. However, in this model the non-linear activation and concentration overpotentials are also considered for the cells. The module current has to be distributed, resulting in every cell delivering the same voltage. This calculation takes place before the calculations for each cell described in the previous section are conducted. Figure 5.10 shows a screenshot of the content of the electric distribution block shown in figure 5.1 for 3 cells in parallel. The block is provided with two inputs: the electric current of the module and the volume flow rate vector of the electrolyte (the hydraulic distribution explained in the following section will cause different volume flow rates for different

cells). Its output is a vector containing the electric current for each cell.

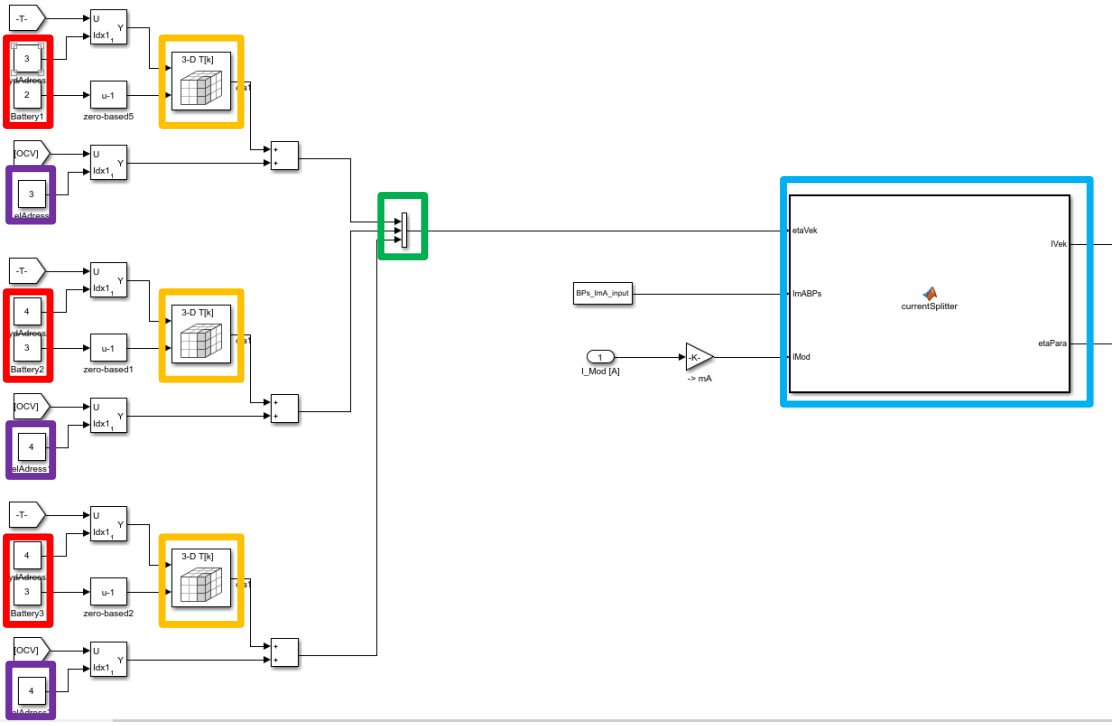

Figure 5.10: Content of the Electric Distribution Block for 3 cells in parallel; red and purple: adresses (user inputs); orange: the Direct Lookup table block; green: merging of the LUT excerpts; blue: the current splitter function

The approach used in this work is a graphical one. Rather than iterating to approximate the distribution of the electric current, the LUTs with the overpotential-current characteristic are utilized. As described before, the overpotentials for each cell are collected in a multidimensional table. The Simulink block *Direct Lookup table* allows to access defined parts of the LUT. In this case we look for the overpotential-current characteristic for the specified cell at the specified volume flow rate. Therefore, the hydraulic address is used to read the correct volume flow rate from the input vector and the battery number is used to access the correct battery in the LUT. Both the hydraulic address and the battery number have to be specified in this block, see the red boxes in figure 5.10. The direct lookup table block (in orange) now provides a vector in the form of $\eta(I)$. Before these enter the Matlab function block (blue), they are arranged in a matrix with the *Vector Concatenate* block (green). If more cells are used, it is necessary to concatenate each LUT-excerpt with this block. If longer simulation times occur (for example when simulating charge-discharge cycling), it is advantageous to also add the OCV of

Input	I_{mod}, $OCV(t-1)$
Parameter	none
Settings	addresses, LUT, breakpoints
Output	I_{vec}

Table 5.12: Electric Distribution for Parallel Connections Summary

the respective cell on top of the overvoltages to improve accuracy (purple). However, the following explanation assumes the aforementioned simple case without OCV-influence.

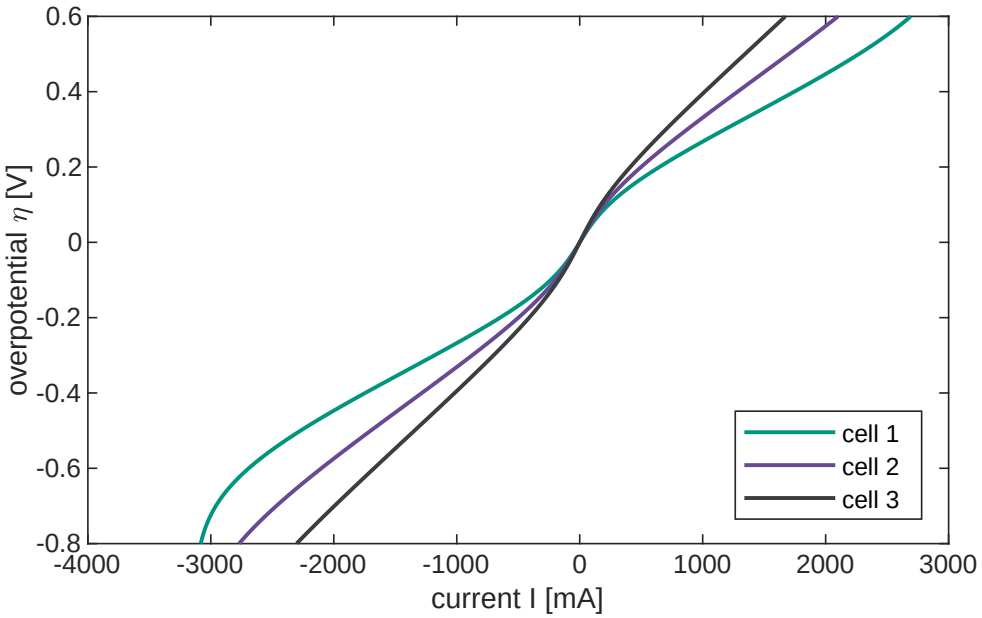

Figure 5.11: Overpotential η in V over electric current I in mA for 3 different cells

The Matlab function is now provided with a overvoltage-current characteristic for each cell. Figure 5.11 shows these characteristics for 3 cells. They represent polarization curves in the form of $\eta(I)$. As one can see, the functions are bijective. Therefore, the dependency can be reverted, resulting in $I(\eta)$, shown in figure 5.12. The (in this example 3) curves are linear interpolated, to have a common η-range.

In a next step, the sum $I_{sum}(\eta)$ of the single $I(\eta)$ is generated, because the single cell electric currents have to add up to the module electric current, see figure 5.13. With the known module current I_{mod} it is now possible to acquire the intersection point with the I_{sum}-curve. The x-coordinate of the intersection point yields the module overvoltage. Inserting the overvoltage into each of the $I(\eta)$ dependencies yields the electric current for each cell.

This described approach is implemented in a Matlab function. Its output is a vector containing the resulting electric current for each cell.

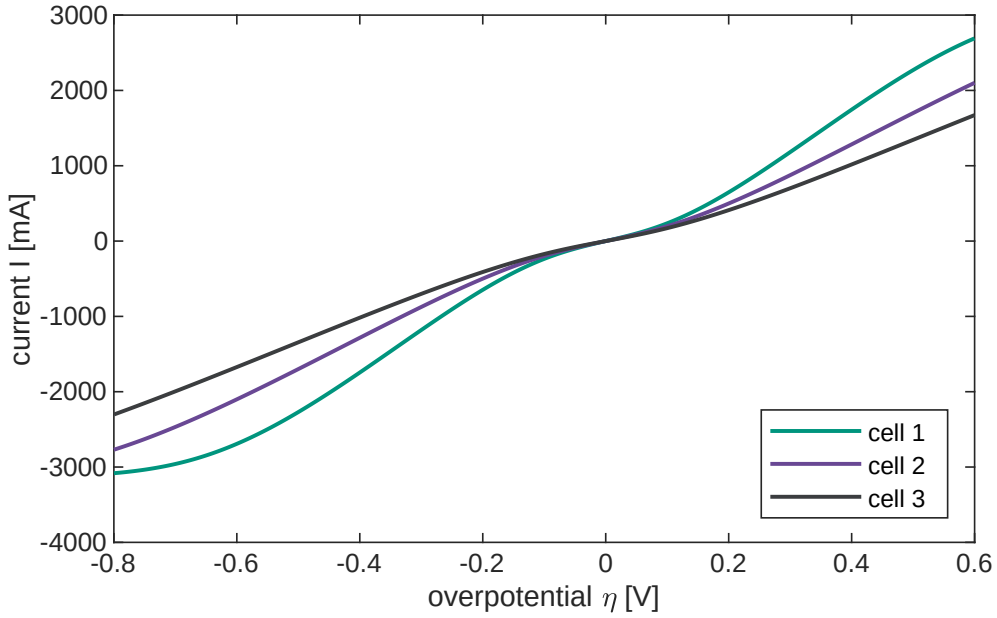

Figure 5.12: Electric current I in mA over overpotential η in V for 3 different cells

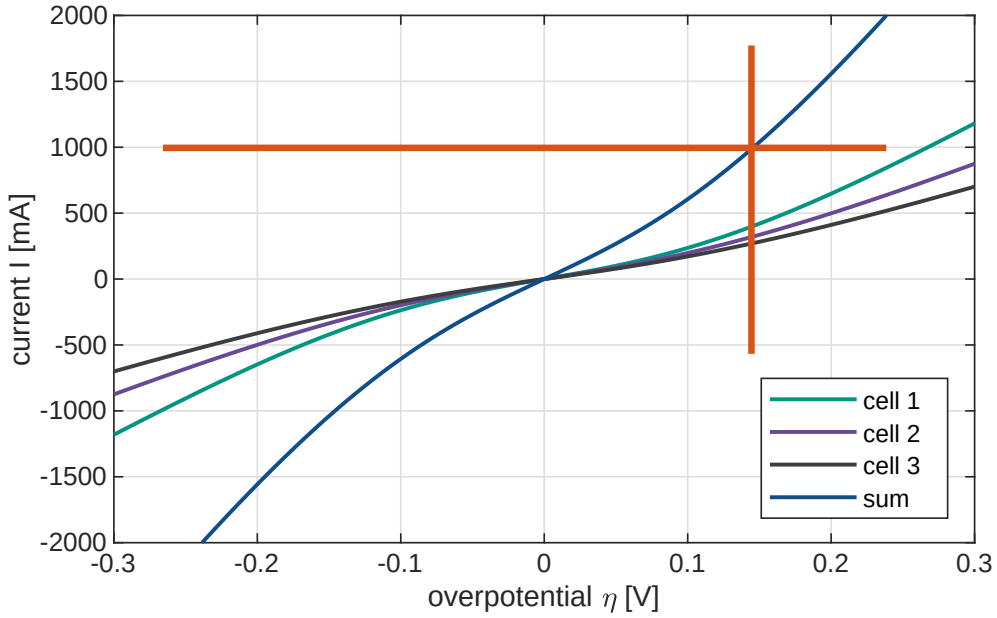

Figure 5.13: Electric current I in mA over overpotential η in V for 3 different cells and the sum of the 3 electric currents. The *crosshair* defines an operating point

5.5.4 Combined Connections

It is also possible to combine serial and parallel electrical connection of cells in a module. Two cases can be discerned. The first one, shown in figure 5.14, will be called serial-parallel in this work, while the second case, shown in figure 5.15, will be called parallel-serial.

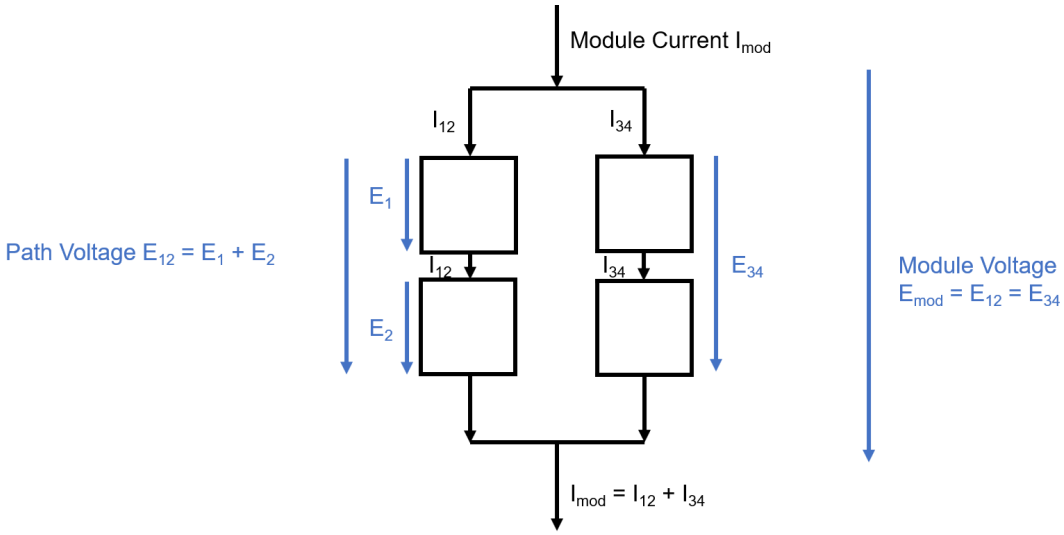

Figure 5.14: Combined Connection of 4 cells: serial-parallel case

From the standpoint of modeling the first case is a variation of the Parallel Connection. The electric distribution can be calculated with the same Matlab function. However, because in this case the path voltages have to be the same, it is necessary to add up the $\eta(I)$-LUTs of each cell in a parallel pathway. In consequence, an *Add*-block is used before the parallel paths are merged into a matrix with the *Vector Concatenate* block (see figure 5.16).

The second case however is even easier. Because the module current is the same before each distribution, the electric distribution from the parallel connection has to be run two times. This results in a distinct current for each cell.

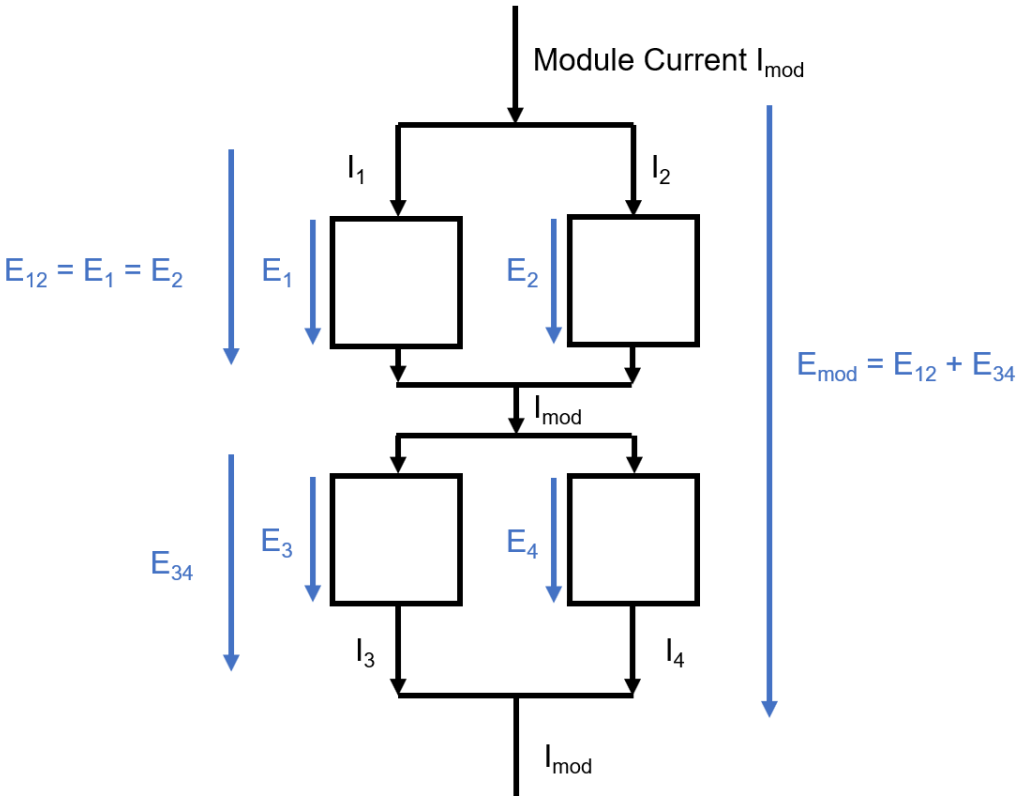

Figure 5.15: Combined Connection of 4 cells: parallel-serial case

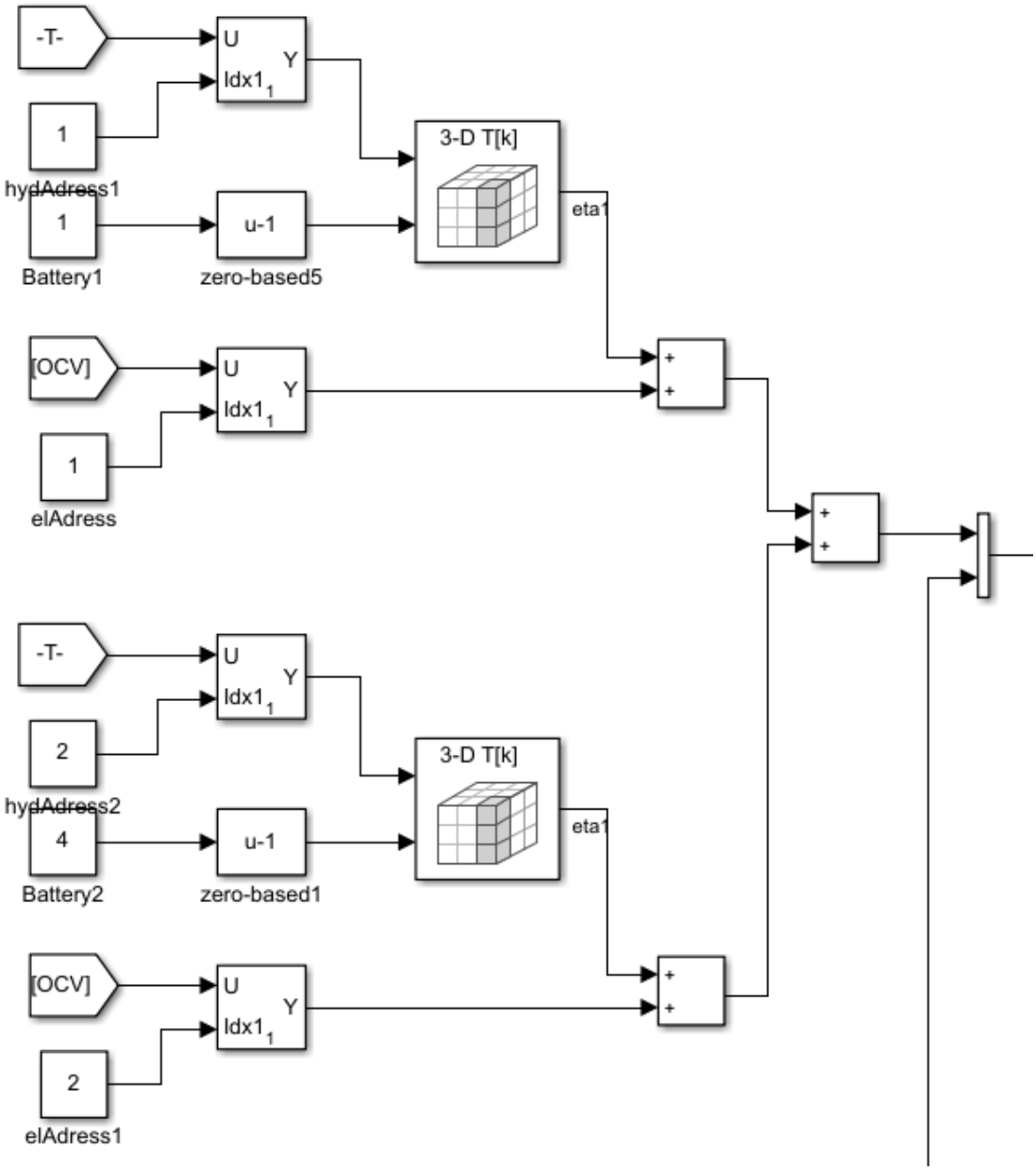

Figure 5.16: Serial-Parallel Connection: The LUTs of each cell in a path are added up

5.6 Hydraulic Distribution

Input	$\dot{V}_{mod}$
Parameter	hydraulic resistance of the cells, geometry of the piping
Settings	none
Output	$\dot{V}_{vec}$, Δp

Table 5.13: Hydraulic Distribution Summary

As already discussed a Redox Flow Battery has to supplied with two different electrolytes, the anolyte and the catholyte. Hence, the cell is connected to two electrolyte circuits. If more than one cell is used in a module or stack, each cell has to be supplied with electrolyte. It acts against the advantage of the Redox Flow Battery to designate an own tank to each cell. Therefore, in a module or stack the fluid flow of the electrolyte has to be distributed to the cells. Figure 5.17 shows an example of how the electrolyte distribution could be realized, as published by Ye et al. in [21].

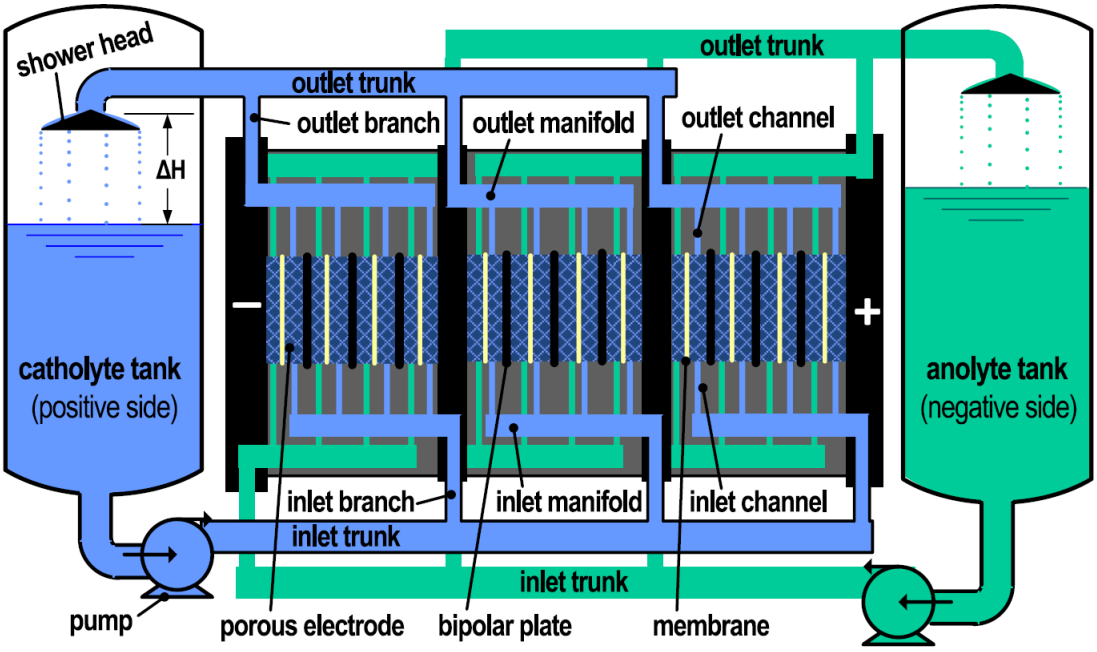

Figure 5.17: Exemplary illustration of the electrolyte circuit of a RFB stack, as published by Ye et al. [21]

Looking at the catholyte tank, one can see that the electrolyte is pumped from the tank into the inlet trunk. The trunk distributes the electrolyte into three branches, which transform without further distribution into manifolds. In the manifold, the electrolyte is distributed into 4 channels, which supply the cells. The same concept is mirrored to merge the electrolyte flow on the other half of the cells.

For the model used in this work, some assumptions are made:

- Electrolytes are incompressible
- Both Electrolytes have the same constant density and viscosity
- The effect of T-junctions on the pressure drop is neglected
- The manifolds are directly connected to the tank
- The effect of valves and tanks on the pressure drop is neglected
- Laminar flow is assumed

5.6.1 Pressure Drop in Cells

Because the flow channel geometry of a vanadium redox flow battery is rather complex, the pressure drop characteristic is simplified in the macro model. Measurements show a nearly linear dependency of the pressure drop Δp_{cell} on the volume flow rate $\dot{V}_{cell}$, although a significant difference between the two half cells is observed, as shown in figure 5.18. By utilizing a linear fit, one can obtain a factor for each half cell which describes the proportionality between the pressure drop and the flow rate. The goal is to obtain two factors $R_{hyd,neg/pos}$ that lead to the following dependency. This approach is analog to the Darcy equation described in equation 2.35.

$$\Delta p_{cell,neg/pos} = R_{hyd,cell,neg/pos} \cdot \dot{V}_{cell,neg/pos} \tag{5.33}$$

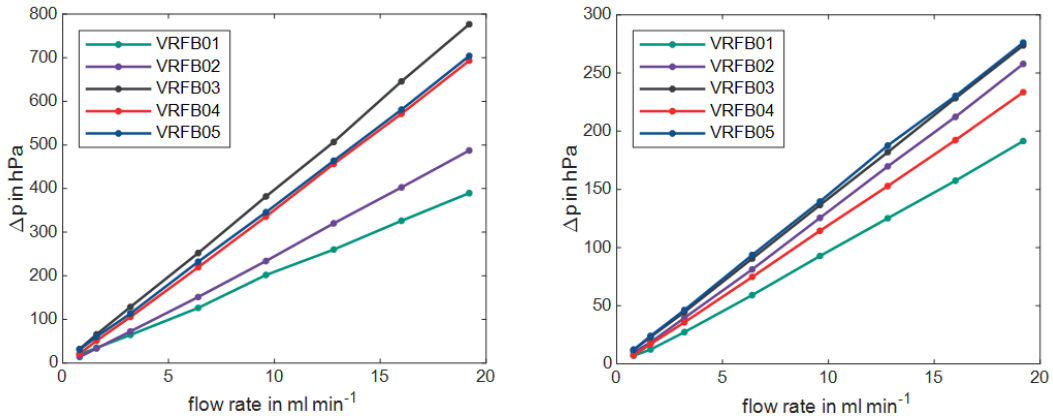

Figure 5.18: Measured Volume Flow Rate dependent Pressure Drop of five different Vanadium Redox Flow Batteries: Negative Half Cell on the left and Positive Half Cell on the right. These are results from the StaTuR work group.

5.6.2 Pressure Drops in Pipes

For the given assumptions, the pressure drop in a pipe with a circular cross-section area is best defined by *Hagen-Poiseuille*, because laminar flow is expected with the operating volume flow rates. While the equation is already described in equation 2.37, it is shown here again for readability's sake.

$$\Delta p = \frac{8 \cdot \mu \cdot l}{\pi \cdot r^4} \cdot \dot{V} = \frac{8 \cdot \mu \cdot l}{\pi \cdot \frac{d^4}{16}} \cdot \dot{V} = \frac{128 \cdot \mu \cdot l}{\pi \cdot d^4} \cdot \dot{V}$$

μ is the dynamic viscosity of the fluid, d and l describe the geometry of the flow channel and $\dot{V}$ is the volume flow rate of the fluid. Similar to the pressure drop in cells, the goal is to obtain a relation similar to the Darcy equation, with a resistance factor $R_{hyd,pipe}$.

$$\Delta p_{pipe} = R_{hyd,pipe} \cdot \dot{V}_{pipe} \tag{5.34}$$

5.6.3 Volume Flow Distribution

In a hydraulic circuit with more than one possible path from point A to point B, the fluid will be divided according to the pressure drop characteristics of the possible paths. To calculate the distribution, the electronic-hydraulic analogy is utilized. The central electric linear model is described by *Ohm's law*.

$$U = R \cdot I \tag{5.35}$$

Direct current electric circuits behave very similar to hydraulic circuits. The central hydraulic linear model is defined by the Darcy equation.

$$\Delta p = R_{hyd} \cdot \dot{V} \tag{5.36}$$

Assuming a hydraulic circuit behaves like a direct current electric circuit, one can use *Kirchhoff's law* to set up an equivalent circuit diagram for the hydraulic circuit. Kirchhoff states:

- The current entering any junction is equal to the current leaving that junction
- The sum of all voltages around a loop is equal to zero.

For the model it is assumed that every cell is connected hydraulically in parallel with the other cells in a *Z-setup*. This means that the fluid influx and outflux are located on opposing sites. An exemplary setup for one of the two electrolyte circuits is shown in figure 5.19. This leads to a periodic set of linear equations (see equations 5.37, 5.38 and 5.39). Special boundaries have to be applied to the first (replace 5.37 and 5.38 with 5.40 and 5.41) and the last cell (replace 5.37 with 5.42 and skip 5.38 and 5.39).

$$\dot{Q}_{cell,n} + \dot{Q}_{in,n-1} + \dot{Q}_{in,n} = 0 \tag{5.37}$$

$$-\dot{Q}_{cell,n} - \dot{Q}_{out,n-1} + \dot{Q}_{out,n} = 0 \tag{5.38}$$

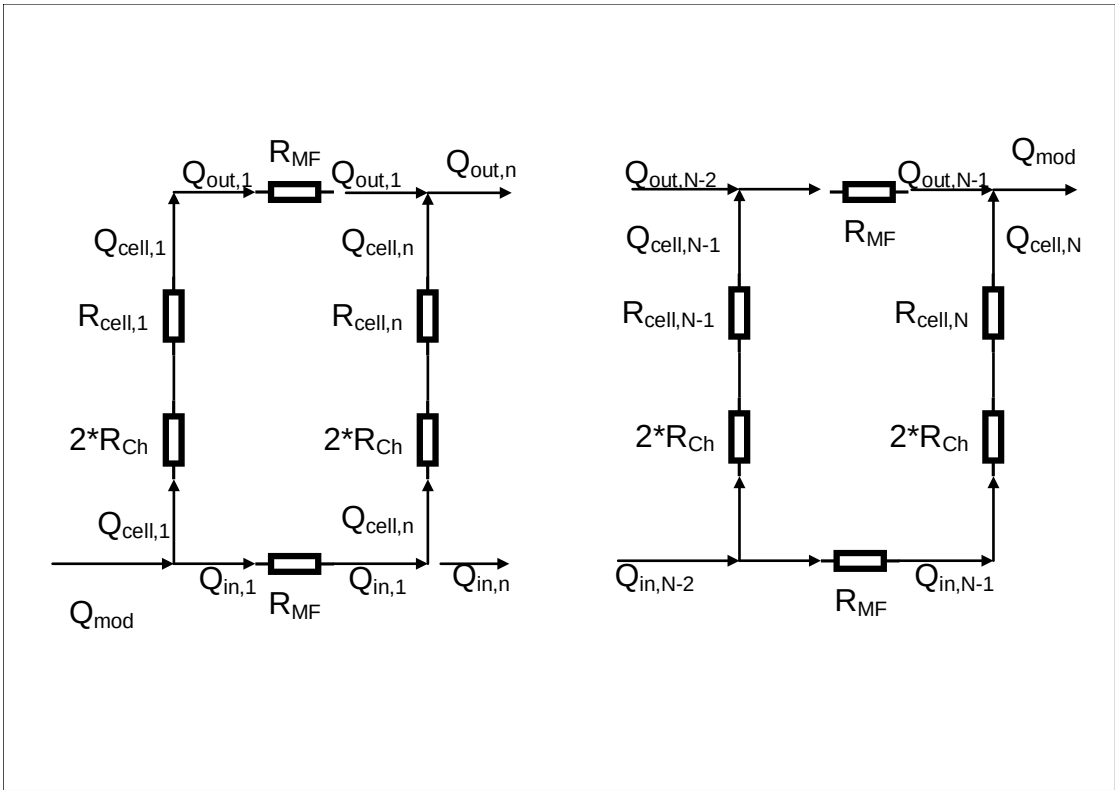

Figure 5.19: Equivalent hydraulic circuit diagram for one of the two electrolytes consisting of N cells connected hydraulically in parallel in a *Z-setup*

$$-\dot{Q}_{cell,n} \cdot (2 \cdot R_{hyd,channel} + R_{hyd,cell,n}) + \dot{Q}_{cell,n+1} \cdot (2 \cdot R_{hyd,channel} + R_{hyd,cell,n+1}) + \dot{Q}_{in,n} \cdot R_{hyd,MF} - \dot{Q}_{out,n} \cdot R_{hyd,MF} = 0 \tag{5.39}$$

$$\dot{Q}_{cell,1} + \dot{Q}_{in,1} = \dot{Q}_{mod} \tag{5.40}$$

$$-\dot{Q}_{cell,1} + \dot{Q}_{out,n} = 0 \tag{5.41}$$

$$\dot{Q}_{cell,N} + \dot{Q}_{in,N-1} = 0 \tag{5.42}$$

Adding every different volume flow rate, a total of $3N-2$ unknowns is determined. The periodic equations mentioned above result in a total of $3N-2$ equations. Therefore, the system can be solved using common methods for linear equation systems.

In order to calculate the total pressure drop of the circuit, one has to pick a path and multiply every volume flow rate with the according coefficient of hydraulic resistance. It is sufficient to do this for one path because of the parallel setup of the circuit.

5.7 Merging of Data

As soon as the model is used to simulate more than one cell, it is necessary to merge some data after each calculation step, as shown in green in figure 5.1.

5.7.1 Merging of the Electrolytes

The setup of the model assumes, that there is one tank for each electrolyte. Electrolyte flows from the tank into the cells, according to the aforementioned hydraulic distribution. From the cells it enters the tank again. The influx concentration to the tank is acquired by relating the cell volume flow rates to the module volume flow rates and add up the vanadium species concentrations accordingly.

5.7.2 Merging of the Cell Voltages

Based on the used electric setup of the cells, the module voltage is calculated. For cells connected in serial, this means adding up every single cell voltage. Cells connected in parallel are not added. It would suffice to take a single cell voltage and use it as the module voltage, however an average of the cell voltages is calculated and used as the module voltage. In combined setups, the module voltage has to be calculated according to the setup. The principles are already discussed in section 5.5.

5.8 Simulation Control

While the inputs for the simulation can be chosen freely (to simulate single operating points or set profiles), standardized charge-discharge cycles feature a logic that has to be applied to the inputs based on the outputs. One cycle consists of one charge and discharge step each. The steps in this work are performed at constant current. When

Input	$E_{cell,min}$, $E_{cell,max}$
Parameter	none
Settings	the desired logic for the simulation
Output	I_{mod}, *ter*, *integ*

Table 5.14: Simulation Control Summary

cycling with constant current, a cell is charged or discharged as long as the cell potential doesn't exceed prior defined boundaries.

To implement this process, a simple simulation control has to be created. The orange block in figure 5.20 is a *Stateflow* block. Stateflow is a sub program of Matlab Simulink, that allows to generate control sequences. The block is provided with the minimum and maximum cell voltage of all cells in the module. It has three outputs: *ter*, a variable that stops the simulation when its value is one, *current*, which serves as the electric current for the top simulation level (module or cell) and therefore the input for the model and *integ*, a variable that is either 0 or 1, which will be used for the efficiency calculation explained in the next section.

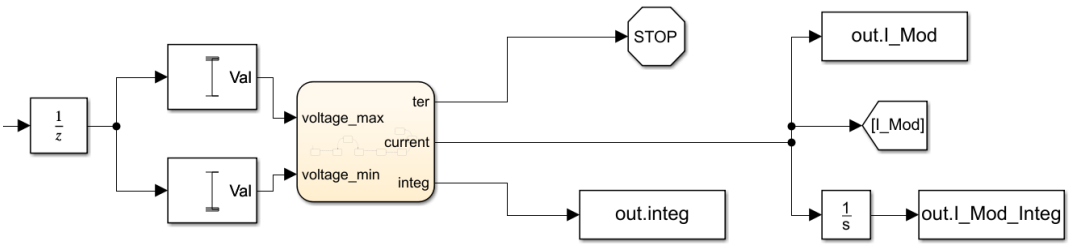

Figure 5.20: The simulation control for charge-discharge cycling

Figure 5.21 shows the stateflow block. The several blocks are states, which are connected with arrows. The transition from one block to another is triggered when the condition stated in the arrow is fulfilled. When a new state is entered, some variables are changed, which is denoted in the block.

5.9 Outputs

5.9.1 Main Outputs

For every simulation time step, the outputs of the simulation are written into the Matlab Workspace. The module voltage E_{mod} and the pressure drop of the module Δp_{mod} are the two main outputs of the model. However, with the *to workspace*-block, the user could track and save every value that is used in the model at every time step. Good examples are the required values for the efficiencies, described in the following. Simulink further allows for simple integration of values.

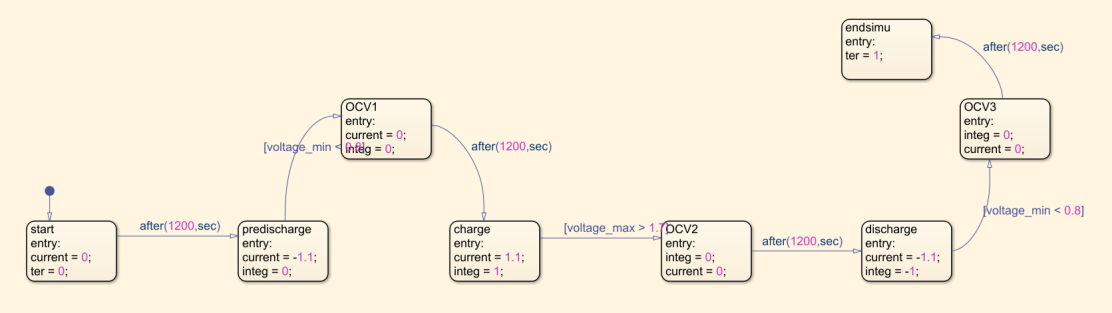

Figure 5.21: The Stateflow block of the simulation control for one charge-discharge cycle

5.9.2 Efficiencies

When the model is used to simulate charge-discharge cycles, it is useful to calculate efficiencies. The efficiency of a redox flow battery is determined by comparing cell currents and potentials during charge and discharge cycles [5]. The Calculations are not integrated into the Simulink model, but are instead run afterwards in Matlab. The aforementioned variable *integ* serves as an indicator for when the following values should be integrated.

Coulombic Efficiency

The *Coulombic Efficiency* CE describes the relation of the transferred charge during discharging ΔQ_{dch} to the transferred charge during charging ΔQ_{ch}.

$$CE = \frac{|\Delta Q_{dch}|}{\Delta Q_{ch}} = \frac{|\int_{t_0}^{t_{dch}} I_{cell}(t)dt|}{\int_{t_0}^{t_{ch}} I_{cell}(t)dt} \tag{5.43}$$

The coulombic efficiency describes the impact of parasitic side reactions, self discharge or capacity losses due to leaks in the half cells. However, none of these effects are modeled yet, so it will always be at 100 %.

Voltage Efficiency

Similar to the Coulombic Efficiency, the *Voltage Efficiency* VE is obtained by relating the cell potential during discharging $E_{cell,dch}$ to the cell potential during charging $E_{cell,ch}$.

$$VE = \frac{\int_{t_0}^{t_{dch}} E_{cell,dch}(t)dt}{\int_{t_0}^{t_{ch}} E_{cell,ch}(t)dt} \tag{5.44}$$

The voltage efficiency decreases with increasing overpotentials and is therefore dependent on the factors which have an impact on the overpotentials, as described in the chapters before.

Energy Efficiency

The power P_{cell} of a cell is defined as the product of the cell current and the cell potential.

$$P_{cell}(I) = I_{cell} \cdot E_{cell}(I) \tag{5.45}$$

Therefore, the *Energy Efficiency EE* is defined as the amount of useful energy during discharging related to the required amount of energy during charging. In the case of constant current it is also the product of the coulombic and voltage efficiency.

$$EE = CE \cdot VE = \frac{|\int_{t_0}^{t_{dch}} P_{cell,dch}(t)dt|}{\int_{t_0}^{t_{ch}} P_{cell,ch}(t)dt} \tag{5.46}$$

The Energy Efficiency describes all occurring losses during charging and discharging in the battery cell. It however, does not describe the losses of auxiliary components of a VRFB, like pumps. The required power to operate a pump can be calculated by using:

$$P_{pump} = \Delta p \cdot \dot{Q} \tag{5.47}$$

These losses are incorporated in the *System Energy Efficiency* EE_{sys}.

$$EE_{sys} = \frac{|\int_{t_0}^{t_{dch}} P_{cell,dch}(t)dt| - \int_{t_{0,dch}}^{t_{dch}} P_{pump}(t)dt}{\int_{t_0}^{t_{ch}} P_{cell,ch}(t)dt + \int_{t_{0,ch}}^{t_{ch}} P_{pump}(t)dt} \tag{5.48}$$

For a quick estimation, it is feasible to assume a pumping efficiency of 60 % [36].

6 Results and Discussion

Because the Macro Model is rather complex, the results are separated into three parts: the first part verifies selected parts of the Model by comparing their results to analytically calculated results. In the second part, the model is used to simulate specific setups, that are then compared to actual measurements of those setups. The final part shows a single example of how the model can be used as a design tool.

6.1 Micro Model

To show the capabilities of the developed Micro Model, the results of an exemplary simulation are shown in the following section.

For the used design parameters an ASR of $1\Omega cm^2$ per current collector and an exchange current density i_0 of $6\frac{mA}{cm^2}$ are chosen. The simulation is conducted at 50 % SOC and a flow rate $\dot{V}$ of $9.6\frac{ml}{min}$. A parameter sweep of the applied current density i ranging from -100 to $100\frac{mA}{cm^2}$ is used.

Figure 6.1 shows the concentration of the vanadium species V^{3+} and VO^{2+} at a discharge current density of $-100\frac{mA}{cm^2}$, while figure 6.2 shows the concentration of the vanadium species V^{2+} and VO_2^+. All of the concentrations show the anticipated behavior, gradually in- or decreasing along the cell length.

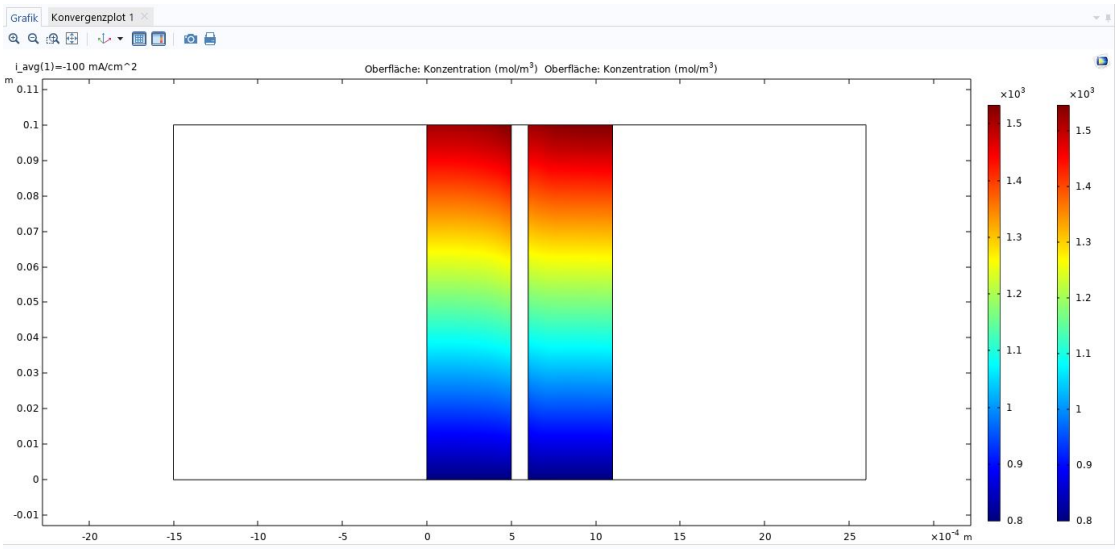

Figure 6.1: V^{3+} and VO^{2+} concentration

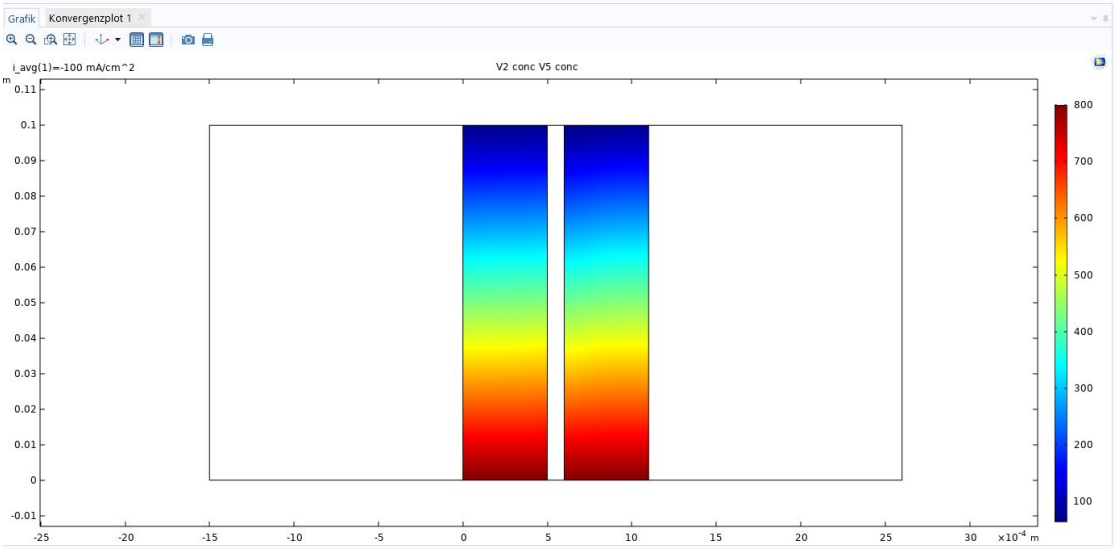

Figure 6.2: V^{2+} and VO_2^+ concentration

The second set of outputs are the potentials. Figure 6.3 shows the solid state potential at a discharge current density of $-100\frac{mA}{cm^2}$ at half cell length. The linear parts of the current collectors to the left and the right are clearly visible. The liquid state potential at a discharge current density of $-100\frac{mA}{cm^2}$ at half cell length is shown in figure 6.4. Because they don't have a liquid state potential, the current collector domains are not shown. The Potential follows the concentration profile as expected. Additionally, the defined Donnan Potential jumps in the membrane are clearly visible. An overview of all potentials including the calculated overpotentials at half cell length for the electrode and the membrane domains is given in figure 6.5.

A polarization curve can be obtained by these potentials, by using the parameter sweep values. It is shown in figure 6.6. The polarization curve features a slight activation part and an ohmic part, just as anticipated. More data points for the low current density area could possible accentuate the activation part. However, these data points can be exported into a table data and are ready to be imported through Matlab to form the data basis for the Macro Model.

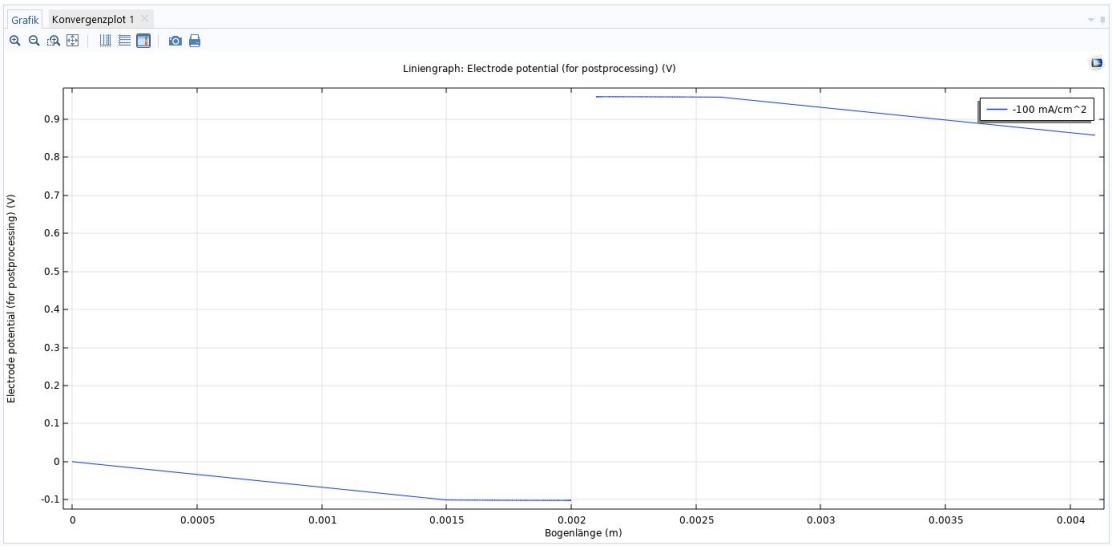

Figure 6.3: Solid state potential at half cell length

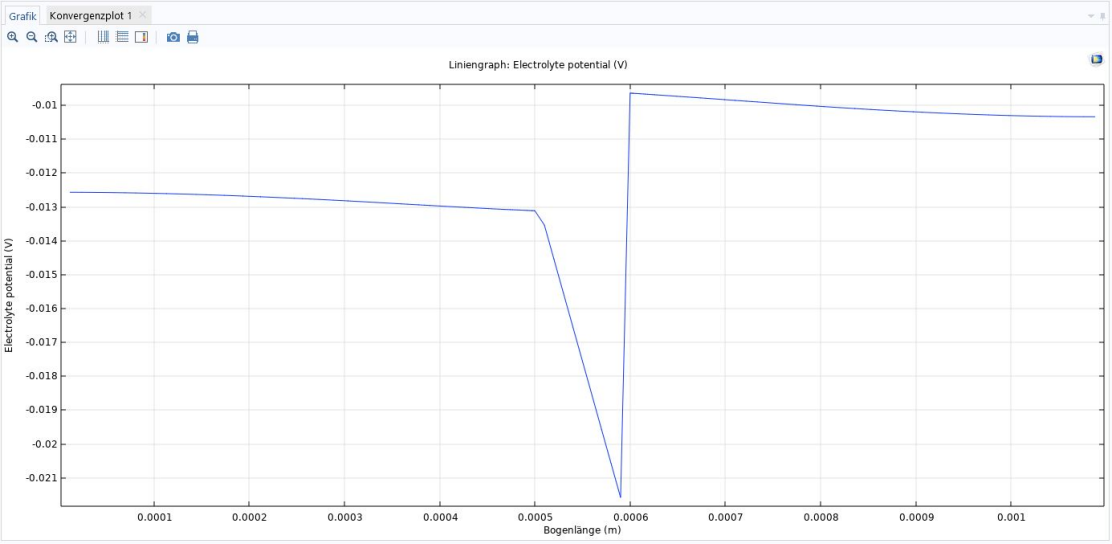

Figure 6.4: Liquid state potential at half cell length without the current collector domains

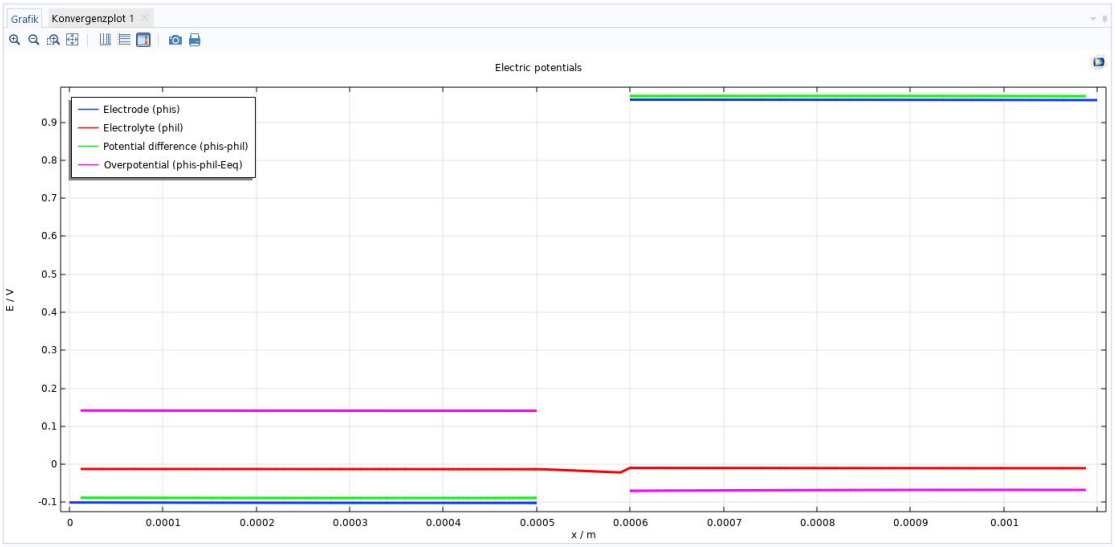

Figure 6.5: Potentials along the cell at half cell length

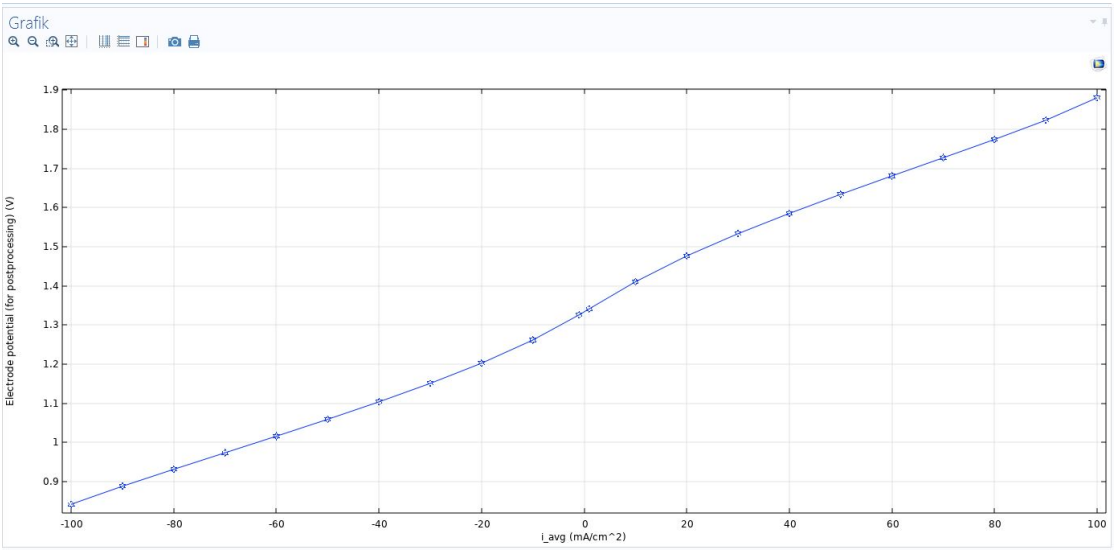

Figure 6.6: Polarization curve for the parameter sweep at half cell length

6.2 Verification Macro Model

The first step of ensuring that the Macro Model works correctly, is to analytically verify selected parts of the model. Alternatively, the results can be compared to results of similar models from literature. If the single parts of the modular Macro Model work correctly, the model as a whole is assumed to be working correctly as well.

6.2.1 Concentrations

Because the concentrations in the electrolytes dictate the OCV of a cell and therefore a big part of the cell voltage, it is crucial to verify the calculation of the concentrations. From the concentrations specified by Knehr in [9] one can derive the total concentration of vanadium $c_{V,neg} = 1040\frac{mol}{m^3}$ and $c_{V,pos} = 1040\frac{mol}{m^3}$. The described electrolyte formation process leads to the total concentration of acid $c_{acid} = 3740\frac{mol}{m^3}$. Knehr specifies the different concentrations at $SOC = 0.15$. By defining these parameters in the Parameter Bus block of the Macro Model, this operating point can be simulated. Figure 6.7 shows the outputs of a reduced cell block. The resulting values match the ones stated in the paper, which indicates that the concentration calculation can be assumed to be correct.

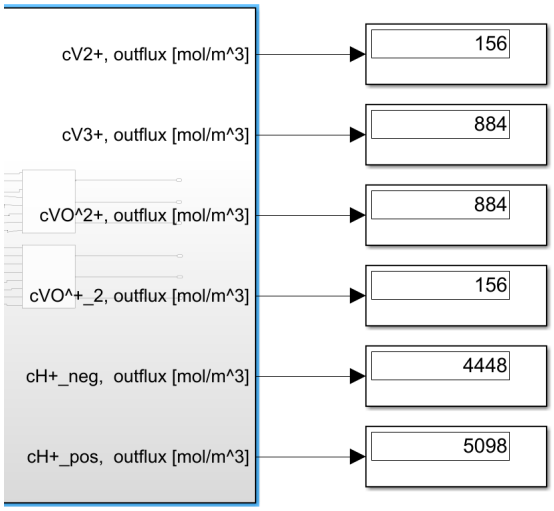

Figure 6.7: Resulting concentrations of the operating point defined in Knehr [9] calculated by using a reduced cell block

6.2.2 OCV

The next step is to check the calculation of the OCV by the concentrations. The OCV can be obtained analytically to validate the simulink model. Therefore, an operating point is defined: state of charge $SOC = 0.15$, temperature $T = 298.15K$ and the total

concentrations of vanadium $c_{V,pos} = 1600\frac{mol}{m^3}$, $c_{V,neg} = 1600\frac{mol}{m^3}$ and the acid $c_{acid} = 2000\frac{mol}{m^3}$.

In a first step, the concentrations are calculated. By using equation 2.17 and 2.18, the concentrations of the vanadium species at the defined state of charged are obtained. The concentrations of the H^+-ions are calculated by using equations 2.19 and 2.20, with $\beta = 0.25$.

Now equation 2.16 can be used to obtain the OCV analytically:

$$OCV = (1.004V - (-0.255V)) + \frac{R \cdot 298.15K}{F} ln \left(\frac{\left(240\frac{mol}{m^3}\right)^2 \cdot \left(\frac{3150\frac{mol}{m^3}}{1000\frac{mol}{m^3}}\right)^3}{\left(1360\frac{mol}{m^3}\right)^2 \cdot \left(\frac{2150\frac{mol}{m^3}}{1000\frac{mol}{m^3}}\right)} \right) = 1.239V \tag{6.1}$$

Simulink computes the same value.

In a next step, the whole OCV range for this electrolyte is simulated with the model. Therefore, a parameter sweep with the state of charge from 0.01 to 0.99 is conducted. Figure 6.8 shows the result. The OCV range behaves as anticipated and is comparable to literature, like stated in Knehr [18] or Ressel [5].

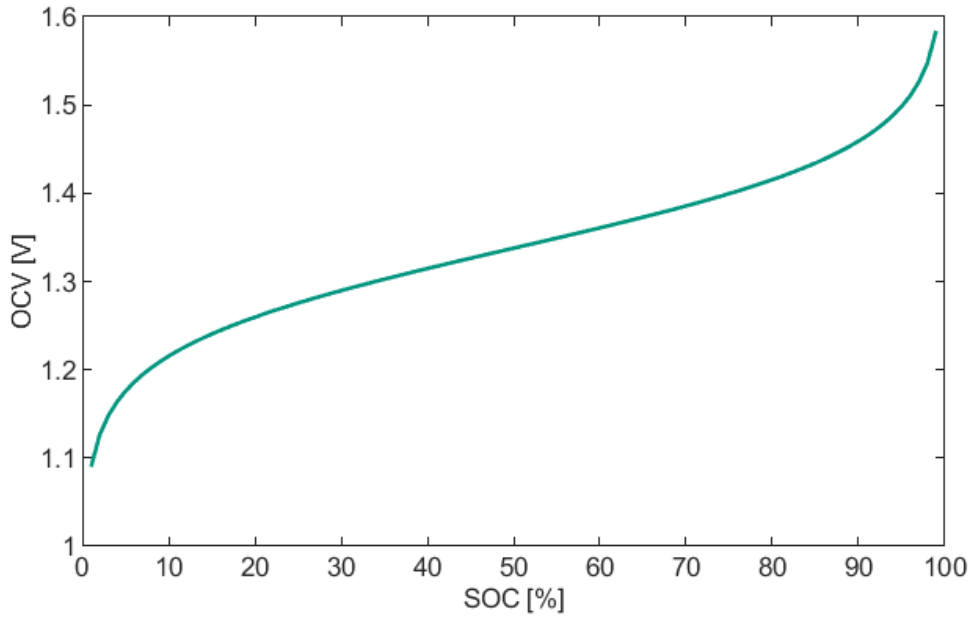

Figure 6.8: OCV range calculated by the Simulink model at $T = 298.15K$, $c_{V,pos} = 1600\frac{mol}{m^3}$, $c_{V,neg} = 1600\frac{mol}{m^3}$ and $c_{acid} = 2000\frac{mol}{m^3}$

6.2.3 Overpotentials

As explained in the modeling chapter, the overpotential characteristic of simulated cells are collected in LUTs, with three options for their creation: from measurements, from the Micro Model and from parameters. The first two options are simply a transfer of data from one format to another and won't be verified here. The third option however uses the principles explained in detail in section 5.2.3.

Consider a VRFB cell with an ASR of $2.5\Omega cm^2$, an exchange current density i_0 of $4mAcm^{-2}$, a limiting current density i_{lim} of $200mAcm^{-2}$ with a membrane area A of $15.708cm^2$ at a temperature T of $298.15K$. With the equations presented in section 5.2.3, we can calculate the overpotentials at a given current density or current. Two operating points are defined: $20mAcm^{-2}$ and $-35mAcm^{-2}$ (which translate to a current I of $314mA$ or $-550mA$ with the given membrane area). Their overpotentials are presented in table 6.1. The polarization curve generated by the LUT-generator in Matlab from the same parameters is shown in figure 6.9. As the two exemplary operating points fall exactly on to the curve, the equations are assumed to be implemented correctly.

	$20\frac{mA}{cm^2}$	$-35\frac{mA}{cm^2}$
η_{ohm}	$0.0500V$	$-0.0875V$
η_{act}	$0.0846V$	$-0.1121V$
η_{conc}	$0.0081V$	$-0.0148V$
η	$0.1427V$	$-0.2144V$

Table 6.1: Overpotentials for 2 operating points

6.2.4 Shunt Currents

The shunt currents are compared to the values stated by Xing in [15]. However, Xing considers only ohmic overpotentials. Therefore, the LUT-generation as explained in section 5.2.3 has to be customized: The activation and concentration parts are turned off. Xing states a cell resistance R of 0.0036Ω with a membrane area A of $476cm^2$, which results in an ASR of $1.7136\Omega cm^2$. The resistances of the channels and the manifolds are stated by Xing with 365.89Ω and 1.23Ω respectively. With these inputs, the shunt current calculation explained in section 5.5.2 can be conducted.

In a first step, 10 identical cells are connected in series and the shunt currents are investigated. The results are identical to the ones found in Xing, as can be seen in figure 6.10.

Xing also investigated the impact of the amount of cells connected in serial on the shunt currents. As can be seen in figure 6.11 this relation also works in the developed model exactly as reported by Xing.

Therefore, the customized calculation method with the LUTs and the iteration described in section 5.5.2 can be assumed to work as intended.

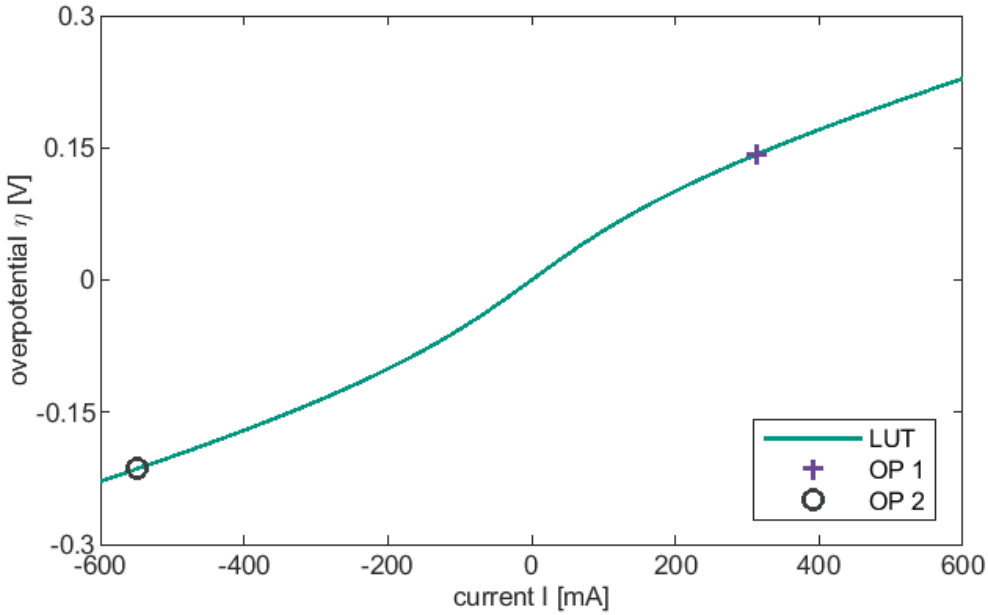

Figure 6.9: Calculated operating points and the whole polarization curve of the LUT

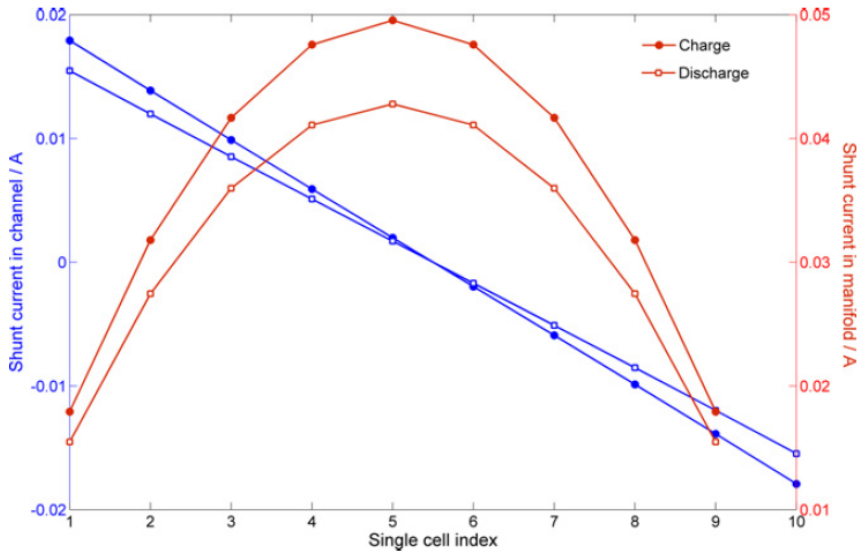

(a)

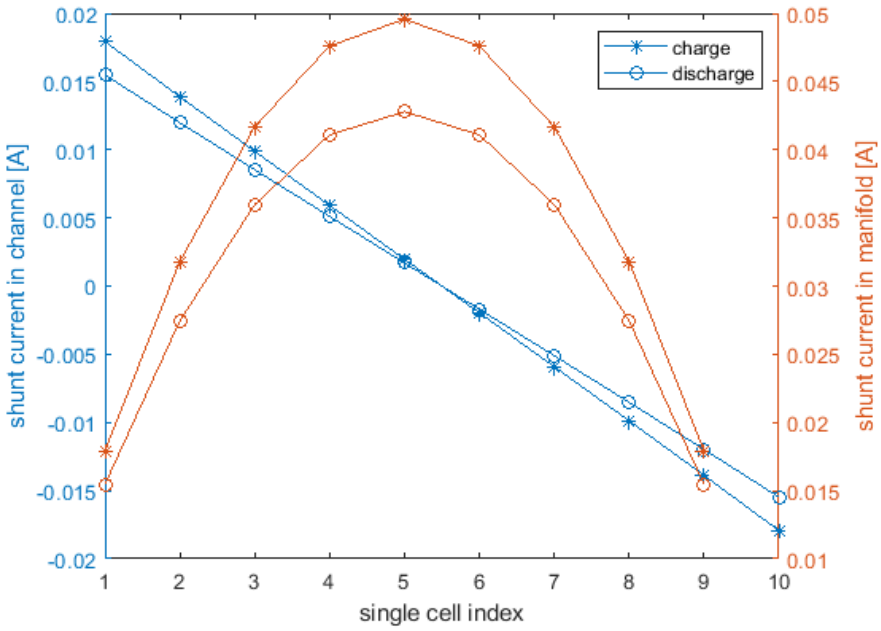

(b)

Figure 6.10: Distribution of shunt currents in manifold and channel during charge and discharge at 50 % SOC for an applied current density of 60 $mAcm^{-2}$ (a) as presented by Xing in [15] (b) simulated with the model in this work

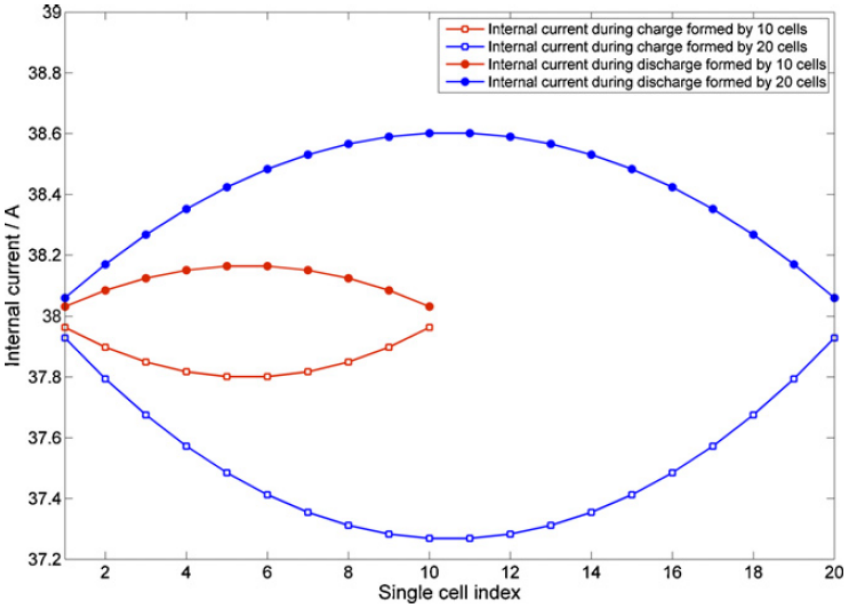

(a)

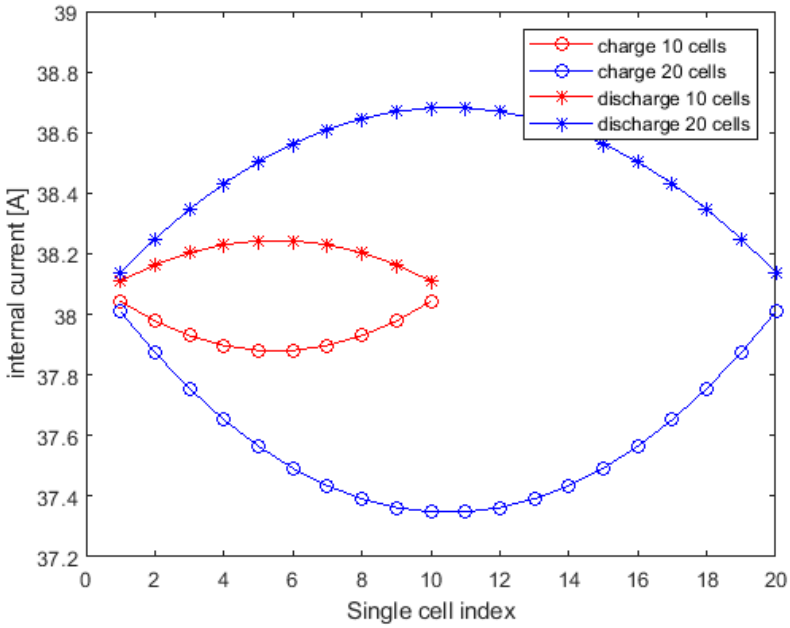

(b)

Figure 6.11: Comparison of internal current for different numbers of cells in series at 50 % SOC for an applied current density of 80 $mAcm^{-2}$ (a) as presented by Xing in [15] (b) simulated with the model in this work

6.3 Validation Macro Model

To validate the macro model, it was compared to polarization curves and charge/discharge cycle measurements that were conducted within the StaTuR-group.

6.3.1 Data Basis

The data basis consists of 4 cells. Their polarization curves (recorded at a volumetric flow rate $\dot{V}_{cell} = 6.4\frac{ml}{min}$ and room temperature each) are shown in figure 6.12. The polarization curves were also recorded at flow rates of 3.2, 9.6 and $12.8\frac{ml}{min}$. These were included in the LUT as well. They were recorded after extensive testing of the cells. While polarization curves exist, that were recorded when the cells were new, the measurements they will be compared to in this section, were conducted rather shortly before the polarization curves shown in figure 6.12 were recorded. VRB01 differs too much from the behavior of the other cells and was ignored for the validation. The other cells vary in their performance. Their polarization curves were used to generate the LUT, according to section 5.2.3. As its current density at the extreme cell voltage values is the highest, VRB04 is considered the best cell among the four, while VRB05 is the worst. The hydraulic characteristic of the cells can be found in figure 5.18.

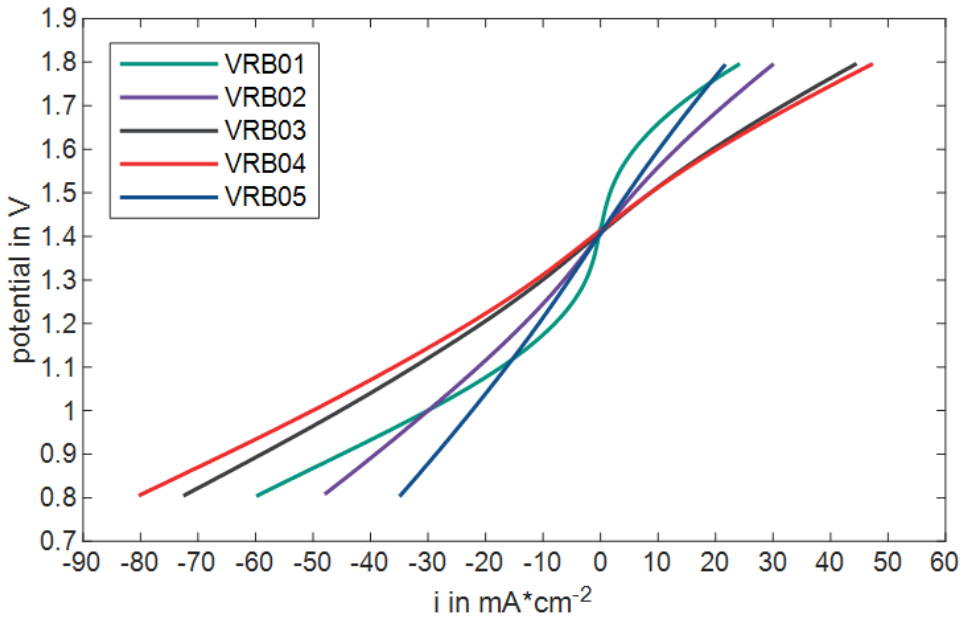

Figure 6.12: Polarization curves of the cells used for the validation

6.3.2 Cell Level

In a first step, only a single cell (the best cell; VRB04) was simulated. The results were compared to the last cycle of a charge/discharge cycle measurement conducted with cell VRB04 as the recording of the data basis shown in figure 6.12 was conducted after the cycling. The starting SOC was taken from the measurement and the OCV in the simulation was corrected by $35mV$ to match that of the measurement at the start. Charging and discharging were executed with $I = 550mA$ and $\dot{V} = 6.4\frac{ml}{min}$ each. The cell is charged or discharged until it reaches the respective cutoff values of $1.7V$ or $0.8V$. Figure 6.13 shows the comparison between the measurement and the simulation.

The upper plot shows the SOC of both electrolytes for the simulation and the measurement. It is notable, that the measured SOC of the negative electrolyte starts out lower but ends higher than the SOC of the positive electrolyte. Also the rate of the SOC change is higher in the measurement than in the simulation. The bottom plot compares the cell voltage. While the charge portion of the cycle from the simulation fits the measurement very good, the OCV after charge and discharge differ considerably. The cell in the measurement reaches the discharge cutoff value roughly $2000s$ earlier than in the simulation with a steeper decrease of the cell voltage. There are multiple possible reasons for this behavior: The SOC change indicates, that the total vanadium concentrations of the electrolytes are smaller than anticipated. This can be estimated analytically by utilizing Faraday's law. Crossover effects are not modeled in the simulation and could also be a reason for the differences. Finally, there is a considerable time gap and multiple measurements that were conducted between the depicted cycle and the measurement of the used data basis for the simulation.

While there is a difference between the measurement and the simulation, it can be assumed that the model works correctly regardless, as both the concentration change as well as the cell voltage show a behavior that would be anticipated with the inputs given to the model.

6.3.3 Module Level

In another series of measurements, the cells were electrically connected in different ways (see figure 6.14) and polarization curves were measured. Hydraulically, the cells were connected in parallel, as can be also seen in figure 6.15, which depicts a photography of the measurement setup. Both of the electrolytes were operated with a volumetric flow rate of $\dot{V}_{mod} = 25.6\frac{ml}{min}$ which translates to roughly $\dot{V}_{cell} = 6.4\frac{ml}{min}$ per cell.

The resulting polarization curves are shown in figure 6.16. All of them were conducted with an electrolyte SOC of 60%. They show the expected behavior with the cells connected in serial yielding a higher module voltage, while the cells connected in parallel cover a bigger current-range. The combined setup falls in between the two extremes.

To replicate this measurement in the Simulink model, the earlier described data basis of the four cells were used. The connection of the cells were then copied in the Simulink model. As the standardized procedure for the generation of polarization curve measurements follows a complex logic, it was decided to take the recorded module current of the

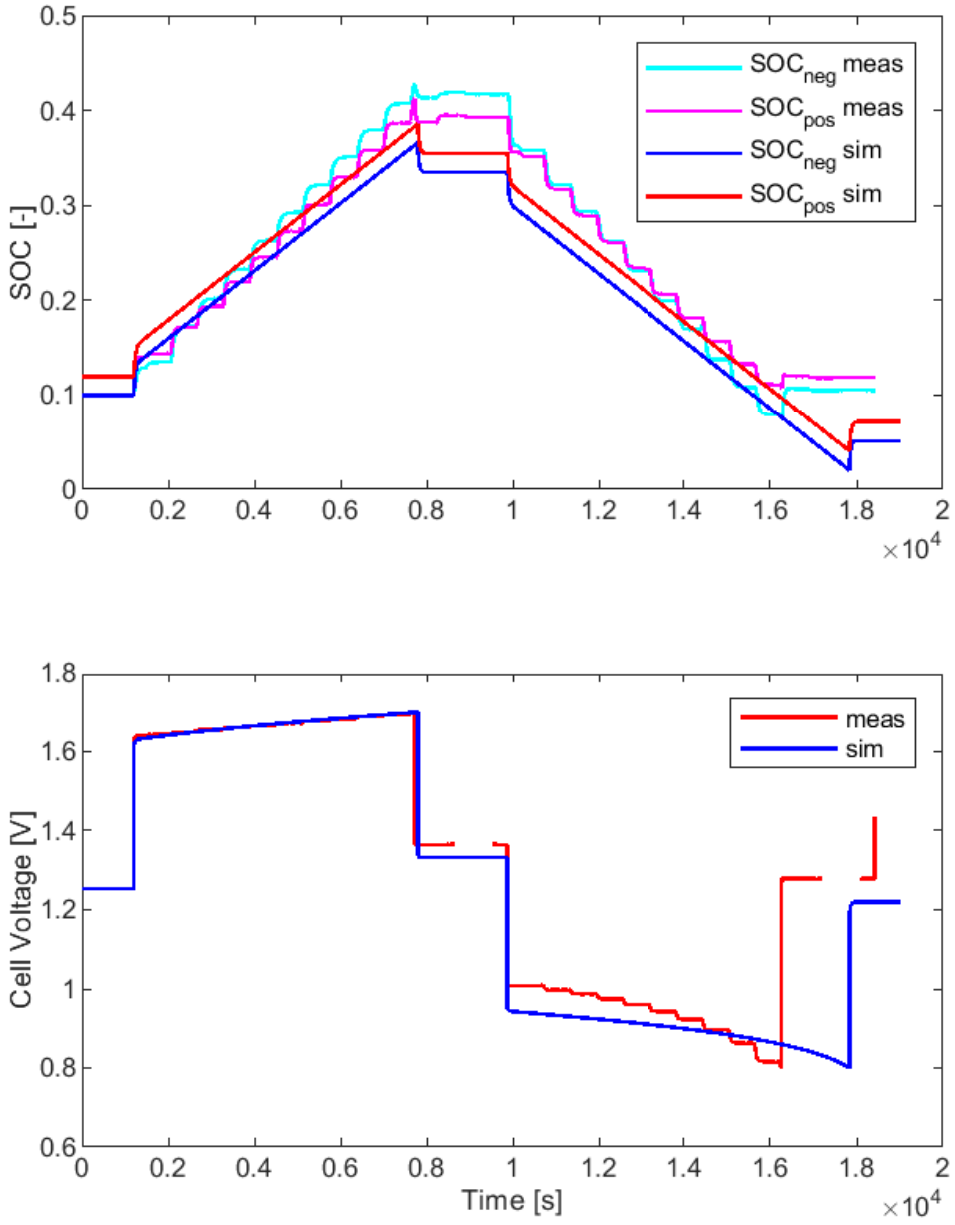

Figure 6.13: Simulated single cell charge/discharge-cycle with an OCV-correction of $35mV$ and the corresponding measurement

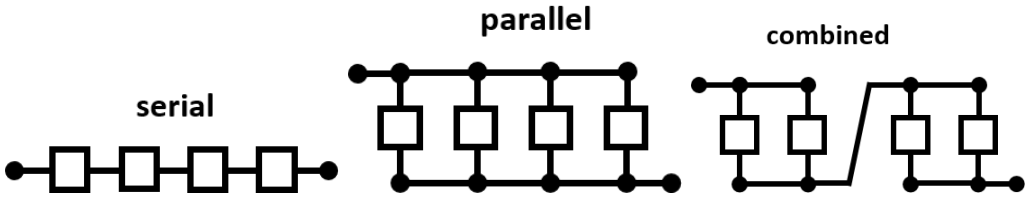

Figure 6.14: The 3 different electrical connections of the 4 cells

measurement as the current input for the model, instead of trying to replicate this logic.

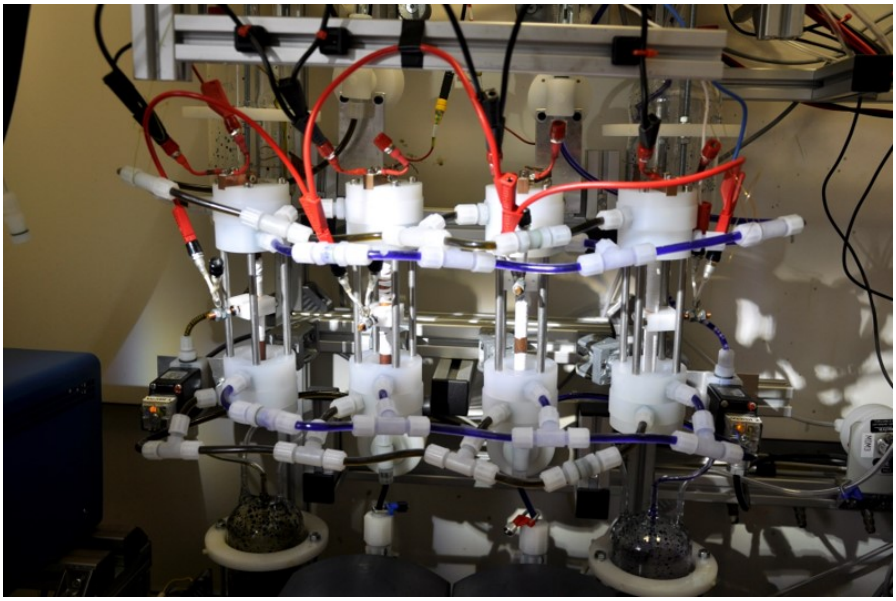

Figure 6.15: Photography of the validation setup

Serial

Figure 6.17 shows a polarization curve conducted with a module consisting of the 4 cells of the data basis connected in serial. The top plot lists the module voltage over the applied module current, while the bottom plot shows the module voltage over the elapsed time. As can be seen in the bottom plot, there are values missing in the simulation towards the ends of the polarization curve. This is due to the fact, that the worst cell of the module (VRB05) is operated in a current range, that is not defined in the data basis used for the model. As already explained, the data basis is gained from the measurements seen in figure 6.12. VRB05 is only defined for a current density roughly ranging from -35 to $20 mA/cm^2$. If a higher current is applied to the cell, the model will deliver an output of NaN for the voltage of this cell, which in turn changes the module voltage also to NaN.

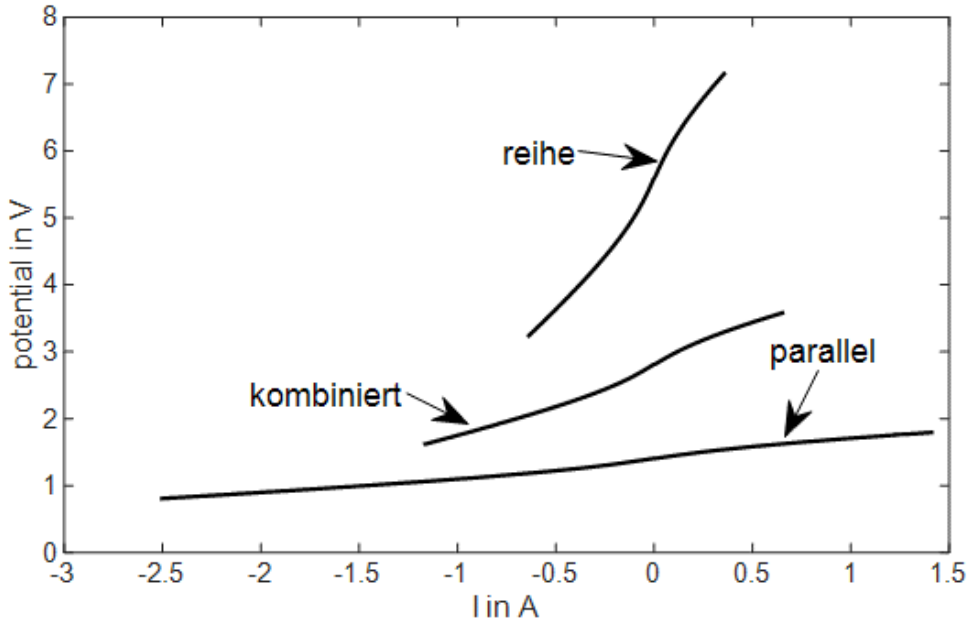

Figure 6.16: Measured polarization curves of 4 different cells in 3 different setups. From top to bottom: serial, combined, parallel. The electric current and the voltage are module values

Comparing the rest of the data, one can see that the simulated polarization curve matches the measured one closely. The qualitative behavior is the same, while the values differ with higher currents. This discrepancy can be retraced to the time gap between the measurement of the data basis and the measurement of the presented combined polarization curve or it could be caused by phenomena like species crossover, which are not covered by the model.

Parallel

Another polarization curve was measured with the four described cells connected in parallel. The distribution of the electric current is shown in figure 6.18. As can be seen in the plot, the distribution of the electric current as done by the simulation matches the distribution of the current in the measurement. However, with higher currents, a developing gap can be observed for the cells 4 and 5. This is interesting because cell 4 is the best performing cell and cell 5 is the worst performing cell. Hence, the model distributes a bigger portion of the module current to the best performing cell and a smaller portion to the worst performing cell, than it is the case in the experimental setup. Qualitatively however, the simulation can be assumed to work as intended.

The polarization curve is included in figure 6.19. It can be observed, that the gap between simulation and measured data rises slightly with higher current. Possible reasons for this discrepancy were already discussed in the last section and remain the same.

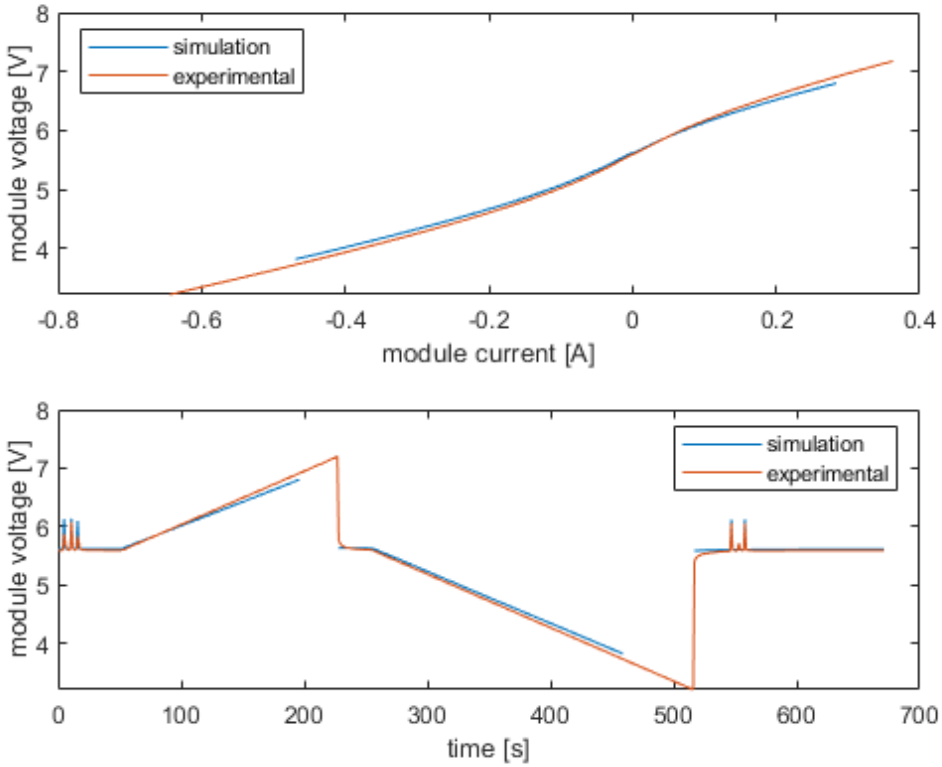

Figure 6.17: Simulated polarization curve of 4 cells in serial and the corresponding measurement

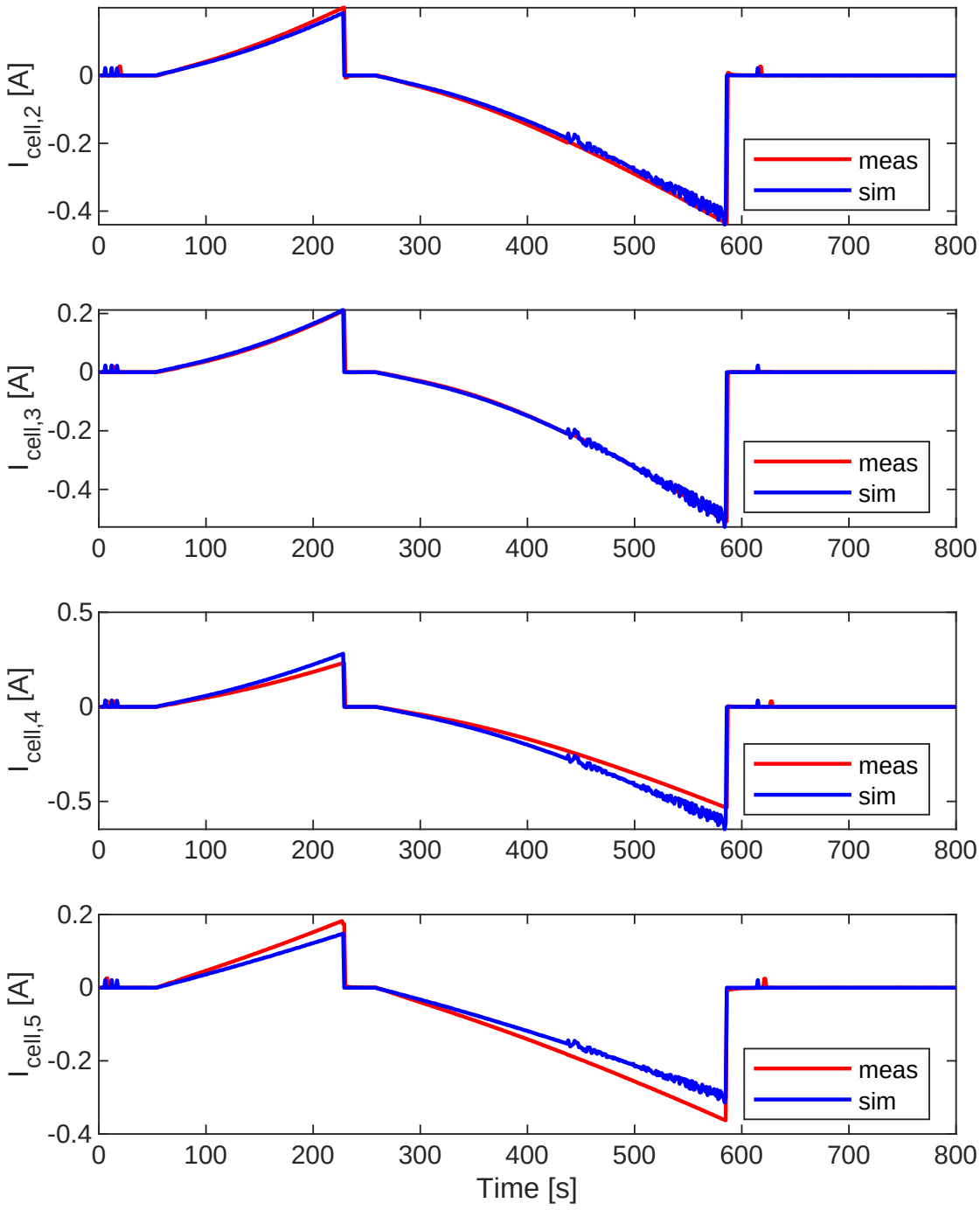

Figure 6.18: Simulated polarization curve of 4 cells in parallel and the corresponding measurement: Distribution of the electric current

Combined

The same relations can be observed for the combined module. Its polarization curve is also included in figure 6.19. An increasing gap can also be observed for this electric setup, the assumed reasons stay the same as for the serial module. In conclusion, the current distribution can assumed to be valid for each shown setup with minor discrepancies.

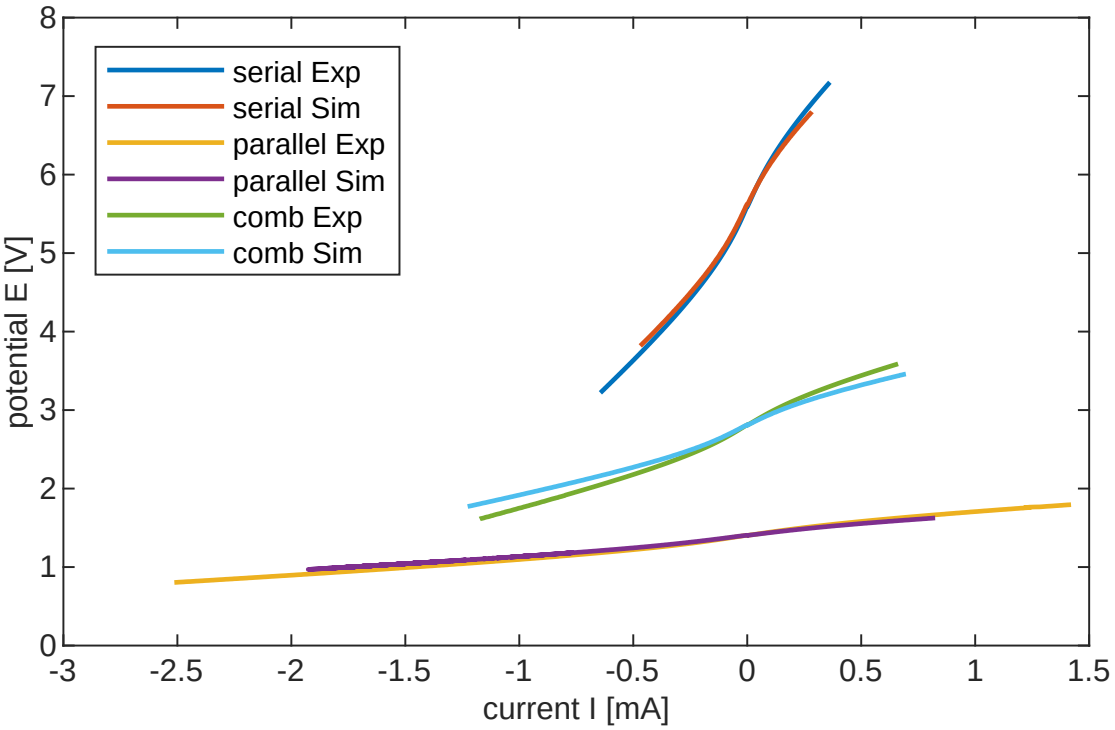

Figure 6.19: Measured polarization curves of 4 different cells in 3 different setups with the results from their respective simulation

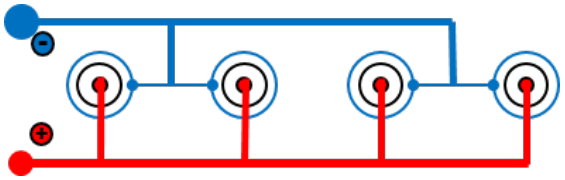

Figure 6.20: Mini-Module consisting of 4 cells connected electrically in parallel

6.4 Simulation Macro Model

The following section will prove the use of the developed model as a design tool. Consider a hypothetical cell with a set exchange current density $i_0 = 4.0\,mA\,cm^{-2}$. Concentration overpotentials are set to $i_{lim} = 200\,mA\,cm^{-2}$. Due to manufactoring processes or other reasons, the ASR is expected to be $ASR = (3 \pm 1)\,\Omega\,cm^2$ with an active membrane area of $A = 15.8\,cm^2$. Four of these cells are set up in a module, with cell 1 being the cell with the lowest ASR and cell 4 with the highest ASR.

In order to evaluate the module performance, the simulation control is used to generate a charge discharge cycle. The sequence is described in the following:

1. 1200s OCV
2. constant current I_{mod} until the first cell voltage reaches $E_{cell} = 0.8\,V$
3. 1200s OCV
4. constant current I_{mod} until the first cell voltage reaches $E_{cell} = 1.7\,V$
5. 1200s OCV
6. constant current I_{mod} until the first cell voltage reaches $E_{cell} = 0.8\,V$
7. 1200s OCV

The four cells are electrically connected in parallel, as depicted in figure 6.20. A module current of $I_{mod} = 2.2\,A$ is applied in the constant current steps, which should average to a cell current of around $I_{cell} = 550\,mA$. Hydraulically the cells are connected in parallel as well, but as their hydraulic characteristic is assumed to be equal, all of them will be delivered with the same flow rate $\dot{V}_{cell} = 6.4\,ml\,min^{-1}$ combining to the module flow rate of $\dot{V}_{mod} = 25.6\,ml\,min^{-1}$.

Figure 6.21 shows the SOC of each electrolyte, the current of each cell and the voltage of each cell (which is equal to the module, as the cells are connected in parallel). After the simulation was conducted, efficiencies were calculated with the exception of CC. It was instead set to 96 % (according to results from [5]) as none of the simulated effects would cause if to differ from 100 %.

As can be seen, the biggest share of the module current is distributed to cell 1, which is expected as it is the best performing cell. At the end of both discharge phases, the current distribution changes, like anticipated: Different cell currents cause slightly

CE	96.0 %
VE	70.1 %
EE	67.3 %

Table 6.2: Mini-Module consisting of 4 cells connected electrically in parallel: Efficiencies

different SOCs in each cell. As can be seen in figure 6.8, the OCV changes rapidly when reaching extreme SOC values. The calculated efficiencies seem to be plausible as well.

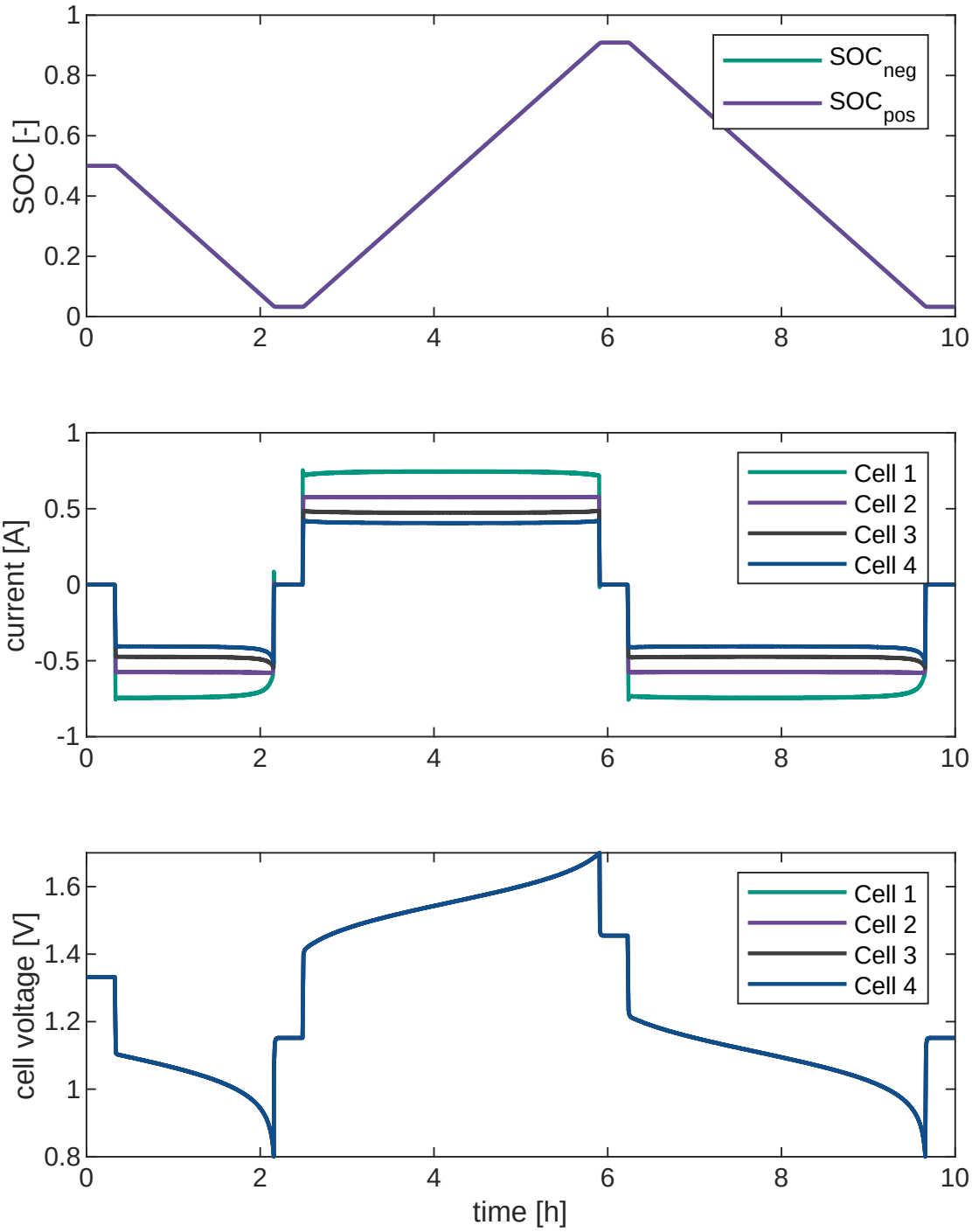

Figure 6.21: Mini-Module consisting of 4 cells connected electrically in parallel: results

7 Conclusions and Outlook

A Micro Model was developed from several existing literature models. It can be used to conduct simple microscopic analysis of potentials and concentrations, based on design parameters. The results can be exported to serve as cell characteristics in the Macro Model.

The developed Macro Model is capable of simulating VRFB modules consisting of cells of varying performance in different setups. It provides values that can be used to quantify the module, like voltages, pressure drops and efficiencies. If possible, the used calculation methods were compared to calculated values or literature. Based on the results, the model is assumed to be working correct, regardless of whether the parts were adopted form literature or were developed by the author himself. The results from simulated polarization curve and charge/discharge cycle measurements also match the actual measurements qualitatively with minor discrepancies qualitatively. Possible reasons for the discrepancies were provided. Using LUTs for the data basis has proven to be an easy way to include characteristics from different sources. Setups can be quickly altered through the use of addresses. The implemented simulation control allows the alteration of inputs by a user-defined logic. A small simulation has shown, that the model is suited to be used as a design tool.

Further development of the model could focus on adding a contact resistance model, as contact resistances arising due to the wiring are assumed to have a significant impact on the performance of a given module.

However, the extensive testing of the model also revealed some flaws. The possibility of realizing every electrical setup of the module decreased user-friendliness. The Simulink-Matlab interface that had to be utilized for the current distribution in parallel setups, in the shunt current calculation and the hydraulic distribution produced severe problems in the testing on multiple occasions. A workaround was eventually found, which would decrease the user-friendliness even further. However, this problem also prevents the envisioned method of upgrading the model from module to stack level. The author has conducted first tests to translate the Macro Model from Simulink to Matlab only and strongly recommends pursuing this route, as the first results look promising.

After a satisfying module and stack concept is developed, it is also possible to use the developed model as a baseline for a new, more accurate model, that simulates this particular setup. Not longer needing the flexibility of simulating a multitude of different setups and therefore following an approach that tries to predict every possibility, specific cases can be modeled. Shunt currents in a non-serial setup are a good example. For strictly serial setups, the equivalent circuit diagram can be set up by periodic equations, as demonstrated in this work. Connecting cells in a mix of serial and parallel adds to the complexity of the equivalent circuit diagram to such an extent, that it can't be

implemented in a way that supports every possible setup. Creating and solving the diagram for a specific setup however, only varying things like cell performance and the geometry of the electrolyte piping, is definitely possible.

Bibliography

[1] International Energy Agency, *Key World Energy Statistics 2019*. IEA, Paris, 2019.

[2] Agora Energiewende, "Power generation and consumption." `https://www.agora-energiewende.de/en/service/recent-electricity-data/chart/power_generation/24.05.2020/27.05.2020/`.

[3] L. Arenas, C. P. de León, and F. Walsh, "Engineering aspects of the design, construction and performance of modular redox flow batteries for energy storage," *Journal of Energy Storage*, vol. 11, pp. 119–153, jun 2017.

[4] M. Skyllas-Kazacos, M. H. Chakrabarti, S. A. Hajimolana, F. S. Mjalli, and M. Saleem, "Progress in flow battery research and development," *Journal of The Electrochemical Society*, vol. 158, no. 8, p. R55, 2011.

[5] S. P. Ressel, *Tubular All Vanadium and Vanadium/Air Redox Flow Cells*. PhD thesis, 2019.

[6] "Project statur." website: `https://www.haw-hamburg.de/forschung/projekte-a-z/forschungsprojekte-detail/project/project/show/statur-q/`.

[7] N. Hagedorn, M. A. Hoberecht, and L. H. Thaller, "Nasa-redox cell stack: Shunt current, pumping power, and cell performance tradeoffs," tech. rep., U.S. Department of Energy, 1982.

[8] S. Ressel, A. Chica, T. Flower, and T. Struckmann, "A tubular cell design for redox flow batteries," in *GDCh Wifo Session: Elektrochemische Energiespeicher und Wandler*, (Berlin), Sept. 2017.

[9] K. W. Knehr, E. Agar, C. R. Dennison, A. R. Kalidindi, and E. C. Kumbur, "A transient vanadium flow battery model incorporating vanadium crossover and water transport through the membrane," *Journal of The Electrochemical Society*, vol. 159, no. 9, pp. A1446–A1459, 2012.

[10] Y. A. Gandomi, D. S. Aaron, T. A. Zawodzinski, and M. M. Mench, "In situ potential distribution measurement and validated model for all-vanadium redox flow battery," *Journal of The Electrochemical Society*, vol. 163, pp. A5188–A5201, nov 2015.

[11] M. W. Nix, *Bachelor's Thesis: Analyse und Implementierung einer mehdimensionalen Mikrosimulation fr eine Vanadium Redox-Flow-Batterie*. Feb. 2017.

[12] F. Moro, A. Trovò, S. Bortolin, D. D. Col, and M. Guarnieri, "An alternative low-loss stack topology for vanadium redox flow battery: Comparative assessment," *Journal of Power Sources*, vol. 340, pp. 229–241, feb 2017.

[13] S. Knig, M. Suriyah, and T. Leibfried, "Model based examination on influence of stack series connection and pipe diameters on efficiency of vanadium redox flow batteries under consideration of shunt currents," *Journal of Power Sources*, vol. 281, pp. 272–284, may 2015.

[14] F. Wandschneider, S. Rhm, P. Fischer, K. Pinkwart, J. Tbke, and H. Nirschl, "A multi-stack simulation of shunt currents in vanadium redox flow batteries," *Journal of Power Sources*, vol. 261, pp. 64–74, sep 2014.

[15] F. Xing, H. Zhang, and X. Ma, "Shunt current loss of the vanadium redox flow battery," *Journal of Power Sources*, vol. 196, pp. 10753–10757, dec 2011.

[16] V. M. Schmidt, *Elektrochemische Verfahrenstechnik*. Wiley, oct 2003.

[17] N. S. Hudak, "Practical thermodynamic quantities for aqueous vanadium- and iron-based flow batteries," *Journal of Power Sources*, vol. 269, pp. 962–974, dec 2014.

[18] K. Knehr and E. Kumbur, "Open circuit voltage of vanadium redox flow batteries: Discrepancy between models and experiments," *Electrochemistry Communications*, vol. 13, pp. 342–345, apr 2011.

[19] T. Struckmann, P. Kuhn, and S. Ressel, "A combined in situ monitoring approach for half cell state of charge and state of health of vanadium redox flow batteries." submitted to Journal of Power Sources.

[20] A. T. Kuhn and J. S. Booth, "Electrical leakage currents in bipolar cell stacks," *Journal of Applied Electrochemistry*, vol. 10, pp. 233–237, mar 1980.

[21] Q. Ye, J. Hu, P. Cheng, and Z. Ma, "Design trade-offs among shunt current, pumping loss and compactness in the piping system of a multi-stack vanadium flow battery," *Journal of Power Sources*, vol. 296, pp. 352–364, nov 2015.

[22] A. Tang, J. McCann, J. Bao, and M. Skyllas-Kazacos, "Investigation of the effect of shunt current on battery efficiency and stack temperature in vanadium redox flow battery," *Journal of Power Sources*, vol. 242, pp. 349–356, nov 2013.

[23] M. Skyllas-Kazacos and M. Kazacos, "State of charge monitoring methods for vanadium redox flow battery control," *Journal of Power Sources*, vol. 196, pp. 8822–8827, oct 2011.

[24] *COMSOL Multiphysics, Documentation.* `https://www.comsol.de/documentation`.

[25] X. Ke, J. I. D. Alexander, J. M. Prahl, and R. F. Savinell, "Flow distribution and maximum current density studies in redox flow batteries with a single passage of the serpentine flow channel," *Journal of Power Sources*, vol. 270, pp. 646–657, dec 2014.

[26] Solved with COMSOL Multiphysics 5.0: Vanadium Redox Flow Battery.

[27] T. Yamamura, N. Watanabe, T. Yano, and Y. Shiokawa, "Electron-transfer kinetics at carbon electrodes," *Journal of The Electrochemical Society*, vol. 152, no. 4, p. A830, 2005.

[28] L. R. F. Allen J. Bard, *Electrochemical Methods*. John Wiley & Sons Inc, 2000.

[29] D. You, H. Zhang, and J. Chen, "A simple model for the vanadium redox battery," *Electrochimica Acta*, vol. 54, pp. 6827–6836, nov 2009.

[30] D. Schmal, J. V. Erkel, and P. J. V. Duin, "Mass transfer at carbon fibre electrodes," *Journal of Applied Electrochemistry*, vol. 16, pp. 422–430, may 1986.

[31] *Matlab R2019b, Documentation*. `https://de.mathworks.com/help/matlab/`.

[32] M. Li and T. Hikihara, "A coupled dynamical model of redox flow battery based on chemical reaction, fluid flow, and electrical circuit," *IEICE Transactions on Fundamentals of Electronics, Communications and Computer Sciences*, vol. E91-A, pp. 1741–1747, jul 2008.

[33] L. J. Ontiveros and P. E. Mercado, "Modeling of a vanadium redox flow battery for power system dynamic studies," *International Journal of Hydrogen Energy*, vol. 39, pp. 8720–8727, may 2014.

[34] C. Yin, S. Guo, H. Fang, J. Liu, Y. Li, and H. Tang, "Numerical and experimental studies of stack shunt current for vanadium redox flow battery," *Applied Energy*, vol. 151, pp. 237–248, aug 2015.

[35] F. Brandes, *Bachelor's Thesis: Implementierung einer Auswertungs-Software fr einen Redox-Flow-Batterie-Prfstand*. Nov. 2017.

[36] V. Viswanathan, A. Crawford, D. Stephenson, S. Kim, W. Wang, B. Li, G. Coffey, E. Thomsen, G. Graff, P. Balducci, M. Kintner-Meyer, and V. Sprenkle, "Cost and performance model for redox flow batteries," *Journal of Power Sources*, vol. 247, pp. 1040–1051, feb 2014.

List of Figures

List of Tables

Hochschule für Angewandte Wissenschaften Hamburg
Hamburg University of Applied Sciences

Erklärung zur selbstständigen Bearbeitung einer Abschlussarbeit

Gemäß der Allgemeinen Prüfungs- und Studienordnung ist zusammen mit der Abschlussarbeit eine schriftliche Erklärung abzugeben, in der der Studierende bestätigt, dass die Abschlussarbeit „– bei einer Gruppenarbeit die entsprechend gekennzeichneten Teile der Arbeit [(§ 18 Abs. 1 APSO-TI-BM bzw. § 21 Abs. 1 APSO-INGI)] – ohne fremde Hilfe selbständig verfasst und nur die angegebenen Quellen und Hilfsmittel benutzt wurden. Wörtlich oder dem Sinn nach aus anderen Werken entnommene Stellen sind unter Angabe der Quellen kenntlich zu machen."

Quelle: § 16 Abs. 5 APSO-TI-BM bzw. § 15 Abs. 6 APSO-INGI

Dieses Blatt, mit der folgenden Erklärung, ist nach Fertigstellung der Abschlussarbeit durch den Studierenden auszufüllen und jeweils mit Originalunterschrift als letztes Blatt in das Prüfungsexemplar der Abschlussarbeit einzubinden.
Eine unrichtig abgegebene Erklärung kann -auch nachträglich- zur Ungültigkeit des Studienabschlusses führen.

Erklärung zur selbstständigen Bearbeitung der Arbeit

Hiermit versichere ich,

Name: Brandes

Vorname: Fabian

dass ich die vorliegende Masterarbeit bzw. bei einer Gruppenarbeit die entsprechend gekennzeichneten Teile der Arbeit – mit dem Thema:

Mehrskalen-Modellierung eines Vanadium Redox-Flow-Batterie Stacks

ohne fremde Hilfe selbständig verfasst und nur die angegebenen Quellen und Hilfsmittel benutzt habe. Wörtlich oder dem Sinn nach aus anderen Werken entnommene Stellen sind unter Angabe der Quellen kenntlich gemacht.

- die folgende Aussage ist bei Gruppenarbeiten auszufüllen und entfällt bei Einzelarbeiten -

Die Kennzeichnung der von mir erstellten und verantworteten Teile der -bitte auswählen- ist erfolgt durch:

Hamburg	29.05.2020	
Ort	Datum	Unterschrift im Original